Use of Climate Model Large Ensembles to Study the Impact of Climate Change on Future Extreme Droughts

by

Cha ZHAO

MANUSCRIPT-BASED THESIS PRESENTED TO ÉCOLE DE TECHNOLOGIE SUPÉRIEURE IN PARTIAL FULFILLMENT FOR THE DEGREE OF DOCTOR OF PHILOSOPHY
Ph.D.

MONTREAL, AUGUST 13, 2020

ÉCOLE DE TECHNOLOGIE SUPÉRIEURE
UNIVERSITÉ DU QUÉBEC

BOARD OF EXAMINERS

THIS THESIS HAS BEEN EVALUATED

BY THE FOLLOWING BOARD OF EXAMINERS

M. François Brissette, Thesis Supervisor
Department of Construction Engineering, École de technologie supérieure

M. Jie Chen, Co-supervisor
State Key Laboratory of Water Resources & Hydropower Engineering Science,
Wuhan University

M. Patrick Terriault, President of the Board of Examiners
Department of Mechanical Engineering, École de technologie supérieure

Mme. Annie Poulin, Member of the jury
Department of Construction Engineering, École de technologie supérieure

M. Alain N. Rousseau, External Independent Examiner
Centre Eau Terre Environnement

THIS THESIS WAS PRESENTED AND DEFENDED

IN THE PRESENCE OF A BOARD OF EXAMINERS AND THE PUBLIC

ON JUNE 29, 2020

AT ÉCOLE DE TECHNOLOGIE SUPÉRIEURE

ACKNOWLEDGEMENTS

Upon writing this thesis, many emotions came to my mind. Throughout these years of my life, I encountered many dilemmas and received many bits of help as well. I am so grateful for all the support I have received while researching and writing this thesis. It would not have been possible without help from so many people in so many ways.

I would like to express my special appreciation and thanks to my Ph.D. supervisor, Professor François Brissette. You have been a tremendous mentor for me. Advice and scientific insights have guided me to complete this thesis under your supervision. You have been a fabulous supervisor because you could always give me some useful suggestions when I was stuck in research problems. Your enthusiasm, inspiration, motivation and patience always encouraged me to go forward and make my research fun. I learned a lot from your simple and clear explanations. I would also like to thank my co-supervisor, Jie Chen, for giving me valuable advice on my research and life. Many thanks to you for helping me solve the research problems, and improve my research papers.

Besides my advisers, I am also very grateful to the jury members who evaluated this thesis. Positive and constructive comments were very helpful in improving my thesis. I am gratefully indebted to your very valuable comments on this thesis.

I am grateful to my colleagues who have graduated and those who remain at the HC3 lab. It would be a hard job for listing all your names. It was great working with all of you over the past few years. Thank you all. Especially, Jean-Luc and Richard, thanks so much for your help.

I would also like to thank my master supervisors Professor WenZhao Liu and Professor Zhi Li. Although I graduated from Northwest A&F University for a few years back, you have always been supporting. This thesis is also dedicated to you.

Plenty of friends are keeping company with me in Montreal. I am very happy to be your friends in this gorgeous city. Besides, I am grateful to my friends in China and other countries. You are always along with me. Many thanks to all of you who supported me to strive towards my goal.

Most importantly, I must express my very profound gratitude to my family for providing moral and emotional support along the way. I have pursued my career in Montreal for over 5 years now. Your support keeps me from sadness and despair. I am also very sorry because I cannot accompany you for the past few years. Thank you for all the sacrifices that you've made on my behalf. Words cannot express how grateful I am to you. With your company, I can face any challenge in life and be successful with great courage.

Last but not least, for those who helped me make this thesis possible I have mentioned or not your name, please accept my sincere appreciation to you. My life is shining because of you. Thank you again for everything you have done.

Utilisation de Grands Ensembles de Modèles Climatiques pour Étudier L'impact du Changement Climatique sur les Futures Sécheresses Extrêmes

Cha ZHAO

RÉSUMÉ

L'évolution des sécheresses dans un climat en évolution a reçu une attention croissante de la communauté scientifique et du public. Des études récentes qui ont examiné l'évolution des futures sécheresses ont montré que ces dernières devraient devenir plus graves et plus fréquentes. L'océan est le principal moteur de la variabilité climatique interne, et la variabilité hydroclimatique régionale peut être liée à des oscillations climatiques à grande échelle. Cette étude vise à explorer l'évolution de la fréquence des sécheresses extrêmes à court et long termes aux échelles mondiale et continentale, et à étudier la relation entre la variabilité climatique future et les modes d'oscillation à grande échelle. Meilleures compréhensions de l'évolution des sécheresses extrêmes futures et de la relation avec la variabilité climatique sont essentielle pour mieux s'adapter au changement climatique.

Deux grands ensembles de modèles climatiques, le grand ensemble de 50 membres du modèle du système terrestre canadien (CanESM2) et celui de 40 membres du modèle du système terrestre communautaire (CESM1), tous deux sous le scénario RCP8.5 ont été utilisés dans ce travail. Les précipitations mensuelles ont été utilisées pour calculer l'indice de précipitation standardisé (SPI) afin de quantifier les sécheresses météorologiques aux échelles mondiale et nord-américaine pour les périodes futures proches (2036-2065) et lointaines (2070-2099). Dans un deuxième temps, l'évolution des sécheresses hydrologiques sur 4521 bassins versants nord-américains a été évaluée à l'aide de l'indice de sécheresse hydrologique (SDI). Dans une dernière étape, la contribution à la variabilité interne de trois indices climatiques à grande échelle a été étudiée. L'impact de l'oscillation australe El Niño (ENSO), de l'oscillation décennale du Pacifique (PDO) et de l'oscillation multidécennale de l'Atlantique (AMO) sur les anomalies climatiques à l'échelle du bassin versant a été étudié. Les interactions constructives et destructives entre ces trois indices ont également été étudiées au cours de la période historique 1961-2010.

Par rapport aux observations, les deux ensembles font un travail raisonnable pour reproduire les profils de précipitations annuelles moyennes et de variabilité interannuelle au cours de la période de référence 1981-2010. Les changements prévus des précipitations pour les deux modèles sont conformes aux tendances prévues par le GIEC. Les deux modèles climatiques prévoient une augmentation de la fréquence des sécheresses météorologiques extrêmes dans de nombreuses régions du monde. Les schémas spatiaux des régions où la sécheresse s'aggrave correspondent à ceux du changement prévu des précipitations annuelles moyennes, bien que le premier soit plus étendu. Ceci qui indique que les changements de la variabilité interne augmenteront la fréquence des sécheresses, même dans certaines régions qui devraient voir une augmentation des précipitations annuelles moyennes. L'augmentation prévue de la fréquence des sécheresses météorologiques est plus importante pour les sécheresses à court terme de juinjuillet-août (JJA) et pour les périodes de retour plus importantes. De grandes augmentations de fréquence sont observées dans de nombreuses régions, jusqu'à 20 fois pendant la sécheresse de 100 ans de JJA, indiquant un changement de période de retour de 100 à 5 ans.

Les résultats montrent des schémas très différents pour les changements futurs des sécheresses hydrologiques extrêmes par rapport aux changements des sécheresses météorologiques. Les sécheresses hydrologiques, qui combinent l'effet des précipitations et des changements de température, montrent un schéma généralement uniforme d'augmentations importantes à très importantes de la fréquence des sécheresses. Cela montre que l'augmentation prévue de la température est un des principaux moteurs des futures sécheresses hydrologiques extrêmes, suffisante pour surmonter l'augmentation prévue des précipitations estivales moyennes prévues pour de nombreux bassins versants nord-américains. Les changements prévus pour les sécheresses météorologiques et hydrologiques s'aggravent constamment pour les périodes de retour considérées plus longues. En d'autres termes, les changements de fréquence pour les sécheresses de 100 ans sont plus importants que ceux attendus pour les sécheresses de 2 et 20 ans.

En ce qui concerne le contrôle des oscillations à grande échelle sur les anomalies climatiques à l'échelle du bassin versant, il a été constaté que l'ENSO domine la variabilité des précipitations annuelles alors que la température annuelle moyenne est principalement influencée par l'AMO sur la majeure partie de l'Amérique du Nord. L'impact de PDO est relativement plus faible. Les rôles dominants de l'ENSO sur les précipitations et de l'AMO sur la température sont préservés mais renforcés ou diminués par les fortes interactions entre les oscillations. Un ENSO négatif (La Niña) couplé à un AMO positif apporte des conditions climatiques favorables aux sécheresses.

Cette thèse illustre l'impact du forçage anthropique et de la variabilité interne sur la fréquence future des sécheresses. Les résultats fournissent des connaissances indispensables nécessaires pour mieux s'adapter au changement climatique.

Mots-clés: changement climatique; modèles climatiques; grands ensembles; sécheresses extrêmes; analyse de fréquence; oscillations à grande échelle

Use of Climate Model Large Ensembles to Study the Impact of Climate Change on Future Extreme Droughts

Cha ZHAO

ABSTRACT

The evolution of droughts in a changing climate has received increasing attention from the scientific community and the public. Recent studies looking at the evolution of future droughts have found that droughts are expected to become more severe. The ocean is the main driver of internal climate variability, and regional hydroclimatic variability can be related to large-scale climate oscillations. This study explored the evolution of the frequency of short- and long-term extreme droughts at the global and continental scales, and studied the relationship between future climate variability and large-scale oscillations. A better understanding of the evolution of future extreme droughts and their relationship with climate variability is the key to better adapt to the changing climate.

Two climate model large ensembles, the 50-member Canadian Earth System Model (CanESM2) and the 40-member Community Earth System Model (CESM1), both under the Representative Concentration Pathway 8.5 were used in this work. Monthly precipitation outputs were used to calculate the Standard Precipitation Index (SPI) to quantify meteorological droughts at the global and North American scales for the near- (2036-2065) and far-future (2070-2099) periods. In a second step, the evolution of hydrological droughts over 4521 North American catchments was assessed using the Streamflow Drought Index (SDI). In the last step, the contribution to internal variability of three large-scale climatic indices was studied. The impact of the El Niño Southern Oscillation (ENSO), Pacific Decadal Oscillation (PDO) and Atlantic Multidecadal Oscillation (AMO) on climate anomalies at the catchment scale was studied. The constructive and destructive interactions between those three indices were also studied over the 1961-2010 historical period.

Compared against observations, both ensembles do a reasonable job at replicating patterns of mean annual precipitation and interannual variability over the 1981-2010 reference period. The projected changes in precipitation for both models are consistent with the predicted IPCC trends. Both climate models project increases in extreme meteorological drought frequency over many of the world's regions. The spatial patterns of regions with worsening droughts match those of projected change in mean annual precipitation, although the former is more extensive, indicating that changes in internal variability will increase drought frequency even in some regions projected to see increased mean annual precipitation. The projected increase in meteorological drought frequency is more significant for short-term June-July-August (JJA) droughts and for the larger return periods. Large increases in frequency are observed in many regions, all the way up to 20 times for the 100-year JJA drought indicating a return period shift from 100 to 5 years.

Results show widely different patterns for future changes in extreme hydrological droughts compared to meteorological ones. Hydrological droughts, which combine the effect of precipitation and temperature changes, show a mostly uniform pattern of large to very large increases in drought frequency. This shows that the projected increase in temperature is a main driver of future extreme hydrological droughts, sufficient to overcome the projected increase in mean summer precipitation projected for many North American catchments. Predicted changes for both meteorological and hydrological droughts get consistently worse for the longer considered return periods. In other words, frequency changes for the 100-year droughts are more important than those expected for the 2- and 20-year droughts.

As to the control of large-scale oscillations on climatic anomalies at the catchment scale, it was found that ENSO dominates annual precipitation variability over North America whereas mean annual temperature is mostly influenced by AMO over most of North America. The impact of PDO is comparatively weaker. The dominant roles of ENSO on precipitation and AMO on temperature are preserved but reinforced or diminished by the strong interactions between oscillations. A negative ENSO (La Niña) coupled with a positive AMO brings climate conditions favorable to droughts.

This Thesis illustrates the impact of anthropogenic forcing and internal variability on future drought frequency under changing climate. The results provide much-needed knowledge necessary to better adapt to a changing climate.

Keywords: climate change; climate models; large ensembles; extreme droughts; frequency analysis; large-scale oscillations

TABLE OF CONTENTS

LIST OF TABLES

LIST OF FIGURES

LIST OF ABREVIATIONS

AMO	Atlantic Multidecadal Oscillation
AOGCMs	Atmosphere-Ocean General Circulation Models
BMF	Best monthly fit approach
CanESM2	Second generation Canadian Earth System Model
CanESM2-LE	Canadian Earth System Model large ensemble
CANOPEX	Canadian model parameter experiment
CCMA	Canadian Centre for Climate Modelling and Analysis
CCSM3	Community Climate System Model Version 3
CESM1	Community Earth System Model
CMIP3	Climate Models Intercomparison Project phase 3
CMIP5	Climate Models Intercomparison Project phase 5
CRU	Climatic Research Unit
DBC	Daily bias correction method
DJF	December-January-February
EEMD	Ensemble empirical model decomposition
ENSO	El Niño Southern Oscillation
EOF	Empirical Orthogonal Function
ESM	Earth System Model
FAO	Food and Agriculture Organization

GCM	General circulation model
GEV	General Extreme Value
GGES	Greenhouse gases emission scenario
GIM	Global impact model
GPCC	Global Precipitation Climatology Centre
IPCC	Intergovernmental Panel on Climate Change
JJA	June-July-August
KGE	Kling-Gupta Efficiency
LENS	Large Ensemble Community Project
LME	Last Millennium Ensemble
LOCI	Local intensity scaling
MIROC	Model for Interdisciplinary Research on Climate
NAO	Northern Atlantic Oscillation
NASST	North Atlantic sea surface temperature
NPI	North Pacific Index
NPSST	North Pacific sea surface temperature
NOAA	National Oceanic and Atmospheric Administration
PC	Principal component
PDF	Probability density function
PDO	Pacific Decadal Oscillation

PDSI	Palmer Drought Severity Index
PET	Potential evapotranspiration
PNA	Pacific North American Pattern
RCP	Representative Concentration Pathways
RDI	Reconnaissance Drought Index
SDI	Streamflow Drought Index
SLP	Sea level pressure
SPEI	Standardized Precipitation-Evapotranspiration Index
SPI	Standardized Precipitation Index
SRI	Standardized Runoff Index
SST	Sea surface temperature
TPSST	Tropical Pacific sea surface temperature
USGS	United States Geological Survey
VIC	Variable infiltration capacity hydrology model
WMO	World Meteorological Organization

INTRODUCTION

The increase in greenhouse gases concentration is affecting local climates all over the world. Over the past 20 years, climate change impacts studies have shown this at an ever-increasing rate. The globally averaged combined land and ocean surface temperature has experienced a warming of 0.85°C [0.65 to 1.06°C] over the 1880 to 2012 period. Since 1950, unprecedented changes have been observed, compared to the recent past tens of thousands of years (IPCC, 2013b). The global climate will continue to change over the 21st century and beyond. This warming trend is expected to have many impacts on the earth's environment. With the increasing global mean surface temperature, the onset of spring snowmelt will be earlier than usual, and the frost-free season will be extended. In the meantime, the amount of sea ice has decreased while the mean sea level has steadily increased, threatening the economy and environment of coastal regions (Wuebbles, D., Fahey, D. & Hibbard, K., 2016). It has become clear that the future potential effect of climate change needs to be quantified to make efficient strategic adaptation decisions.

It is now widely accepted and recognized that climate change is likely to have significant impacts on the hydrological cycle, posing a threat to water resources systems throughout the world (Arnell, N. W. & Gosling, S. N., 2016; Haddeland, I., Heinke, J., Biemans, H., Eisner, S., Flörke, M., Hanasaki, N., Konzmann, M., Ludwig, F., Masaki, Y., Schewe, J. et al., 2014; Hegerl, G. C., Black, E., Allan, R. P., Ingram, W. J., Polson, D., Trenberth, K. E., Chadwick, R. S., Arkin, P. A., Sarojini, B. B., Becker, A. et al., 2018). A warming climate will result in the intensification of the hydrological cycle amplifying the difference between dry and wet regions and leading to more extreme precipitation events (Donat, M. G., Lowry, A. L., Alexander, L. V., O'Gorman, P. A. & Maher, N., 2016). High-latitude regions have been shown to be more vulnerable to the changing climate because of the change of surface albedo, an additional mechanism of water vapor transpiration and feedback from the ocean and sea-ice (Barnett, T. P., Adam, J. C. & Lettenmaier, D. P., 2005; Swann, A. L., Fung, I. Y., Levis, S., Bonan, G. B. & Doney, S. C., 2010). The continued warming could drive changes in the seasonality of streamflow, such as earlier spring freshet, reduced summer flows (Bonsal,B.R., P. D. S. F. R. A. & Berg, A., 2019). The impacts of climate change on hydrological regimes vary with regions and time scales, because the temporal and spatial patterns of temperature and precipitation, which are key factors at the regional and local scales, are both affected by climate change. Climate change can also affect water balance by intensifying evapotranspiration, mainly through increasing temperature, change of rainfall patterns and by affecting the fraction of solid/liquid precipitation, and therefore affecting the snowpack storage dynamics (Boyer, C., Chaumont, D., Chartier, I. & Roy, A. G., 2010).

The hydrological response to global warming is expected to result in an increase in the frequency of extreme hydrological events. Changes in extreme events are expected to have more impacts on human safety, infrastructure, agriculture, and natural ecosystems than changes in mean values (Wuebbles *et al.*, 2016). Droughts, for example, are a recurring extreme event that can last several weeks to a few years and are arguably the most severe natural disaster, due to their pronounced societal and economic impacts, especially in semi-arid and arid areas. For example, droughts can lead to reduced crop productivity, diminished water resources, along with an increase in wildfires and poor soil quality. Furthermore, droughts can be a catalyst for water rights conflicts in many countries (Alahdin, S., Ghafouri, H. & Haghighi, A., 2018; Burrows, K. & Kinney, P., 2016).

Droughts always come with below-average precipitation, above-average temperature, low relative humidity and diminished cloud cover over a significant time period (Dai, A., 2011). A drought is a temporary natural phenomenon and is periodic, and can be characterized by its intensity, duration, and probability of occurrence. Droughts are typically classified into four main classes: meteorological droughts, agricultural droughts, hydrological droughts and socio-economic droughts (Dracup, J. A., Lee, K. S. & Paulson Jr, E. G., 1980; Wilhite, D. A. & Glantz,

M. H., 1985). Meteorological droughts are related to an abnormal precipitation deficit, over a given time period. Since all droughts ultimately result from a precipitation deficit, monthly precipitation data has been commonly applied to analyze droughts (Dai, 2011; Marengo, J. A., Tomasella, J., Alves, L. M., Soares, W. R. & Rodriguez, D. A., 2011; Vicente-Serrano, S. M., Beguería, S. & López-Moreno, J. I., 2010). Meteorological droughts impact industrial and domestic water supply as well as agricultural production. Below-average precipitation is not only the primary cause of meteorological droughts, but also a main driver for other types of droughts.

Agricultural droughts are related to low soil moisture conditions that cannot meet the water demand for crop growth. Low soil moisture content restricts crop growth, decreases yields and may ultimately lead to total crop failure. Several drought indices combining temperature, precipitation and soil moisture have been widely applied to study agricultural droughts (Mishra, A. K. & Singh, V. P., 2010). The onset of agricultural droughts may lag that of meteorological droughts, depending on prior surface soil moisture status and the type of precipitation at the end of the meteorological droughts (Heim, J. & Richard, R., 2002).

Hydrological droughts are the results of river streamflows being insufficient to support a water resource management system over a given period (Dai, 2011). Hydrological droughts are always analyzed by using streamflow data (Clausen, B. & Pearson, C., 1995; McCarthy, J. J., Canziani, O. F., Leary, N. A., Dokken, D. J. & White, K. S., 2001; Zelenhasić, E. & Salvai, A., 1987).

Socio-economic droughts are different from the other three types of droughts. Its occurrence is due to the unbalance between the supply and demand of economic goods associated with the weather-related shortage of water supply.

Even though hydrological droughts are always related to meteorological droughts, there can be significant differences in the magnitude and duration of both types of droughts, and the former may persist well past the end of the latter depending on watershed size, usage and non-linear impacts between precipitation and other meteorological variables such as temperature (Heim & Richard, 2002). Meteorological droughts play an important role in subsequent droughts formation and propagation across different droughts types (Potop, V., 2011). The commonly accepted drought types and sequences of droughts are shown in Figure 0.1 (NDMC, 2020; Wilhite, D., 2006).

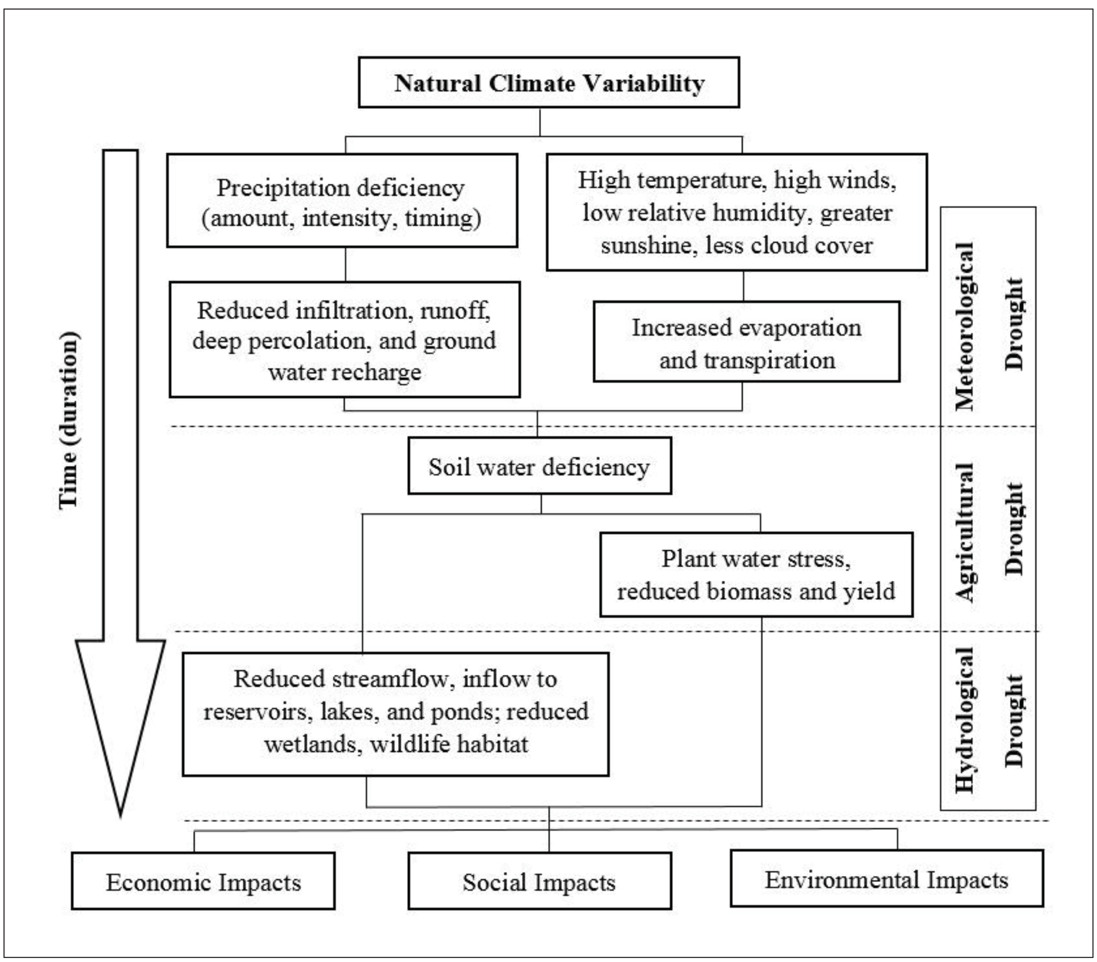

Figure 0.1 Type of droughts and sequence of drought occurrence
Taken from NDMC, 2020

There are many recent examples of severe droughts resulting in significant socio-economic impacts. Droughts are considered among the costliest natural disasters over United States (U.S.) on the sole basis of economic losses (NOAA/NCEI, 2019). The 2015 California droughts, the fourth consecutive year with severe droughts, led to a $2.7 billion total economic impact and 21,000 job losses across the state (Howitt, R., MacEwan, D., Medellín-Azuara, J., Lund, J. R. & Sumner, D., 2015). The duration of droughts in California during 2012 to 2015 period was unprecedented and was estimated as a 10,000-year event (Robeson, S. M., 2015). The exceptional 2017 droughts over the northern High Plains in U.S. caused $2.5 billion of economic losses and also led to an unprecedented wildfire (Wang, H., Schubert, S. D., Koster, R. D. & Chang, Y., 2019a). Droughts that occurred in 2018 in the Southwest U.S. and Southern US Plains affected the growth of field crops, increased cattle feeding costs, and led to $3 billion economic losses (NOAA/NCEI, 2019). Many recurrent major droughts have also affected Canada and particularly in Western Canada. Regions, like British Columbia's interior valley and the Prairies are often affected, because they are on the leeside of large mountain ranges and subject to high precipitation variability (Bonsal, B. R., Wheaton, E. E., Chipanshi, A. C., Lin, C., Sauchyn, D. J. & Wen, L., 2011; Masud, M., Khaliq, N., Wheater, H. & Zilefac, E., 2015). Forest fires linked to an exceptionally dry winter completely destroyed the town of Fort McMurray in May 2016, causing damages nearing $5 billion (McDonald, C., 2016). The provincial government of British Columbia relocated 2800 cattle and paid around $2 million to replace the damaged fencing due to the droughts in 2017 (Cherneski, P., 2018). Eastern North American droughts typically affect smaller areas and have a shorter duration than their Central and Western counterparts, but are nonetheless susceptible to significant economic impacts (Barrie Bonsal,Grace Koshida, E. T. O. E. W., 2004). The Canadian Prairies and northern Central Canada are the two well-defined drought regions with a 8 to 40 months periodicity (Asong, Z. E., Wheater, H. S., Bonsal, B., Razavi, S. & Kurkute, S., 2018).

Rare extreme events tend to cause a disproportionate amount of damage, despite their low probability of occurrence (Leng, G., Tang, Q. & Rayburg, S., 2015; Wuebbles *et al.*, 2016). There are several reasons for this, the most important likely being that adaptation measures that have been put in place to deal with the more frequent events are not sufficient to deal with the rarer ones. However, most of the previous work on droughts under a changing climate has focused on those frequent droughts and comparatively little has been done on changes of rare and very rare droughts.

Potential changes in drought occurrence is an important consequence of climate change. Climate change refers to a change in the state of the climate that can be characterized by changes in its mean and/or variability (IPCC, 2007). Global warming is not only caused by external forcing, but also due to the internal interactions within the chaotic and complex non-linear climate system. There are two main components driving climate change: anthropogenic forcing and natural climate variability (IPCC, 2001). Anthropogenic climate change, also called human-induced climate change, as its name suggests, is the result of the increase in greenhouse gases concentration in the atmosphere, due to human activities. Human influence has been the dominant driver of the observed warming since the mid-twentieth century (IPCC, 2013a; Lins, H. F. & Cohn, T. A., 2011). Human activities alter the energy balance at the Earth's surface and destabilize the climate system. The effects of human-induced climate change are likely to be insidious, with a gradual increase in the number and intensity of many extremes, including floods, droughts, heatwaves and heavy precipitation over a number of decades (IPCC, 2001). Natural (or internal or unforced) climate variability is the manifestation of the chaotic behavior of the climate system. The impact of natural climate variability on global temperature change is weaker than anthropogenic forcing over a long enough period (Martel, J.-L., Mailhot, A., Brissette, F. & Caya, D., 2018). The characteristics of climate variability are easier to capture in regions with low natural variability. At the catchment scale, the impacts of natural variability may be greater even over a multi-decadal time span (Hulme, M., Barrow, E. M., Arnell, N. W., Harrison, P. A., Johns, T. C. & Downing, T. E., 1999). Due to its non-linear nature, the climate system displays a quite large variability at different time scales. The importance of natural climate variability increases with shorter time scales and smaller spatial scales (Matthews, R., Kropff, M., Horie, T. & Bachelet, D., 1997).

There are several natural dynamic processes at the decadal time scale affecting the climate in addition to sources of high-frequency variability. The North Atlantic and Pacific Oceans are the key drivers of the internal multidecadal variability of Northern Hemisphere temperatures. Pacific- and Atlantic-based internal multidecadal variability were found to explain a large proportion of the Northern Hemisphere internal variability of mean annual temperatures (Steinman, B. A., Mann, M. E. & Miller, S. K., 2015). Decadal fluctuations modulate the regional climate and also account for 20-40% of the annual precipitation variance (Cayan, D. R., Dettinger, M. D., Diaz, H. F. & Graham, N. E., 1998; Newman, M., Alexander, M. A., Ault, T. R., Cobb, K. M., Deser, C., Di Lorenzo, E., Mantua, N. J., Miller, A. J., Minobe, S., Nakamura, H. et al., 2016; Valdés-Pineda, R., Cañón, J. & Valdés, J. B., 2018; Yang, Q., Ma, Z., Fan, X., Yang, Z.-L., Xu, Z. & Wu, P., 2017). Natural climate variability may introduce some inherent limitations to climate projection and adaptation guidance in some places, and it is unlikely to be mitigated through model improvement and increasingly certain greenhouse gas trajectories (Deser, C., Knutti, R., Solomon, S. & Phillips, A. S., 2012a). The effect of natural variability could still be larger than the human-induced climate change until the mid-late 21st century over some regions (Dai, A. & Bloecker, C. E., 2019; Martel *et al.*, 2018). Lack of considering the effect of natural climate variability can lead to poor climate projections (He, J., Valeo, C. & Bouchart, F.-C., 2006; Lins & Cohn, 2011). A better understanding of natural climate variability in the present and future climate will help us better understand its contribution to variability and especially how it impacts climate extremes (Pierce, D., Barnett, T., Schneider, N., Saravanan, R., Dommenget, D. & Latif, M., 2001).

This thesis consists of five parts: an introduction, a literature review, the main body of the thesis, a general discussion and a conclusion. The introduction covered the background and main scientific problems. The literature review presents relevant scientific articles published on climate change impacts on droughts and role of natural climate variability. The objectives of the thesis are presented at the end of the literature review. The main body of the thesis consists of three research articles. A general discussion describing the main limitations of this work and presenting recommendations for further work follows. A general conclusion closes this thesis.

Three research articles are presented in Chapters 2, 3 and 4. The frequency change of future extreme meteorological droughts is first assessed at the global scale in Chapter 2. The frequency change of future extreme meteorological and hydrological droughts are then assessed at the watershed scale over 5797 North American catchments in Chapter 3. Finally, in order to better understand the contributions of natural climate variability to North American droughts, the relationship between three large-scale oscillations and climate variability is explored in Chapter 4. The flow chart of this research is presented in Figure 0.2.

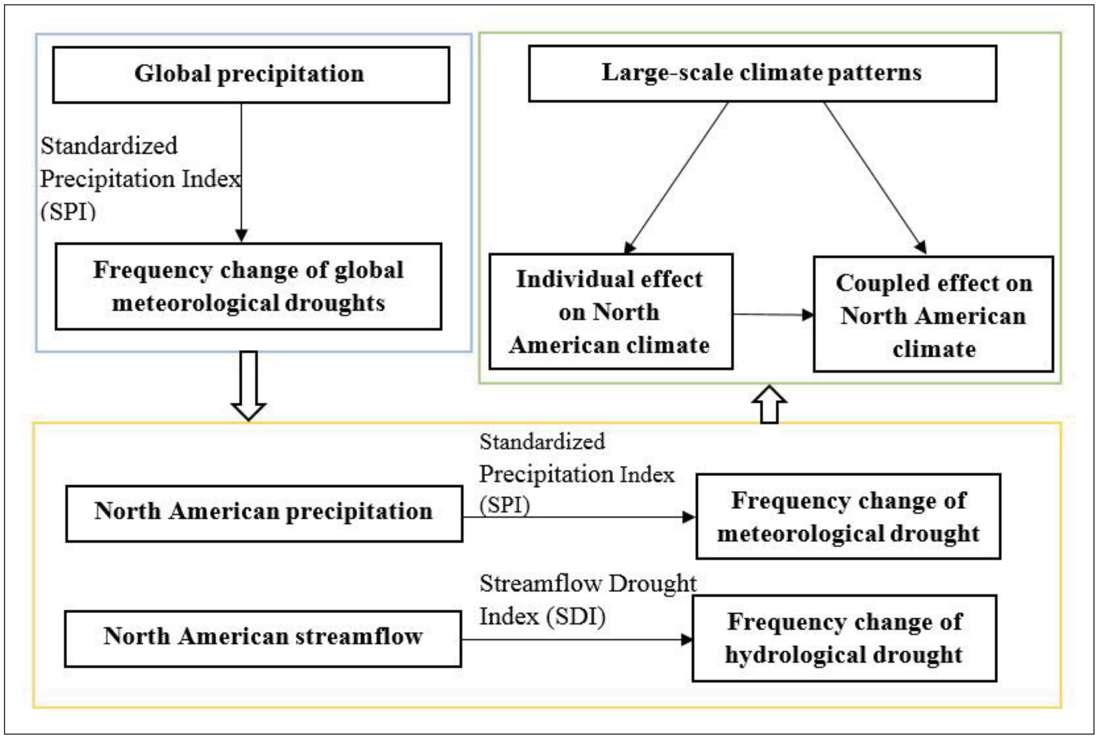

Figure 0.2 Flow chart of this work

LITERATURE REVIEW

This section describes the relevant recent body of work on the impact of climate change and natural climate variability on drought frequency and magnitude.

1.1 Droughts under a changing climate

The most recent Intergovernmental Panel on Climate Change (IPCC) report described an increase in drought frequency and intensity in some parts of the world. Nowadays dry regions are likely to experience increased agricultural droughts by the end of this century under Representative Concentration Pathway (RCP) 8.5 scenario (IPCC, 2013b).

In general, drought assessments are focused on the frequent events and less attention has been paid to their extreme counterpart. Extreme droughts can be defined by their frequency, intensity or duration. The United States Drought Monitor uses a percentile approach to classify the magnitude of droughts into five categories, from abnormally dry to exceptionally dry (Svoboda, M., LeComte, D., Hayes, M., Heim, R., Gleason, K., Angel, J., Rippey, B., Tinker, R., Palecki, M., Stooksbury, D. et al., 2002). This is based on the percentile chance of occurrence in any given year out of 100 years. Extreme droughts are ranked within the fourth class of the drought monitor and are defined as having less than a 5% chance of occurring. The Canadian Drought Monitor classifies droughts into five classes based on the return period, and extreme droughts are characterized with a return period larger than 20 years, which is equivalent to the US definition albeit defined in return period instead of a probability. Extreme droughts can also be defined by their magnitude. For example, in some studies, extreme droughts are identified when the Standardized Precipitation Index (SPI) is less than -2.0 (Livada, I. & Assimakopoulos, V., 2007; Lloyd-Hughes, B. & Saunders, M. A., 2002; Zhang, Q., Li, J., Singh, V. P. & Bai, Y., 2012). This threshold could be interpreted as an extreme event that occurs two or three times in a 100-year period (Hayes, M. J., Svoboda, M. D., Wiihite, D. A. & Vanyarkho, O. V., 1999). Extreme droughts can also be defined by their duration. For example, megadroughts are prolonged droughts lasting a decade or even longer.

1.1.1 Climate change impacts on meteorological droughts

Many researches have looked at the changes in droughts from a purely meteorological perspective. Meteorological droughts express the precipitation's departure from normal over some period of time (Wilhite & Glantz, 1985). Relative to current conditions, at the global scale, the frequency and duration of many droughts are expected to increase by the second half of the 21st century (Burke, E. J., Brown, S. J. & Christidis, N., 2006; Sheffield, J. & Wood, E. F., 2008). Zarch, M. A. A., Sivakumar, B. & Sharma, A. (2015) assessed the global annual meteorological droughts in a warming climate for the periods 1850-2005 and 2006-2100 based on the CSIRO Mk 3.6 climate model under the RCP8.5 scenario. The results showed that the tropical and subtropical regions would turn drier while the droughts over the middle to high latitudes would see a downward trend in the future. Touma, D., Ashfaq, M., Nayak, M. A., Kao, S.-C. & Diffenbaugh, N. S. (2015) analyzed the global meteorological drought characteristics of 15 general circulation models (GCM) from the Coupled Model Intercomparison Project Phase 5 (CMIP5, Taylor, K. E., Stouffer, R. J. & Meehl, G. A., 2012) in the early (2010-2054) and late (2055-2099) 21st century under RCP8.5 relative to the 1961-2005 baseline period. They found no noticeable changes in the spatial extent of 6-month exceptional meteorological droughts in nearly all regions, with the exception of the Mediterranean, Southern South America, and Central America in the future periods. In the latter half of the 21st century, the number of drought events and their duration were found to increase, with the exception of some high-latitude regions (e.g., Alaska, Greenland).

Some studies about meteorological droughts in a changing climate were conducted at the regional scale. Sushama, L., Khaliq, N. & Laprise, R. (2010) studied dry spell characteristics across Canada, over three time periods (1971-2000, 2041-2070, and 2071-2100) using a regional climate model. Results showed an increase in the mean number of dry days in southern Canada, and a decrease over the rest of Canada. Penalba, O. C. & Rivera, J. A. (2016) assessed the change of future meteorological droughts based on 15 GCMs from CMIP5 under RCP4.5 and RCP8.5 scenarios for the 2011-2040 and 2071-2100 periods over Southern South America. A large increase in the number of events and a decrease in the mean duration were found in both 3-month and 12-month meteorological droughts. Tam, B. Y., Szeto, K., Bonsal, B., Flato, G., Cannon, A. J. & Rong, R. (2018) studied future meteorological droughts over Canada using 29 GCMs under three emission scenarios. The results showed that drought frequency would increase in Southwestern Canada and the Prairies in the latter half of the 21st century, largely due to a larger interannual variability of precipitation and temperature.

A comparatively much smaller number of researches have focused on extreme meteorological droughts and over the historical period. Livada & Assimakopoulos (2007) found that the frequency of extreme 12-month meteorological droughts (defined as having a SPI inferior to -2) was very low over the whole of Greece during the 1950-2000 period. The same definition of extreme droughts was also adopted by Ayala, J. J. H. & Heslar, M. (2019) to identify the seasonal extreme meteorological drought events in the Caribbeans for the 1981-2018 period.

1.1.2 Climate change impacts on agricultural droughts

Agricultural droughts are usually expressed in terms of needed soil moisture of a particular crop over a particular time period (Hisdal, H. & Tallaksen, L., 2000; Wilhite & Glantz, 1985). Sheffield & Wood (2008) used soil moisture data from eight Atmosphere-Ocean General Circulation Models (AOGCMs) under SRES B1, A1B and A2 emission scenarios to analyze changes in agricultural droughts occurrence. The results showed that the AOGCMs could represent the occurrence of large-scale agricultural droughts very well, although long-term droughts (duration exceeding 12 months) were overestimated. By the end of the 21st century, the frequency of short-term droughts (4-6 months duration) would experience a two-fold increase while long-term droughts would be three times more common when compared to the pre-industrial control period. Leng *et al.* (2015) used the soil moisture data generated by the Variable Infiltration Capacity (VIC) hydrological model forced by five climate models under RCP8.5 scenario to assess the severity, duration and frequency of future agricultural droughts in China. Results showed that China would experience more frequent droughts over the 2020-2049 period (1.5 times more frequent on average) relative to the 1971-2000 period, with the exception of parts of northern and northeastern China. Drought duration was predicted to become longer, compared to the same reference horizon. Results indicated that agricultural droughts would experience the largest changes compared to their meteorological and hydrological counterparts. In addition, long-term droughts (duration longer than 4 months) would experience larger frequency increases than for short-term ones (duration shorter than 4 months).

Various criteria have been used in the literature to study extreme agricultural droughts. Yu, C., Huang, X., Chen, H., Huang, G., Ni, S., Wright, J. S., Hall, J., Ciais, P., Zhang, J., Xiao, Y. et al. (2018) assessed the impacts of extreme agricultural droughts in China based on nine GCMs under three RCPs (2.6, 4.5 and 8.5) during the past (1955-2014) and future (2006-2100) periods. The frequency of agricultural droughts was estimated by using historical yield loss data fitted with a General Extreme Value (GEV) distribution. Future frequency of agricultural droughts was projected to increase under all examined RCPs. The current 100-year drought is expected to become a 30-year drought under RCP2.6, 13-year under RCP4.5 and 5-year under RCP8.5. Grillakis, M. G. (2019) assessed the severe and extreme 7-month agricultural droughts based on the Joint UK Land Environment Simulator simulations forced by four CMIP5 GCMs under the RCP2.6 and RCP6.0 scenarios for near- (2020-2059) and far-future (2060-2099) periods. Severe and extreme droughts were defined by a Soil Moisture Index inferior to -3. They projected an increasing trend in European extreme agricultural droughts. The frequency of future agricultural droughts was expected to increase from 11 to 28 times depending on the emission scenarios and analysis periods compared to the historical 1961-2005 period.

1.1.3 Climate change impacts on hydrological droughts

Hydrological droughts are usually expressed by the deficiencies in surface and subsurface water supplies (Hisdal & Tallaksen, 2000; Wilhite & Glantz, 1985). Hydrological droughts are more complex since in addition to precipitation deficit, they result from the combination of several hydroclimatic variables, such as cloud cover, humidity, and temperature which all impact evapotranspiration. Lehner, B., Döll, P., Alcamo, J., Henrichs, T. & Kaspar, F. (2006) explored an integrated global water model (Water-Global Assessment and Prognosis) with two GCMs (ECHAM4 and HadCM3) to compute time series of river flows. The results showed that southern and southeastern Europe would experience significant increases in hydrological drought frequencies. The 100-year drought would be 2 to 10 times more frequent by the end of the century, compared to the 1901-1995 historical period. Hirabayashi, Y., Kanae, S., Emori, S., Oki, T. & Kimoto, M. (2008) used daily runoff simulated by the MIROC GCM to project future hydrological droughts under the SRES A1B scenario. Results showed that future hydrological drought frequency was mostly expected to increase globally over the 2071-2100 period although northern high latitudes, eastern Australia, and eastern Eurasia showed a small decrease or no change. Prudhomme, C., Giuntoli, I., Robinson, E. L., Clark, D. B., Arnell, N. W., Dankers, R., Fekete, B. M., Franssen, W., Gerten, D., Gosling, S. N. et al. (2014) used seven global impact models (GIM) and five GCMs under four RCPs to study hydrological droughts in projected future climates. They predicted a likely increase in the severity of hydrological droughts (measured by Global Deficit Index) at the global scale by the end of the 21st century (2070-2099). Wanders, N., Wada, Y. & Van Lanen, H. (2015) applied a global hydrological model (PCR-GLOBEWB) forced by five GCMs under four RCPs to simulate global daily streamflows at a 0.5 grid resolution from 1971 to 2099. Droughts in this study were defined by conventional (based on a static reference period) and transient (based on the previous 30 years) thresholds respectively. Results showed that roughly half of all land areas would experience a negative trend of future low flows. Drought duration was projected to increase in 27% of global land area. Leng *et al.* (2015) fed the VIC hydrological model with bias-corrected climate outputs from five GCMs under the RCP8.5 to project the changes of future hydrological droughts in China. Results showed that the intensity of severe hydrological droughts over the 2020-2049 period would be three times larger than over the 1971-2000 reference period.

A few researches specifically looked at the impact of climate change on extreme hydrological droughts. Huang, S., Krysanova, V. & Hattermann, F. (2015b) used sixteen regional climate change simulations to project future floods and droughts in Germany. They found that in the Rhine basin, the current 50-year extreme hydrological droughts would be twice as frequent in the future 2061-2100 period. Roudier, P., Andersson, J. C., Donnelly, C., Feyen, L., Greuell, W. & Ludwig, F. (2016) used eleven bias-corrected climate model outputs from the CMIP5 ensemble and three hydrological models to study the impacts of a 2°C temperature increase on hydrological droughts in Europe. Extreme droughts in this study were defined as those with 10-year and 100-year return periods. Results showed that the magnitude of extreme hydrological droughts would increase compare with the 1971-2000 baseline period, especially in southern France, parts of Spain, Portugal and Greece.

1.1.4 Uncertainty in future drought assessment

Several sources of uncertainties are typically found in drought assessment studies, similar to those existing in hydrological impacts studies. The uncertainties are likely to come from the climate models, downscaling methods, natural climate variability, emission scenarios, impact models, and the selection of drought indices (Chen, J., Brissette, F. P., Poulin, A. & Leconte, R., 2011b; Clark, M. P., Wilby, R. L., Gutmann, E. D., Vano, J. A., Gangopadhyay, S., Wood, A. W., Fowler, H. J., Prudhomme, C., Arnold, J. R. & Brekke, L. D., 2016; Dai, A. & Zhao, T., 2017; Troin, M., Arsenault, R., Martel, J.-L. & Brissette, F., 2018; Zhao, T. & Dai, A., 2017). The exception is that the uncertainty originating from downscaling methods or impact models (e.g., hydrological model) typically does not exist for meteorological droughts. Therefore, the sources of uncertainty depend on the type of droughts considered.

Burke, E. J. & Brown, S. J. (2008) explored the uncertainties in the parameter space of the HadCM3 climate model and inter-model uncertainty in a multimodel ensemble, respectively, using four drought indices and two greenhouse gases emission scenarios (GGES). Results showed that the selection of drought indices introduces significant uncertainties in the drought impact studies, affecting the magnitude of droughts. Different indices consider different processes (e.g., water input, water demand) thus affecting the quantification of droughts. Those indices that take atmospheric demand for moisture into consideration will lead to more severe future drought conditions (Spinoni, J., Barbosa, P., De Jager, A., McCormick, N., Naumann, G., Vogt, J. V., Magni, D., Masante, D. & Mazzeschi, M., 2019). Chen, J., Brissette, F. P. & Leconte, R. (2011a) explored the uncertainty introduced by different downscaling methods in the quantification of the impacts of climate change on hydrology. Results showed that the uncertainty envelope produced by downscaling methods is large, and, in some cases, similar to that produced by climate models. Climate scenarios issued from different downscaling methods would therefore translate to additional uncertainty of simulated discharge. Chen *et al.* (2011b) studied the relative uncertainty of all components of the hydroclimatic modeling chain of a hydrological impact study. Two GGES, six GCMs, five GCM initial conditions, four downscaling methods, three hydrological model structures, and ten sets of hydrological model parameters were considered. They found that the largest uncertainty comes from GCMs, followed by downscaling methods, natural climate variability, GGES and hydrological model structure. The hydrological model parameter sets play the least important role in the uncertainty envelope. Orlowsky, B. & Seneviratne, S. I. (2013) separated the different sources of uncertainty in projections of meteorological and hydrological droughts. They found that internal climate variability was the main source of uncertainty for the near future while GCMs became the dominant source of uncertainty by the end of the 21st century. Prudhomme *et al.* (2014) explored the uncertainty related to hydrological drought studies by using bias-corrected outputs from three GCMs, seven GIMs and four RCPs. They found that the uncertainty from the GIMs is greater than that from GCMs. Diverse GIMs should therefore be considered to better capture the uncertainties. Zhao & Dai (2017) assessed the agricultural droughts simulated from CMIP3 and CMIP5 climate model outputs during historical and future periods. A large uncertainty was found to result from the internal climate variability at the regional scale. In a companion paper (Dai & Zhao, 2017), they also found that the choice of meteorological forcing datasets (e.g., precipitation) and chosen calibration period for the definition of drought indices also contribute to significant uncertainties in estimating historical drying trends. Troin *et al.* (2018) generated a 105-member ensemble by combining seven snow models, five potential evapotranspiration (PET) calculation methods, and three hydrological model structures to assess structural uncertainty over two snowmelt-dominated watersheds in Canada. The uncertainty introduced by natural climate variability was also evaluated in their study. Results showed that the largest source of uncertainty comes from hydrological model components, followed by PET and natural variability. Snow models only make a very small contribution to the uncertainty envelope. There are numerous different formulas used to calculate PET based on different climatic variables (temperature-based, radiation-based and physically based), thus bringing large uncertainties to the drought assessment studies, especially in semi-arid and arid regions (Dai & Zhao, 2017; Kay, A. & Davies, H., 2008).

1.2 The impact of natural variability

1.2.1 The impact of natural variability on climate change

The climate is affected by sea surface temperature anomalies resulting from the normal thermohaline ocean circulation. This variability is represented at many time scales, from the seasonal to the multi-decadal scales. The representation of sea surface temperature (SST) anomalies is typically characterized by the computation of large-scale oscillations. Many such oscillations affecting the North American climate have been described in the literature, the most important being the El Niño-Southern Oscillation (ENSO), the Pacific North American pattern (PNA), the North Atlantic Oscillation (NAO), the Pacific Decadal Oscillation (PDO) and the Atlantic Multi-decadal Oscillation (AMO) (Barlow, M., Nigam, S. & Berbery, E. H., 2001; Cayan, D. R., Redmond, K. T. & Riddle, L. G., 1999; Déry, S. J. & Wood, E. F., 2004; Enfield, D. B., Mestas-Nuñez, A. M. & Trimble, P. J., 2001; Rogers, J. C. & Coleman, J. S., 2003; Stewart, I. T., Cayan, D. R. & Dettinger, M. D., 2005). It is generally acknowledged that El Niño has the strongest impact and leads to reduced precipitation in the Midwest, increased precipitation and higher streamflow in the Gulf of Mexico region in the U.S. (Kurtzman, D. & Scanlon, B. R., 2007; Schmidt, N., Lipp, E., Rose, J. & Luther, M., 2001; Trenberth, K. E. & Guillemot, C. J., 1996). The PDO is the dominant pattern of Northern Pacific Decadal Variability (Mantua, N. J., Hare, S. R., Zhang, Y., Wallace, J. M. & Francis, R. C., 1997). The impacts of PDO on winter precipitation are however mostly significant only in the southern Central United States (Trenberth & Guillemot, 1996). The AMO is known to have an influence on precipitation in North America (Enfield *et al.*, 2001; McCabe, G. J., Palecki, M. A. & Betancourt, J. L., 2004). The correlation between precipitation and AMO is mostly negative in the Southeast U.S. (Enfield *et al.*, 2001; Maleski, J. J. & Martinez, C. J., 2018).

The coupled effect of dominant oscillations on hydroclimatic variability has also been studied. Precipitation in North America is affected by both ENSO and AMO and interactions between the two are likely. For example, a negative AMO could help increase the correlation between ENSO and precipitation in the Southeast (Enfield *et al.*, 2001). The interaction between the North Pacific Index (NPI, area-weighted sea level pressure over the region 30°N-65°S, 160°E-140°W) and ENSO results in a larger amplitude of surface temperature anomalies over North America when they are out of phase compared to their in-phase combinations (Yu, B., Shabbar, A. & Zwiers, F., 2007). In addition, ENSO phases tend to be stronger and more stable during a positive PDO (Yu *et al.*, 2007). The combination of these two modes of variability has implications for future climate projections over North America (Gershunov, A. & Barnett, T. P., 1998; Mantua *et al.*, 1997). When PDO and ENSO are in phase, typical ENSO conditions are in effect over the U.S., whereas the signal is less clear for out of phase or neutral conditions (Dai, A., 2013b; Kurtzman & Scanlon, 2007). El Niño coupled with positive PDO or AMO would lead to below-normal precipitation, whereas the impact of La Niña on temperature and precipitation (increased temperature and decreased precipitation) is significantly increased during positive AMO and PDO phases in the Southeast U.S. (Maleski & Martinez, 2018).

Different methods have been applied to study the coupled effects of climatic indices. Kurtzman & Scanlon (2007) used a statistical descriptive analysis of ENSO and PDO impacts on winter precipitation throughout the entire Southern U.S. The relationship between precipitation, temperature and ENSO, NAO, AMO and PDO was evaluated using a canonical correlation analysis (Stevens, K., 2008). Nonparametric ranks-sum tests were used to learn about the individual and coupled effects of ENSO, AMO and PDO on temperature, precipitation (Maleski & Martinez, 2018) and streamflow (Johnson, N. T., Martinez, C. J., Kiker, G. A. & Leitman, S., 2013) over Southeast U.S. river basins during the 1895-2009 period. Results showed that the AMO has a significant effect on the precipitation and temperature. The effect of ENSO on precipitation would be intensified when PDO and AMO are in their positive phases.

Some researches have linked changes in drought frequency to the variance of oscillations directly, because precipitation deficit is usually related to the anomalous atmospheric circulation caused by persistent sea surface temperature anomalies in the Pacific and Atlantic Oceans (Dai, A., Zhao, T. & Chen, J., 2018; Hoerling, M., Eischeid, J., Kumar, A., Leung, R., Mariotti, A., Mo, K., Schubert, S. & Seager, R., 2014; Liu, Z., 2012). More frequent droughts were recorded in Southern Europe when NAO was in its positive phase. When NAO went to its negative phase, drought conditions were relieved (López-Moreno, J. I. & Vicente-Serrano, S. M., 2008; Trigo, R. M., Osborn, T. J. & Corte-Real, J. M., 2002). Santos, J. F., Pulido-Calvo, I. & Portela, M. M. (2010) extracted monthly precipitation over the 1910 to 2004 period to study the spatial and temporal variability of droughts in Portugal. The results showed that NAO had an immediate and significant influence on drought patterns, especially in the south where drought conditions had a 3 to 4-year periodicity. Espinoza, J. C., Ronchail, J., Guyot, J. L., Junquas, C., Vauchel, P., Lavado, W., Drapeau, G. & Pombosa, R. (2011) found that precipitation deficit and very low flow in the western Amazon basin were associated with positive SST anomalies in the tropical North Atlantic (Marengo, J. A. & Espinoza, J., 2016). Furthermore, Jiménez-Muñoz, J. C., Mattar, C., Barichivich, J., Santamaría-Artigas, A., Takahashi, K., Malhi, Y., Sobrino, J. A. & Van Der Schrier, G. (2016) found that extreme droughts in Amazonia in 2015-2016 was associated with ENSO. The most severe Iranian droughts occurred between 1998 and 2001 and coincided with a prolonged La Niña (Golian, S., Mazdiyasni, O. & AghaKouchak, A., 2015). Dai & Zhao (2017) found that regional drying trends are related to multi-decadal oscillations in Pacific SSTs. Rojas, O. (2018) found that agricultural droughts are often associated with ENSO at the global level. Jiang, P., Yu, Z. & Acharya, K. (2019) explored the connections between leading drought indicators and large-scale oceanic oscillations in the Western U.S. over the 2003-2016 period. They showed that the spatial pattern of winter droughts was related to ENSO, PDO and AMO, while PDO controlled the spatial pattern of summer droughts. ENSO was also found to be the main large-scale driver for hydrological droughts over many regions, while the Ocean Indian Dipole and NAO were also found to have regional influences (Forootan, E., Khaki, M., Schumacher, M., Wulfmeyer, V., Mehrnegar, N., van Dijk, A., Brocca, L., Farzaneh, S., Akinluyi, F., Ramillien, G. et al., 2019).

1.2.2 Methods for studying natural climate variability

We can study natural climate variability by either looking at the historical record or by using climate models.

A long historical record documents the evolution of the past climate and can reveal important modes of natural climate variability. Long historical records can be analyzed by looking at the main frequency of modes of variability, using a spectrum of wavelet analysis (Torrence, C. & Compo, G. P., 1998). Alternatively, the historical records can be divided into several time slices, with natural climate variability accounting for differences between the different periods. In the latter approach, detrending may be needed to remove the impact of anthropogenic forcing. However, many countries or regions lack long-enough observational records to enable researchers to bring to light the impact of natural climate variability. Paleoclimatic studies may provide long proxy records useful to study multidecadal variability, but the proxies (e.g., tree rings, ice cores) are often only imperfectly related to the physical process under study (e.g., droughts), and may not be adequate to study the impacts at shorter time scales.

Climate model outputs can also be used to study natural variability but most simulations also cover relatively short periods for the historical past, and suffer from a strong anthropogenic forcing component in future periods. Alternatively, natural climate variability can also be studied by using a multi-member ensemble originating from a single climate model. Such ensembles consist of multiple climate projections from the same climate model under the same forcing, using only slightly different initial conditions. Also known as large ensembles, these simulations provide a unique opportunity to investigate questions related to the linearity of an externally forced signal and how the characteristics of the internal variability of the coupled system may be changing in a warmer climate (Hu, Z.-Z., Kumar, A., Jha, B. & Huang, B., 2012). Large ensembles allow for the study of natural climate variability and enable researchers to study the relationship between natural climate variability and anthropogenic climate change. Such ensembles are now more widely used to learn about natural climate variability and its impact on the climate (von Trentini, F., Schmid, J., Wood, R., Willkofer, F., Leduc, M., Frigon,

A. & Ludwig, R., 2018). In her seminal paper, Deser *et al.* (2012a) studied the range of internal climate variability over North America using a 40-member ensemble from the Community Climate System Model Version 3 (CCSM3) forced by the A1B emission scenario over the 2000-2060 period. von Trentini *et al.* (2018) compared the natural variability of the 50-member ensemble from the second generation Canadian Earth System Model (CanESM2) under the RCP8.5 scenario against that of EURO-CORDEX models. They found that natural variability plays an important role in climate projections, and that the variability within a multi-model ensemble is significantly larger than that in the multi-member ensemble from CanESM2. Chen, J. & Brissette, F. P. (2018) assessed the reliability of multi-member ensembles at estimating internal variability, by comparing it to CRU data over the historical period. They found that multi-member ensembles represent multi-decadal natural variability well, at both the global and regional scales.

1.3 Summary and work objectives

Severe drouhts are the greatest recurring natural disaster (Cook, E. R., Seager, R., Cane, M. A. & Stahle, D. W., 2007). Large drying trends have been observed over many low-latitude regions since the 1950s (Dai, 2011), and most land areas are projected to experience increasing droughts by the end of the 21st century (Dai, A., 2013a; Dai *et al.*, 2018; Sheffield & Wood, 2008). However, most previous drought assessment studies have been confined to relatively small areas (Lehner *et al.*, 2006). Drought studies over North America have mostly been concentrated on the southern Canadian Prairies, western and southeastern U.S. (Barrie Bonsal, 2004; Gan, T. Y., 2000; Miskus, D., 2017; Quiring, S. M. & Papakryiakou, T. N., 2003). Little attention has been paid to the evolution of extreme droughts. Extreme droughts are of particular concern since they carry a disproportionate part of economic losses associated to droughts.

Regional drying patterns associated with precipitation change in North America are thought to be related to multi-decadal oscillations in Pacific SSTs (Dai & Zhao, 2017). Accordingly, the impact of natural climate variability on droughts is also an important study area. As of now, despite a large number of studies on droughts, there are comparatively much fewer studies that have looked at the impact of both climate change and natural variability on extreme droughts.

The primary goal of this Thesis is therefore to explore the impact of climate change on future extreme droughts at the global scale, but also with an emphasis over North America. This work is especially concerned with extreme droughts, defined in this work as having a return period larger than 20 years. The specific objectives of this thesis are therefore to:

1) assess the impacts of climate change on meteorological droughts at the global scale;

2) assess the impacts of climate change on hydrological droughts over a large number of North American watersheds;

3) explore the relationship between large-scale oscillations and climate variability over North America.

A better understanding of droughts in a changing climate is required to implement successful adaptation strategies and/or mitigate future impacts.

CHAPTER 2

PROJECTION OF FUTURE EXTREME METEOROLOGICAL DROUGHTS USING TWO LARGE MULTI-MEMBER CLIMATE MODEL ENSEMBLES

Cha Zhao[1], François Brissette[1], Jie Chen[2]

[1] Department of Construction Engineering, École de Technologie Supérieure,
1100 Notre-Dame West, Montreal, Quebec, Canada H3C 1K3
[2] State Key Laboratory of Water Resources & Hydropower Engineering Science,
Wuhan University,
299 Bayi Road, Wuchang Distinct, Wuhan, Hubei, China 430072

Paper submitted for publication, April 2019

2.1 Abstract

Several studies have looked at the evolution of droughts in a changing climate in various locations and have typically found that droughts are expected to become more severe in the future. However, relatively little work has been done on extreme droughts. This study focuses on the evolution of extreme meteorological droughts over near- (2036-2065) and far- (2071-2100) future time periods. Monthly precipitation from two large multi-member climate model ensembles: the 50-member Canadian Earth System Model (CanESM2) and the 40-member Community Earth System Model (CESM1), was used to calculate the Standard Precipitation Index (SPI) to quantify and explore the evolution of future meteorological droughts. The use of these large ensembles allows for the very precise calculation of the 20- and 100-year droughts return period, and offer a unique perspective into those rare events.

Both climate models project increases in extreme meteorological drought frequency over many of the world's regions. South America, Oceania and the Mediterranean basin are predicted by both models to be the most affected regions. The spatial patterns of regions with worsening meteorological droughts generally match those of projected change in mean annual precipitation, although the former is more extensive, indicating that changes in internal variability will increase drought frequency even in some regions projected to see increasing mean annual precipitation. The projected increase in meteorological drought frequency is more important for short-term June-July-August (JJA) droughts, and for the larger return periods. Larger increases in frequency are observed in many regions, all the way up to 20 times for the 100-year JJA drought indicating a return period shift from 100 to 5 years.

Keywords: climate change; extreme meteorological droughts; Standardized Precipitation Index; large ensemble

2.2 Introduction

It is now widely accepted and recognized that climate change will have significant impacts on the hydrologic cycle (Arnell & Gosling, 2016; Feng, D., Beighley, E., Raoufi, R., Melack, J., Zhao, Y., Iacobellis, S. & Cayan, D., 2019; Hegerl *et al.*, 2018; Mukherjee, S., Mishra, A. & Trenberth, K. E., 2018; Trenberth, K. E., Dai, A., Van Der Schrier, G., Jones, P. D., Barichivich, J., Briffa, K. R. & Sheffield, J., 2014). Climate change will affect the distribution and frequency of precipitation events (Mauger, G., Casola, J., Morgan, H., Strauch, R., Jones, B., Curry, B., Busch Isaksen, T., Whitely Binder, L., Krosby, M. & Snover, A., 2005). At one end of the spectrum, changes in extreme precipitation frequency are expected to result in ever increasing damages to infrastructures and to affect populations in most parts of the world (Mailhot, A. & Duchesne, S., 2009; Rosenberg, E. A., Keys, P. W., Booth, D. B., Hartley, D., Burkey, J., Steinemann, A. C. & Lettenmaier, D. P., 2010; Wilhelmi, O. V. & Morss, R. E., 2013). However, at the other end of the spectrum, lack of precipitation is also a critical issue in many regions of the world.

Droughts are recurring extreme events which can last from a few days to a few years and arguably constitute the most severe natural disaster, due to their pronounced socio-economic impacts, especially in semi-arid and arid areas. They are typically classified into four main classes: meteorological droughts, hydrological droughts, agricultural droughts and socio-economic droughts (Dracup *et al.*, 1980; Wilhite & Glantz, 1985).

Protection from droughts is complex and substantial structural adaptation measures are typically required. In this context, a better understanding of the potential impacts of climate change on drought is essential to any drought mitigation strategy. Many studies have shown an increasing drought risk over the 21st century (e.g., Burke & Brown, 2008; Cook, B. I., Ault, T. R. & Smerdon, J. E., 2015; Dai, 2011; Grillakis, 2019; Sheffield & Wood, 2008; Teuling, A. J., 2018; Zhao, P., Lü, H., Yang, H., Wang, W. & Fu, G., 2019). Most of these studies concluded that more regions would experience more severe and long-duration droughts, especially in the summer. With temperature increases predicted by all climate projections, water demand is expected to exceed water supply in many regions of the world and to lead to more severe water deficit and droughts afterward. Dai (2011) assessed changes in droughts by calculating the Palmer Drought Severity Index (PDSI) using the CMIP3 (Meehl, G. A., Covey, C., Delworth, T., Latif, M., McAvaney, B., Mitchell, J. F., Stouffer, R. J. & Taylor, K. E., 2007) multi-model ensemble mean monthly climate data, and found that severe droughts ($-3.99 \leq PDSI \leq -3.00$) would likely occur in the latter half of this century over most continents. This assessment was confirmed for the United States by Cook *et al.* (2015). Zarch *et al.* (2015) assessed global droughts in a warming climate with and without considering the impact of PET, using the Standardized Precipitation Index (SPI) and Reconnaissance Drought Index (RDI), respectively. Both indices were calculated based on the CSIRO Mark 3.6 climate model simulation for the 1850-2005 and 2006-2100 periods. The results point to more severe droughts by the end of this century. The areal extent of droughts would increase with global warming and the most affected regions would mostly be in the low- to mid-latitude regions.

However, most of the previous work has focused on frequent droughts and comparatively little has been done on changes in rare and very large droughts. As is the case for most types of extremes events, the consequences of such events do not scale linearly with their probability of occurrence. In other words, rare extremes events (defined here as having a return period $T \geqslant 20$ years) cause a disproportionate amount of damages, despite their low probability of occurrence. There are several reasons for this, the most important likely being that adaptation measures that have been put in place to deal with the more frequent extreme events are not sufficient to deal with the rare ones. Since meteorological droughts are the primary driver of subsequent formation and propagation across different droughts types (Potop, 2011). This work therefore focuses specifically on extreme meteorological droughts ($T \geqslant 20$ years) and contrast future frequency changes in extreme droughts against those in average droughts.

The rest of this paper is organized as follows. Section 2.3 and 2.4 describes the different datasets and the methodology used in this study. Results are shown in section 2.5. A discussion and a conclusion follow in section 2.6.

2.3 Data

Daily precipitation data from two Earth System Model (ESM) large ensembles were selected to analyze extreme meteorological droughts over the historical (1981-2010), near- (2036-2065) and far- (2071-2100) future periods. The Canadian Earth System Model (CanESM2) large ensemble (spatial resolution of $2.8^\circ \times 2.8^\circ$) covers the 1950-2100 period. To produce the 50-member ensemble, 5 simulations of the ocean state were performed over 1850 to 1950, from which 10 runs with small random atmospheric perturbations were initialized over the remaining 1950-2100 period. From 2006 on, the representative concentration pathway (RCP8.5) was used as the forcing scenario (Arora, V., Scinocca, J., Boer, G., Christian, J., Denman, K., Flato, G., Kharin, V., Lee, W. & Merryfield, W., 2011; Sigmond, M. & Fyfe, J. C., 2016; von Salzen, K., Scinocca, J. F., McFarlane, N. A., Li, J., Cole, J. N., Plummer, D., Verseghy, D., Reader, M. C., Ma, X., Lazare, M. et al., 2013). This large ensemble results in 1500 equivalent years (30 years $\times$ 50 members) for each period considered. The Community Earth System Model (CESM1) is a coupled climate model for simulating Earth's climate system (spatial resolution of $1^\circ \times 1^\circ$), which covers the 1920-2100 period. The CESM1 large ensemble has 40 members, each obtained from random atmospheric perturbations (Kay, J., Deser, C., Phillips, A., Mai, A., Hannay, C., Strand, G., Arblaster, J., Bates, S., Danabasoglu, G., Edwards, J. et al., 2015). This results in 1200 equivalent years for each considered period (30 years$\times$ 40 members). Considering the large computational cost of running these large ensembles, both ensembles are only available for the RCP8.5 scenario. At the time of conducting this work, these were the only two global large ensembles readily available to the scientific community.

Since this is a study solely based on climate models, some level of validation against observation is therefore necessary. Although many climate change studies are only concerned with climate model data, it is nonetheless always preferable to validate some climate characteristics relevant to a specific study. This is especially the case when a small number of climate models are used, as is the case in the present study. Since droughts originate from temporal variability in precipitation fields, there is also a need to validate some measure of variability in the models. To this end, mean annual and inter-annual standard deviation of total annual and seasonal precipitation were chosen as validation metrics. The metrics were calculated for all climate model members and each grid point. The 0.5°, 2018 monthly version from Global Precipitation Climatology Centre (GPCC) was used as the reference dataset. This dataset covers the period 1891-2016 over land areas (Schneider, U., Becker, A., Finger, P., Meyer-Christoffer, A. & Ziese, M., 2018). The GPCC dataset was first upscaled to the respective resolution of both climate models (1° and 2.8° respectively) prior to computing the differences between metrics.

2.4 Methodology

There are several potential indices that can be used to quantify droughts (Dai, 2011). In this study on extreme meteorological droughts, SPI was chosen because of its simplicity and widespread use. It is also recommended by World Meteorological Organization (WMO) as the main meteorological drought index. The SPI is a dimensionless indicator, which represents the precipitation deficit (or excess) relative to a long-term mean at a given location and time scale (McKee, T. B., 1995; McKee, T. B., Doesken, N. J., Kleist, J. et al., 1993). The SPI is normalized by its mean and standard deviation, typically after fitting a 2-parameter gamma distribution to monthly precipitation values, followed by a transformation to a Gaussian distribution (Guttman, N. B., 1999). Positive SPI values indicate precipitation above average, while negative values are representative of a rainfall deficit over a given time duration. The SPI has been widely used to quantify meteorological droughts over different time scales, typically ranging from 1 month to 24 months (Hayes, M., Svoboda, M., Wall, N. & Widhalm, M., 2011; Mo, K. C., 2008). In this study, SPI values were calculated every month for both 1 month (SPI-1, representing short-term droughts) and 24 months (SPI-24, representing multi-year droughts). Monthly SPI-24 values represent the water deficit (or surplus) over the previous 24 months. Both indices were calculated over the reference and future periods.

The study looked at both the annual and seasonal scales. At the annual scale, the smallest value of SPI-1 and SPI-24 (out of 12 monthly values) was selected for the extreme value analysis, irrespective of the month associated with its occurrence. This follows the guidelines used in flood frequency analysis (Hamed, K. & Rao, A. R., 2019). A threshold approach, in which a drought is defined by a given SPI value, could also have been used, therefore allowing multiple droughts in a single year. For seasonal (June-July-August (JJA) and December-January-February (DJF)) droughts, the lowest SPI-1 value associated with these months was chosen.

In hydrological terminology, a return period refers to a recurrence interval of some specified hydrological events, and is usually used to express the frequency of an extreme event (Sharma, T. & Panu, U., 2015; Sigdel, M. & Ikeda, M., 2010). For both ensembles, the very large number of available equivalent-years allows for the calculation of large return period events without having to resort to fit a theoretical distribution as is typically done in the analysis of extreme events to extrapolate toward larger quantiles. Different probability density distributions (PDF) have differences mainly at the tail level and estimating large quantiles always result in large sampling uncertainties. Since both ensembles provide respectively 1500 and 1200 years for each 30-year period, the estimation of the 100-year return period can reliably be estimated from the empirical distribution. This paper will look at droughts with a 2-, 20- and 100-year return periods. The 2-year drought represents a typical drought that should be exceeded every other year on average (referred to as a moderate drought), while the 20- and 100-year droughts represent extreme droughts that are only to be exceeded every 20 and 100 years on average (respectively referred to as severe and extremely severe droughts). The empirical return period T of future SPI values was calculated based on the Cunnane's formula (1978). Considering the large sample size, the use of other estimators would have essentially yielded the same result, since different plotting formulas give very similar results except at the very end of the distribution (Rakhecha, P. & Singh, V. P., 2009). To sum up, for both ensembles, the 2-, 20- and 100-year meteorological droughts were characterized by their 1 and 24-months SPI values at both the annual and seasonal (DJF and JJA) scales.

In order to better display changes at the regional scale, all land areas in the world (with the exception of Antarctica) were divided into 21 regions defined by Giorgi & Francisco (2000). Table 2.1 and Figure 2.1 present details of each of the 21 individual regions.

Table 2.1 List of the 21 geographical regions
Adapted from Giorgi & Francisco, 2000, p. 172

Continent	**ID**	**Region**	**Acronym**	**Latitude(°)**	**Longitude(°)**
Oceania (OC)	1	Australia	AUS	45-11S	110-155E
South America (SA)	2	Amazon Basin	AMZ	20S-12N	82-34W
	3	Southern South America	SSA	56-20S	76-40W
	4	Central America	CAM	10-30N	116-83W
North America (NA)	5	Western North America	WNA	30-60N	130-103W
	6	Central North America	CNA	30-50N	103-85W
	7	Eastern North America	ENA	25-50N	85-60W
	8	Alaska	ALA	60-72N	170-103W
	9	Greenland	GRL	50-85N	103-10W
Europe (EU)	10	Mediterranean Basin	MED	30-48N	10W-40E
	11	Northern Europe	NEU	48-75N	10W-40E
Africa (AF)	12	Western Africa	WAF	12S-18N	20W-22E
	13	Eastern Africa	EAF	12S-18N	22-52E
	14	Southern Africa	SAF	35-12S	10W-52E
	15	Sahara	SAH	18-30N	20W-65E
Asia (AS)	16	Southeast Asia	SEA	11S-20N	95-155E
	17	East Asia	EAS	20-50N	100-145E
	18	South Asia	SAS	5-30N	65-100E
	19	Central Asia	CAS	30-50N	40-75E
	20	Tibet	TIB	30-50N	75-100E
	21	North Asia	NAS	50-70N	40-180E

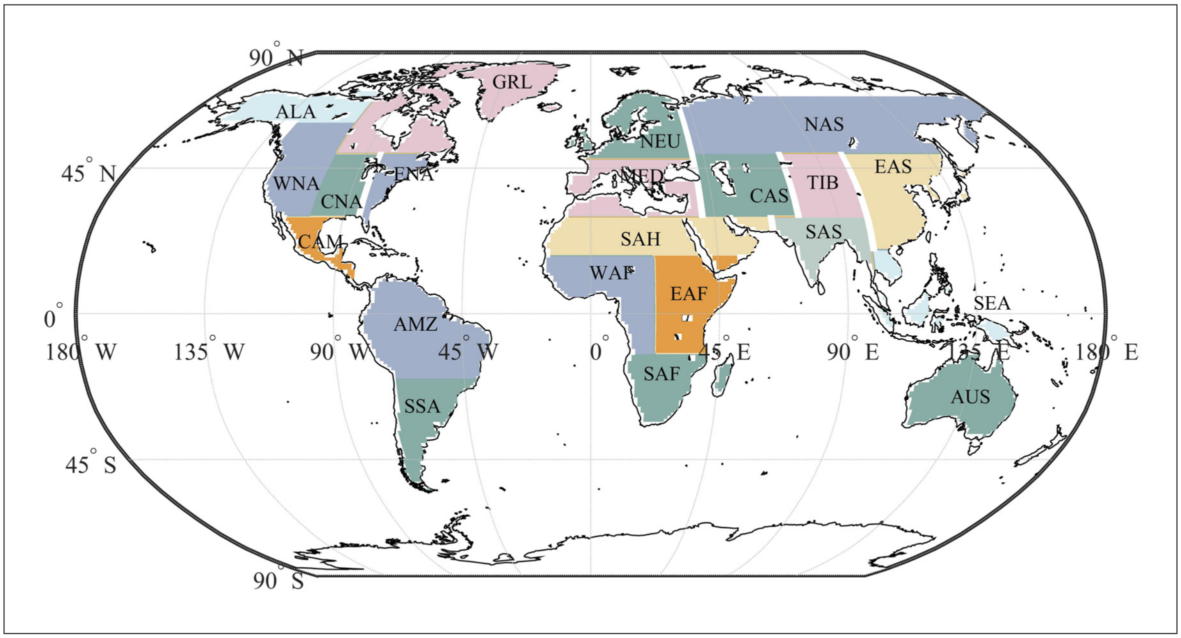

Figure 2.1 The spatial distribution of 21 regions over the world
Taken from Giorgi & Francisco, 2000, p. 172

2.5 Results

2.5.1 Comparison of model outputs against observations

Figure 2.2 presents maps of mean annual and seasonal (DJF and JJA) precipitation for the 1981-2010 reference period for both ensembles and for the GPCC dataset. The ensemble mean (mean of all members for each ensemble) is used to represent both ensembles. The spatial distribution of precipitation is very well represented by both climate models at both the annual and seasonal scales. However, both climate models are generally wetter than observation over the reference period. This is especially the case for North America, South Africa, Australia, and Central Asia. Only in Northern South America and Southeast Asia are model simulations drier. CESM1 is generally wetter than CanESM2 over the reference period.

Once again, the global spatial patterns are very similar in Figure 2.3, indicating that both climate models do a reasonably good job at representing the inter-annual variability of precipitation. Overall, the variability tends to be larger in climate models in most parts of the world, with the exception of Southeast Asia and the northern end of South America. To further explore climate model performance in simulating total precipitation amounts and standard deviation, differences between both models and observations are shown in Figure 2.10 and 2.11. Both models underestimate precipitation amounts and interannual variability in South America, parts of Africa at the annual, JJA and DJF temporal scales. Both models underestimate precipitation amounts over the Mediterranean Basin and North America in JJA, and during the DJF over North Africa and North Australia. In all cases discussed above, model performance is best in DJF, when variability is lower.

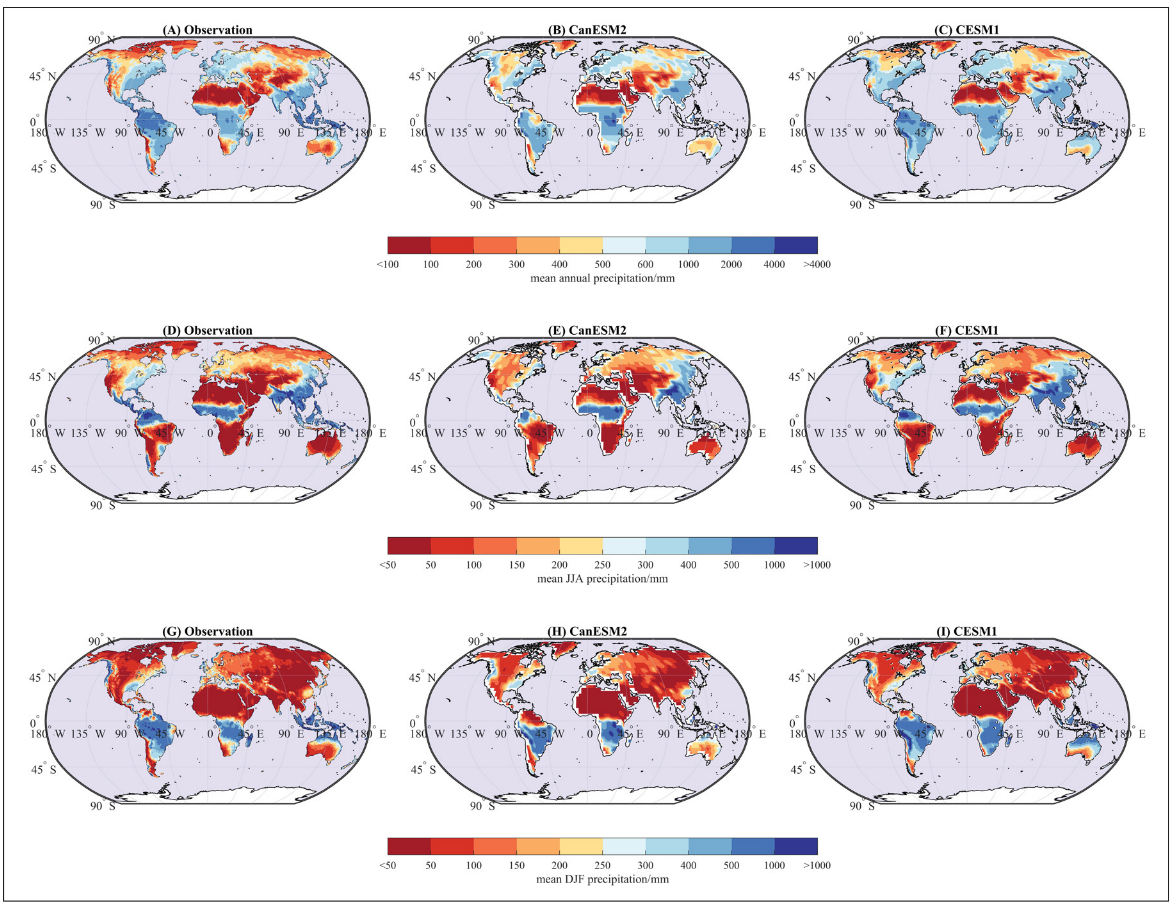

Figure 2.2 Mean annual precipitation in observations (A. GPCC), and two large climate model ensembles, CanESM2 (B) and CESM1 (C) in the reference period (1980-2010). In the second and third rows are mean summer JJA (D. GPCC, E. CanESM2, F. CESM1) and mean winter DJF (G. GPCC, H. CanESM2, I. CESM1) total precipitations

In the following section, Figures 2.4 to 2.7 present results for short-term meteorological droughts (with accompanying Tables 2.2, 2.3 and 2.4). Section 2.5.3 presents results for long-term droughts within Figures 2.8, 2.9 and Table 2.4. Change patterns are very similar between the near- and far-future periods, and are essentially more pronounced for the latter. Accordingly, only results from the far future are shown in the main body of the paper. Results for the near-future period are presented in the supplementary material section 2.8.

2.5.2 Short-term droughts

Figure 2.4 presents annual frequency changes for the moderate (2-year), severe (20-year) and extremely severe (100-year) droughts for both ensembles in the far-future period (results for the near future are shown in Figure 2.12). These figures do not display absolute values of drought severity, but rather, show changes in the frequency of occurrence, as done by Martel *et al.* (2018). For example, for the 20-year drought, a future value of 10 years indicates a doubling in frequency, and a value of 5 years means a four-fold increase in frequency. Warm colors indicate an increase in frequency whereas cold colors show a decrease.

Results from both climate ensembles display similar spatial patterns for all three return periods. Increases in drought frequency are particularly noticeable for the Southern Hemisphere, especially for the CanESM2 model. Patterns are similar for all three return periods, but changes in drought frequency become more severe for larger return periods. Moderate meteorological droughts become less severe for all of the Northern Hemisphere with the exception of the Mediterranean basin, whereas this pattern progressively reverses over some northern regions for larger return-period droughts. CESM1 generally predicts a larger increase of extreme droughts frequency, as compared to CanESM2. This is especially clear for North America, Asia and Australia. The changes in SPI values behind these results were found to be statistically significant ($\alpha = 0.05$) at the annual scale for more than 80% of all land grid points for both climate models (80.5% for CanESM2 and 86.41% for CESM1).

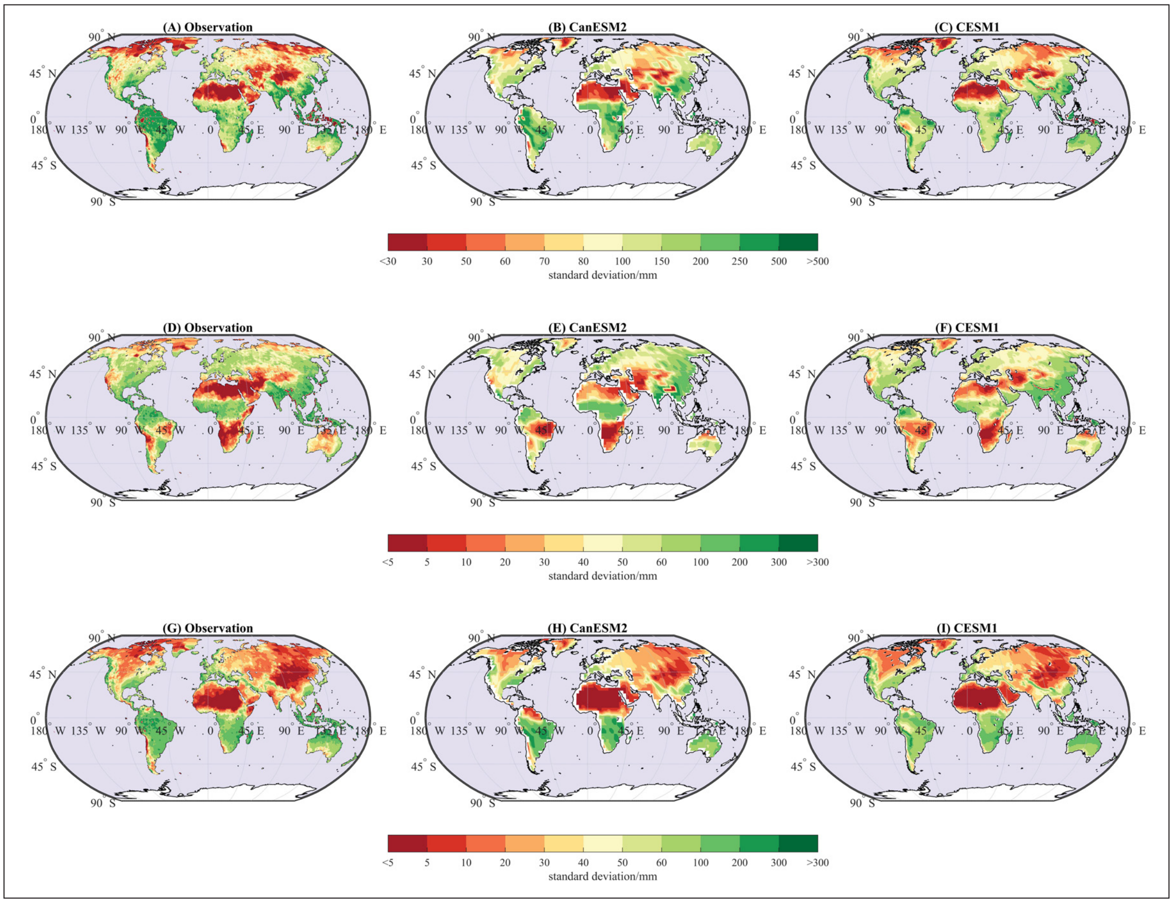

Figure 2.3 Standard deviation of mean annual precipitation (mm) in observations (A. GPCC) and climate model ensembles (B. CanESM2 and C. CESM1) over the reference period (1981-2010). The Second row (D to F) shows the standard deviation in seasonal precipitation (mm) in JJA (D. GPCC, E. CanESM2, F. CESM1) and the third row (G to I) for DJF (G. GPCC, H. CanESM2, I. CESM1). Red in the map means low standard deviation, while green means large standard deviation

Despite the general agreement between both climate models, there are some regional differences. In order to better summarize these differences, Figure 2.5 presents boxplots of the 100-year drought frequency change at the annual scale for each region of Figure 2.3 (the corresponding figure for the 20-year drought is shown in Figure 2.13). Each boxplot is comprised of all grid points within each region. The boxplots show the median and interquartile range (centered box) while the lower and upper whiskers respectively display the grid point with the most and least dramatic change in drought frequency. Quantiles below the horizontal line indicate a worsening in the recurrence of 100-year droughts (decreasing return period/increasing drought frequency), whereas quantiles above the horizontal line indicate increasing return periods.

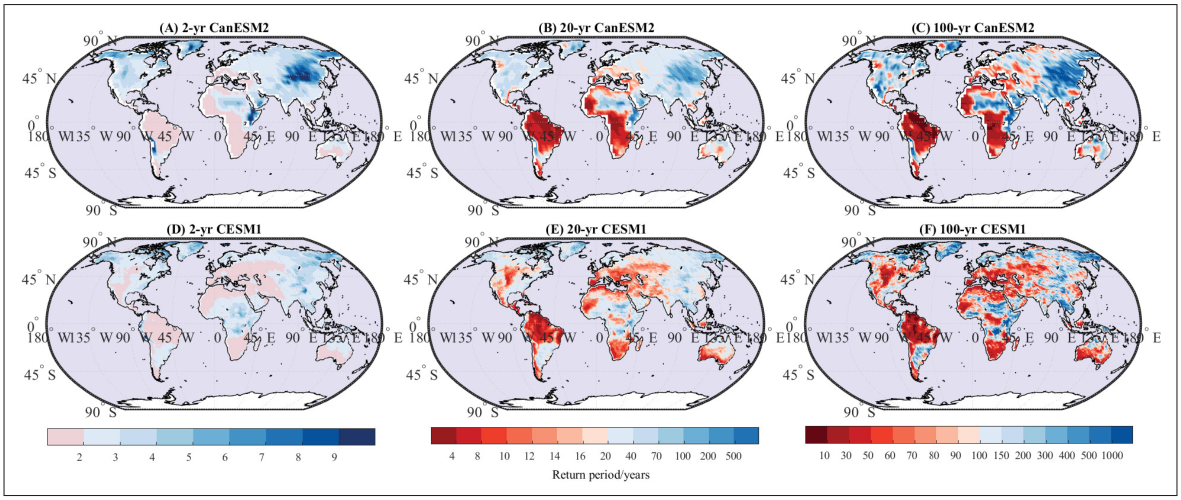

Figure 2.4 Change in the mean annual 1-month SPI drought frequency in the far future relative to the reference period. The upper panel (A-C) is for the 2-year, 20-year, and 100-year return period changes relative to the reference period in CanESM2. The bottom panel (D-F) presents changes in frequency for 2-, 20- and 100-year return periods in CESM1. Red means an increase in drought frequency while cooler colors indicate a decrease

Results show that CESM1 consistently predicts larger drought frequency increases, as compared to CanESM2 with the exception of South America (SA) and West Africa (WAF). The regions of South America (SA), Oceania (OC) and the Mediterranean basin (MED) show the clearest signature of worsening extreme droughts for most of the grid points, and for both models. Asia (AS), North America (NA) and Northern Europe (NEU) are the regions least affected by a worsening of extreme meteorological droughts, although there is significant variability within sub-regions within NA and AS.

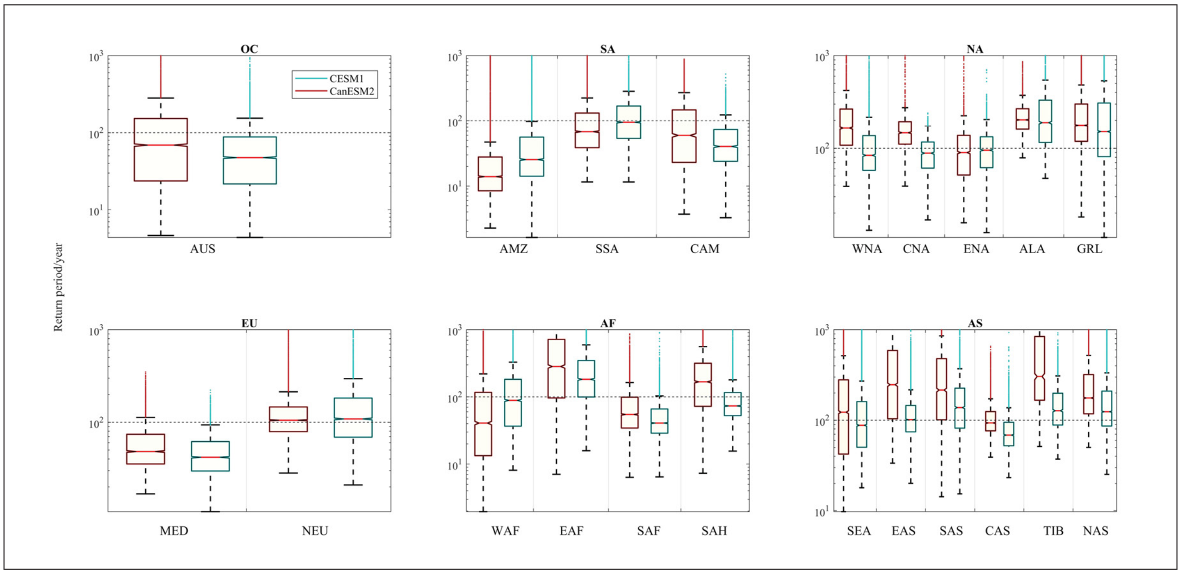

Figure 2.5 Drought frequency change of future short-term extremely severe droughts (drought with 100-year return period in the reference period) in 21 regions over the annual scale in the far future

The main similarities and differences between both climate models are summarized in Table 2.2. Regions in which more than 55% of grid points experience increasing (decreasing) drought frequency are labeled with an increasing (decreasing) trend. The 55% value was semi-quantitatively chosen as the best threshold to contrast regional behavior. The probability of having more than 55% of positive trends in a random sample is less than 5% for a region containing 300 grid points. Both climate ensembles project opposite trends for only 4 out of 21 regions. There are 13 regions where both models project trends in the same direction and only four regions where models predict opposite trends. These regions correspond to regions identified by the IPCC as having large internal variability compared to the expected climate change signal.

Table 2.2 Agreements and disagreements between CanESM2 and CESM1 large ensembles for short-term extremely severe droughts over annual scale in the far-future

Regions with the same trend			**Regions with the different trend**	
Increase	Decrease	No change in ensembles	Opposite trend	No change in one ensemble
AUS, AMZ CAM, MED SAF, CAS	ALA, GRL EAF, SAS TIB, NAS	NEU	WNA, CNA SAH, SEA	SSA, ENA WAF, EAS

Note: 'Regions with the same trend' means that two large ensembles predicted the same change direction of extreme droughts of 3 different return periods. 'Regions with the different trend' means that two large ensembles predicted reverse trends, for example, region A was predicted to be with increasing drought frequency in CanESM2 while CESM1 projected a decreasing trend, or CanESM2 and/or CESM1 predicted the no change in the drought frequency

Figure 2.6 shows the changes in the return periods of moderate, severe and extremely severe droughts in JJA for the far-future period for both ensembles (Figure 2.14 presents results for the near-future period). Compared to the annual scale, the patterns are more severe for all regions and particularly so for the Northern Hemisphere. East Asia (EAS), Tibet (TIB), Alaska (ALA), Greenland (GRL), Southern US and part of Sahara (SAH) and Eastern Africa (EAF) are the only regions with a projected decrease in extreme meteorological droughts. The amplitude of changes gets progressively larger for the larger return period.

Figure 2.7 displays regional changes for the far-future JJA extremely severe droughts. Results are similar for the 20-year droughts presented in Figure 2.15. The regional changes are extremely similar to those presented in Figure 2.5, with the difference being that JJA increases in drought frequencies are consistently more severe than at the annual scale. This is particularly striking for the Europe domain, where increases in 100-year frequency are now observed over almost all grid points. Both climate models predict opposite trends for only 2 out of 21 regions (Table 2.3).

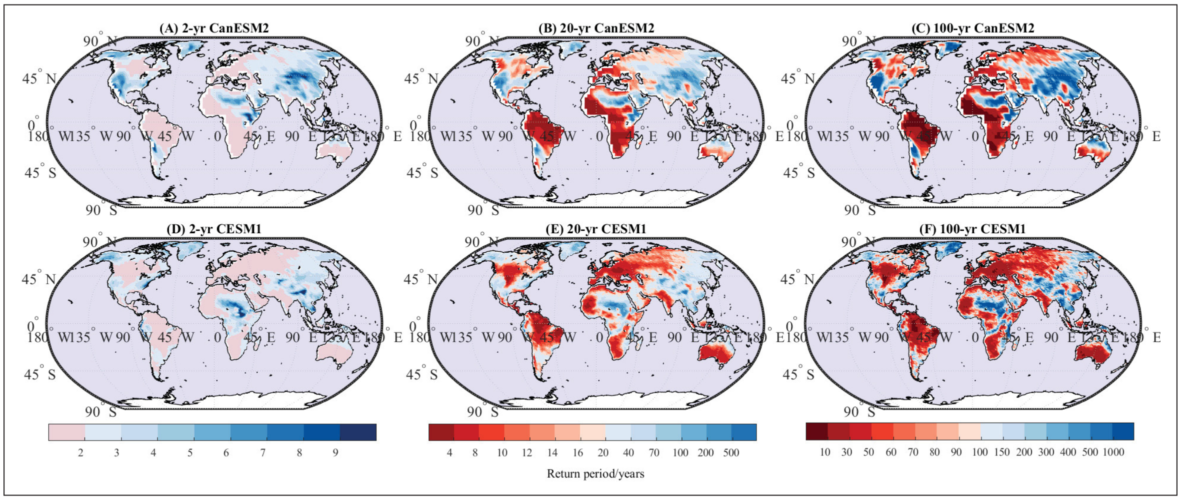

Figure 2.6 Same as Figure 2.4, but for the mean JJA 1-month SPI drought frequency

Changes in drought frequency for DJF are presented in Figures 2.16 to 2.18 and Table 2.5. Patterns are similar between both climate models and frequency changes are noticeably smaller than for JJA, even for the Southern Hemisphere.

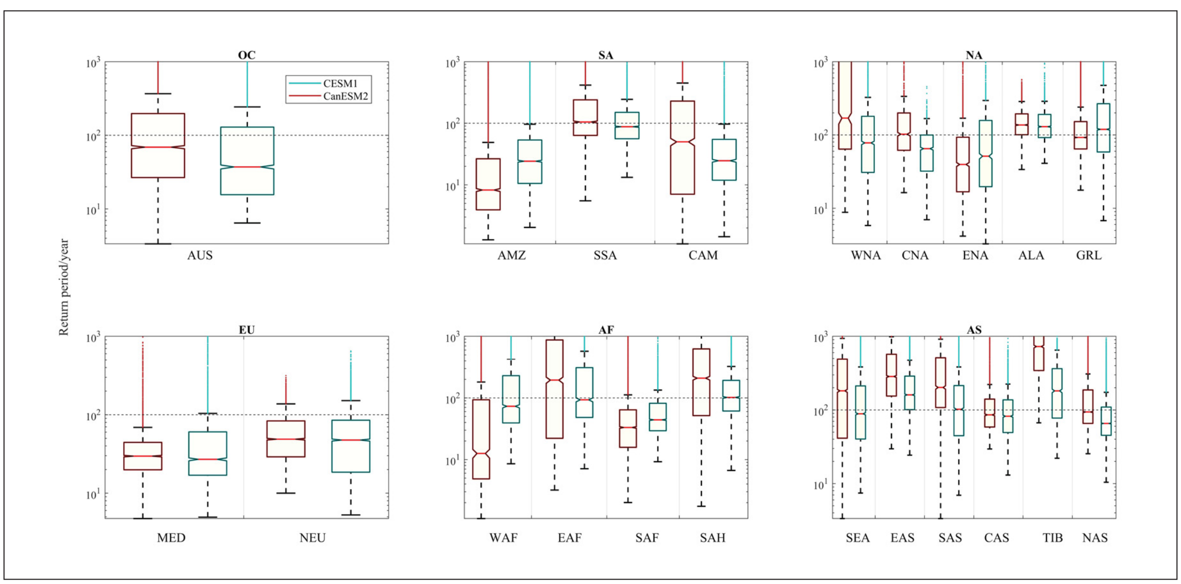

Figure 2.7 Same as Figure 2.5, but for the short-term extremely severe droughts in far-future JJA

Table 2.4 presents a summary of the regions most affected by a frequency increase in extreme meteorological droughts at the yearly and seasonal (JJA, DJF) scales. These regions are listed under two categories: highest percentage of grid points experiencing frequency increases, and highest mean magnitude of grid points with increasing extreme drought frequency at the regional scale. Results show that four regions are particularly affected by increases in extreme meteorological droughts. They are all mid-latitude regions located either in South America or around the Mediterranean Sea. The largest frequency increases are found in the Amazon basin (AMZ) with a mean frequency increase of 19.72 (CanESM2) and 9.32 (CESM1) for extremely severe droughts in JJA. These respectively correspond to future return periods of roughly 5 and 11 years for the current 100-year droughts.

2.5.3 Long-term droughts

Long-term droughts are represented in this work by the 24-month SPI index as a representation of multi-year droughts. Figure 2.8 presents future changes in the frequency of long-term droughts for both climate model ensembles. The results are more consistent across both climate model ensembles than they were for short-term droughts. A much smaller percentage of land areas is affected by a worsening of droughts, compared to short-term droughts. In particular, most of Asia and North America are expected to see a decrease in the frequency of long-term droughts. In the Northern Hemisphere, the Mediterranean Basin (MED) and Western Africa are the only areas to see a worsening in long-term droughts. In the South Hemisphere, South America (SA), Southern Africa (SAF) and South Australia all see an increase in the severity of long-term meteorological droughts. CanESM2 predicts the worst future extreme droughts conditions.

The above results are well emphasized in the regional plots presented in Figure 2.9. The agreement between both climate models is also quite clear from this figure. There are only two regions where both climate models differ on the direction of the trend (WAF and CAS), and both of these regions encompass zones with significant variability. Overall, those results indicate that future frequency increases will be more important for short-term meteorological droughts (and especially in the future JJAs), as compared to long-term meteorological droughts. In both cases, the changes in frequency are more important for larger return period, emphasizing the amplification of extremes.

Table 2.3 Agreements and disagreements between CanESM2 and CESM1 large ensembles for short-term extremely severe droughts in far-future JJA

Regions with the same trend			**Regions with the different trend**	
increase	Decrease	No change in ensembles	Opposite trend	No change in one ensemble
AUS, AMZ, CAM, ENA, MED, NEU, WAF, SAF, CAS	ALA, EAS, TIB	–	WNA, GRL	SSA, CNA, EAF, SAH, SEA, SAS, NAS

Note: ’Regions with the same trend’ means that two large ensembles predicted the same change direction of extreme droughts of 3 different return periods. ‘Regions with the different trend’ means that two large ensembles predicted reverse trends, for example, region A was predicted to be with increasing drought frequency in CanESM2 while CESM1 projected a decreasing trend, or CanESM2 and/or CESM1 predicted the no change in the drought frequency

Table 2.4 The worst region influenced by more frequent extreme droughts and the regions with the largest change of short-term extreme drought frequency over different time scales

Change	**Severe drought(20-year)**		**Extremely severe drought(100-year)**	
	Most affected region (%)	Region with the largest change in frequency (times)	Most affected region (%)	Region with the largest change in frequency (times)
Annual				
CanESM2	MED (89.36)	AMZ (6.32)	AMZ (84.41)	AMZ (10.35)
CESM1	MED (96.53)	AMZ (4.28)	MED (93.47)	AMZ (6.41)
June-July-August				
CanESM2	MED (87.61)	AMZ (8.52)	MED (87.97)	AMZ (19.72)
CESM1	CAM (84.96)	CAM (4.88)	CAM (86.02)	AMZ (9.32)
December-January-February				
CanESM2	CAM (85.19)	AMZ (4.99)	CAM (79.20)	AMZ (8.28)
CESM1	SAH (93.31)	AMZ (5.27)	SAH (95.0)	AMZ (9.01)

Note:‘MED (89.36)’ means that 89.36% in MED would be with increasing frequency of severe droughts in the far future. A 4 times change indicates that the drought would become 4 times more frequent in the far future. The 20-year (100-year) drought would therefore become a 5-year drought (25-year)

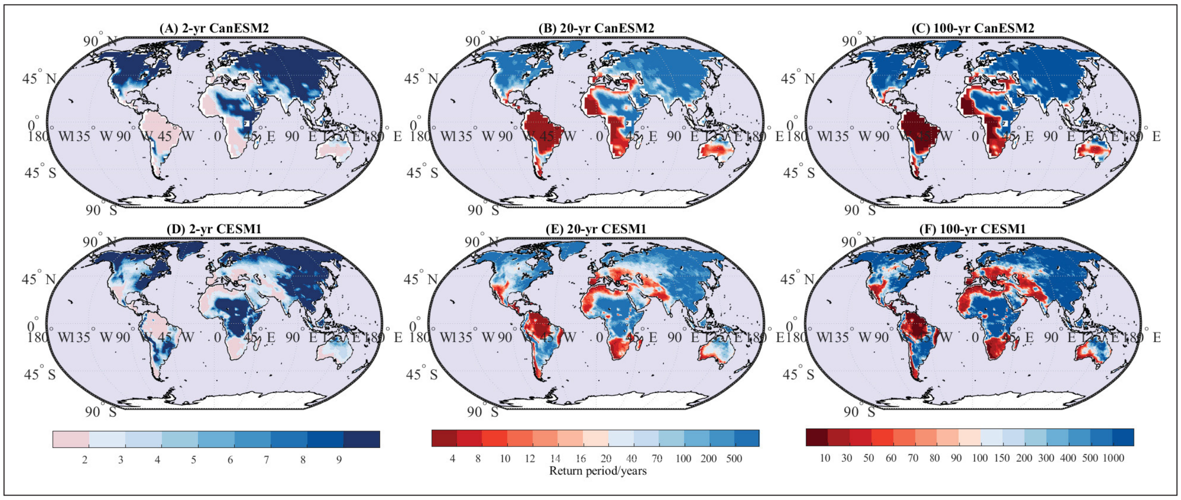

Figure 2.8 Same as Figure 2.4, but for the mean annual 24-month SPI drought frequency

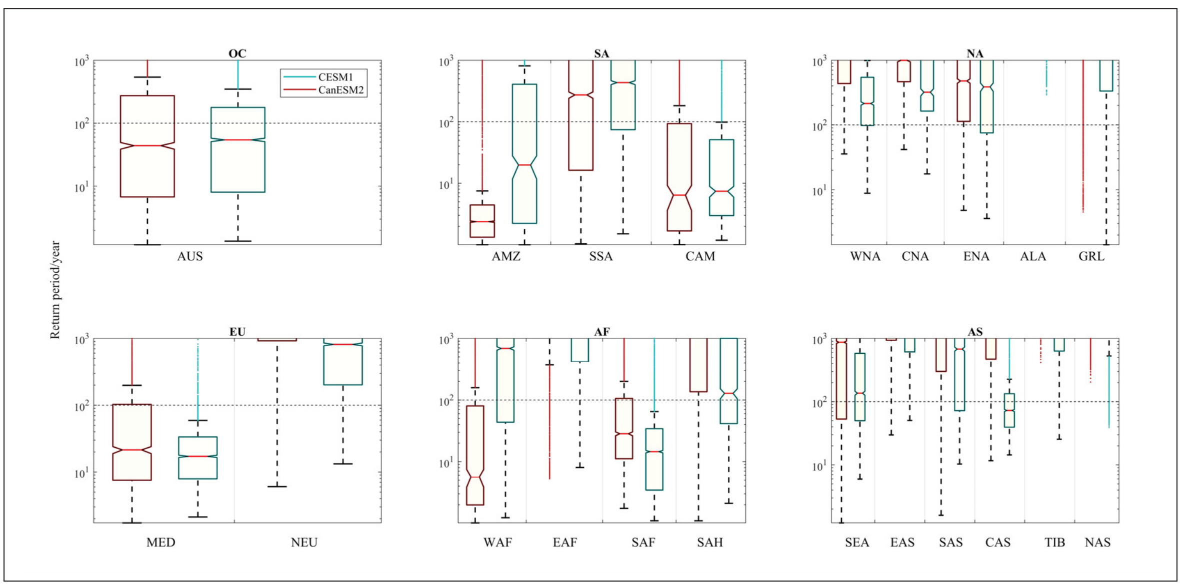

Figure 2.9 Same as Figure 2.5, but for the long-term extremely severe drought over annual scale

2.6 Discussion and Conclusion

2.6.1 Discussion

The results presented in this paper indicate a worsening of extreme meteorological droughts in many regions of the world, and particularly so for seasonal short-term droughts. These results are based on two large ensembles from two different climate models. The use of two large ensembles provides the important advantage of allowing a study extreme events with little uncertainty. The disadvantage of using large ensembles is that such use does not allow a proper sampling of GCM/ESM uncertainty as would be the case if using a global (CMIP5, Taylor *et al.*, 2012) or regional (e.g., NARCCAP, Mearns, L. O., Arritt, R., Biner, S., Bukovsky, M. S., McGinnis, S., Sain, S., Caya, D., Correia Jr, J., Flory, D., Gutowski, W. et al., 2012) multi-model ensemble. Using large ensemble therefore provides a unique opportunity to look at extremely rare events with minimal uncertainty, whereas multi-model ensembles are specifically used to investigate model structural uncertainty. The CMIP6 (Eyring, V., Bony, S., Meehl, G. A., Senior, C. A., Stevens, B., Stouffer, R. J. & Taylor, K. E., 2016) ensemble should provide the opportunity to do both, as all climate model will provide a minimum number of members for the core simulation. Since we only used two climate models, it is therefore important to frame our results in comparison to others, even though little previous work has been dedicated to extreme droughts.

In Sheffield & Wood's work (2008), soil moisture data from 8 GCMs (from IPCC AR4, forced by SRES A2, A1B and B1 scenarios) was used to study global drought occurrence under future warming (2070-2099). In this study, droughts were defined as the sequence of consecutive months with soil moisture quantiles lower than a threshold corresponding to a 10-year return period in the historical period (1961-1990). Results showed that the Mediterranean, West African, Central Asia and Central American regions showed large increases in drought frequency, and particularly for long-term droughts (more than 12-month duration). A doubling in the frequency of short-term droughts (4-6 months duration) was observed by Sheffield & Wood (2008), as compared to the mid-twentieth century, under the future projections. Zhao & Dai

(2017) used the outputs from 12 CMIP3 models under the A1B scenario and 14 CMIP5 models under RCP4.5 to project changes in the frequency of future agricultural droughts for the 2070-2099 period. Moderate to severe droughts were defined as having respective anomalies below the 20^{th} and 10^{th} percentiles, based on the reference period (1970-1999). Both ensembles project an increase over almost all land areas, with severe droughts seeing a larger frequency increase than their moderate counterparts. This amplification of extremes is consistent with the results presented in this paper. Overall, the spatial extent of warming future droughts was more expansive than presented in this study, because they both considered agricultural droughts, a point that will be discussed later. The results presented in this paper are also mostly consistent with those of Dai (2011). The general distribution of areas affected by increasing drought frequency is also in line with areas where mean annual precipitation is expected to decrease, and particularly in tropical and subtropical zones (IPCC, 2013b). To further this point, the JJA relationship between the frequency change of extreme droughts and mean total precipitation was also explored. Unsurprisingly, there is a good spatial correlation between future mean JJA precipitation changes and increases in future meteorological drought frequency. The projected change for JJA total precipitation for both models is shown in Figure 2.22. Areas affected by an increase in meteorological droughts are however larger than those affected by decreases in mean JJA precipitation, indicating that many regions where mean JJA precipitation is expected to increase will nonetheless see worsening drought conditions. For example, this is especially clear for Northern Russia in CanESM2, and in many regions of South America in CESM1. There is also a clear link with drought return periods, with more extreme droughts more likely to increase in regions with increasing mean JJA precipitation than for more common droughts. This observed tendency in drought frequency to increase in regions getting wetter can only be explained by changes in temporal precipitation variability.

Overall, results obtained from both climate ensembles are fairly consistent, with only some regional differences. In all cases, the observed differences correspond to regions already identified by the IPCC as having low inter-model agreement. These regions are typically characterized by high internal variability compared to the expected climate change signal. For example, two regions WNA and GRL, see different trends (depending on the climate model) for the far-future JJA. Both of those regions are characterized by a lot of variability and both barely exceed the 55% cutoff to declare a regional trend. Slightly changing the region boundaries could reverse the trends. Better agreement was found at the seasonal scale for short-term extreme droughts, and especially in future DJFs, which corresponds to the season in which inter-annual variability is lower. This lower inter-annual variability is also likely the reason why JJA extreme droughts will see a greater frequency increase than will DJF.

As with any studies dealing with climate change in future horizons, this work is impacted by many sources of uncertainty. The work focused on meteorological droughts using a single index, and with only two climate models under the pessimistic RCP8.5 scenario. The choice of models and scenario was imposed by the main objective of focusing on extreme droughts. The focus on large ensembles was dictated by the need to reduce statistical uncertainty for large return period droughts, and this led to the use of the only two global large ensembles available: CanESM2 and CESM1. Large ensembles are expected to become more common in the future, and this will help better frame extreme drought-related inter-model uncertainty. Such ensembles are now available at the regional scale (Leduc, M., Mailhot, A., Frigon, A., Martel, J.-L., Ludwig, R., Brietzke, G. B., Giguére, M., Brissette, F., Turcotte, R., Braun, M. et al., 2019). Droughts were only assessed under the RCP8.5 scenario because no other RCPs were available for the two existing (at the time of starting this work) large ensembles. The use of different drought indices has been shown to potentially have an influence on the magnitude and sign of the change of drought (Burke & Brown, 2008). The SPI was chosen especially because of its simplicity and its widespread use. However, the use of this index will likely result in an underestimation of the severity of future droughts under climate change because it ignores the role of temperature, a critical contributor (Marcos-Garcia, P., Lopez-Nicolas, A. & Pulido-Velazquez, M., 2017). Some drought indices (e.g., PDSI and SPEI), also categorized as meteorological drought indices (Svoboda, M., Fuchs, B. et al., 2016), consider water supply and demand simultaneously, thus showing more severe drought conditions under a warming climate (Burke & Brown, 2008; Sheffield & Wood, 2008). Since surface moisture/water balance is related to agricultural droughts, some researches have explored the characteristics of agricultural droughts based on those same indices (Dai, 2011; Touma *et al.*, 2015).

This study has only looked at meteorological droughts since precipitation deficit is the main driver of all other types of droughts. Considering the complexity of using large ensembles, the focus was therefore to exploit their ability at looking extremely rare events rather than look at the propagation of meteorological droughts into other types of droughts. Clearly, agricultural and hydrological droughts are also affected by other climate variables, such as wind, humidity and temperature, which control evapotranspiration and may worsen the impact of meteorological droughts. Global surface temperatures have been steadily on the rise over the past decades, and the observed changes have already been larger than internal variability for most of the world's regions, and sharp increases are expected everywhere, especially at high latitudes, by the end of the century (Fischer, E. M. & Knutti, R., 2015). While this study did not look at agricultural and hydrological droughts, it can be inferred with good confidence that results presented in this paper for meteorological droughts, however dire they are for many regions of the world, will pale in comparison to the combined impact of higher temperatures with the increasing frequency of extreme precipitation deficit.

Further studies should focus on a better understanding of these combined effects and the interplay between anthropogenic forcing and climate's internal variability. Studies on hydrological and agricultural droughts could easily be carried out using the methodological approach presented in this paper. However, runoff and soil moisture outputs from climate models should be treated with caution, because there is lack of suitable observation to verify (Burke & Brown, 2008). Ultimately, developing a better ability to forecast droughts will become critical to the development of adaptation strategies to cope with the increase frequency and severity of droughts.

2.6.2 Conclusion

This study has explored the evolution of the frequency of future extreme meteorological droughts at the global scale using precipitation outputs from two large climate ensembles (CESM1 and CanESM2) under the RCP8.5 emission scenario. The major findings are summarized as follows:

1) The very large number of simulated years from two climate model large ensembles (CanESM2-7550 years; CESM1-7240 years) were used to study extreme meteorological droughts, defined here as having a return period exceeding 20 years. Such extreme droughts have not received much attention in previous work.

2) Both ensembles do a good job at replicating spatial patterns and magnitude of annual total precipitation and interannual variability over the reference period (1981-2010). This provides confidence in each model's ability to adequately represent short-term (1-month) and long-term (24-month) drought frequency.

3) Projected increases in future extreme meteorological drought frequency are mostly consistent across both climate ensembles, although there are many regional differences, mostly in regions that have already been labeled as having high internal variability by the IPCC.

4) The projected increases in meteorological drought frequency are much more severe for short-term droughts than for long-term droughts.

5) The patterns of increasing extreme meteorological drought frequency are consistent with those of future changes in mean annual precipitation, indicating that regions with decreasing precipitation are, unsurprisingly, more at risk. However, the extent of the drought frequency increase patterns is larger than those for mean annual precipitation, indicating a worsening of extreme droughts in some regions projected to see an increase in mean annual precipitation.

6) The total area affected by a worsening of droughts gets larger with the drought return periods. In other words, the frequency increase of the 100-year drought is more important than for the 20-year drought. For the most vulnerable region, the JJA short-term drought frequency could increase by up to 20 times for the 100-year drought, and by 9 times for the 20-year drought. This means that the future return periods of the current 20 and 100-year droughts, would become 2 and 5 years in the future, for the most affected region.

7) The amplification of the impact of climate change toward more extreme droughts has been observed in other studies, but the frequency changes are much larger in this study, likely the result of looking at droughts with a much larger return period.

2.7 Acknowledgments

The authors acknowledge the contribution of the Canadian Centre for Climate Modelling and Analysis (CCMA) for making the CanESM2 Large Ensemble simulations available in this study. The authors would also like to thank the Ouranos Consortium for helping with the data transfer. The data is now available for the 1950-2020 period from the CCMA website (http://collaboration.cmc.ec.gc.ca/cmc/cccma/CanSISE/output/CCCma/CanESM2/). The CESM1 large ensemble was downloaded from the Large Ensemble Community Project (LENS) website (http://www.cesm.ucar.edu/projects/community-projects/LENS/). The GPCC database was downloaded from (https://opendata.dwd.de/climate_environment/GPCC/html/download_gate .html). This work was funded by the Canadian Natural Science and Engineering Research Council (Grant RGPIN-2015-05048).

2.8 Supplementary materials

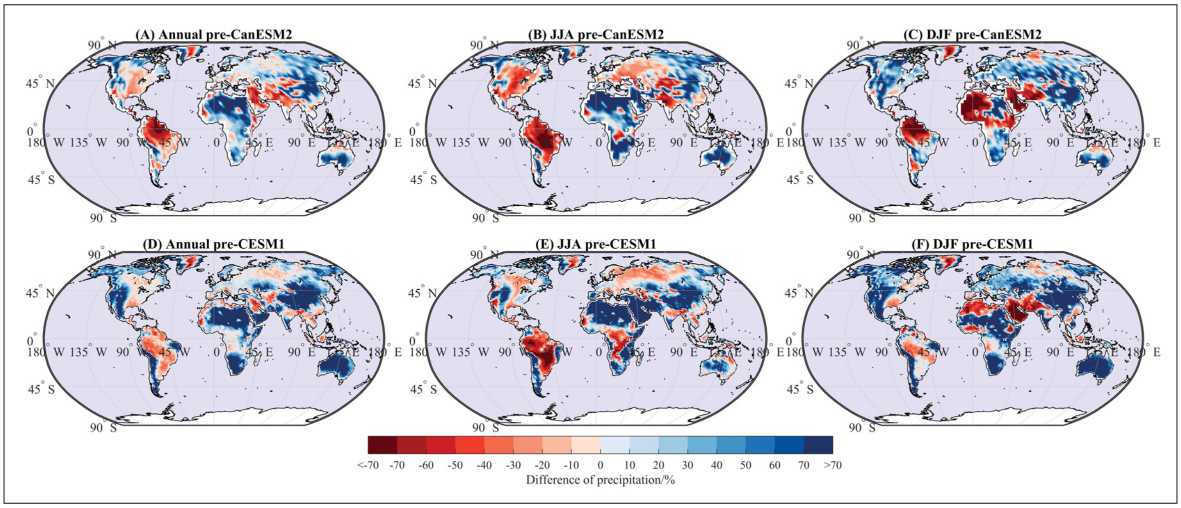

Figure 2.10 Difference in total annual (JJA/DJF) precipitation amount between CanESM2 (upper row, A to C) or CESM1 (lower row, D to F) and observation. Red represents underestimation while blue means overestimation of the precipitation amount

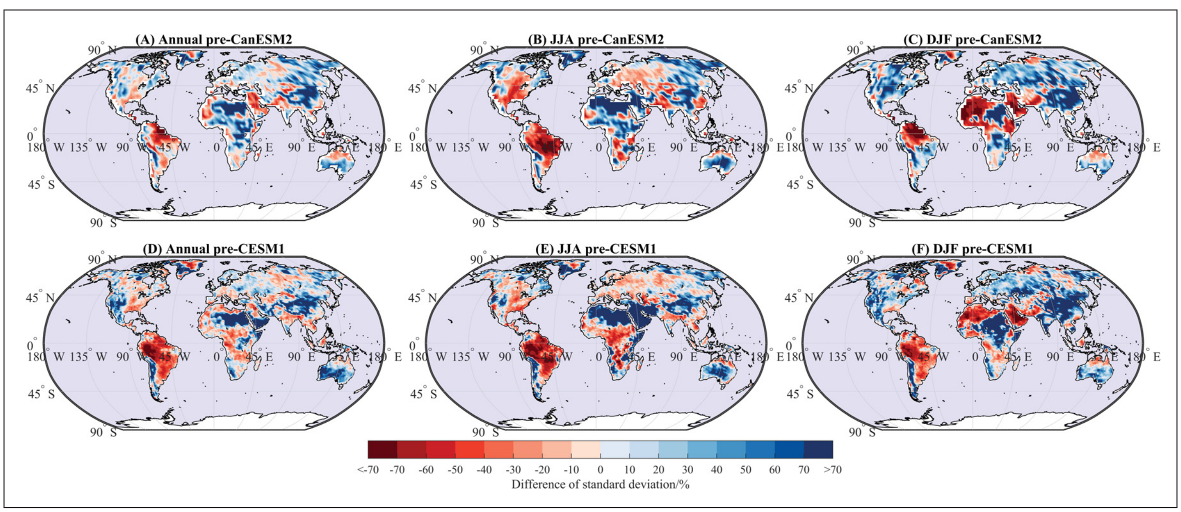

Figure 2.11 Difference in standard deviation of annual (JJA/DJF) precipitation between CanESM2 (upper row, A to C) or CESM1 (lower row, D to F) and observation. Red represents underestimation while blue means overestimation of the standard deviation

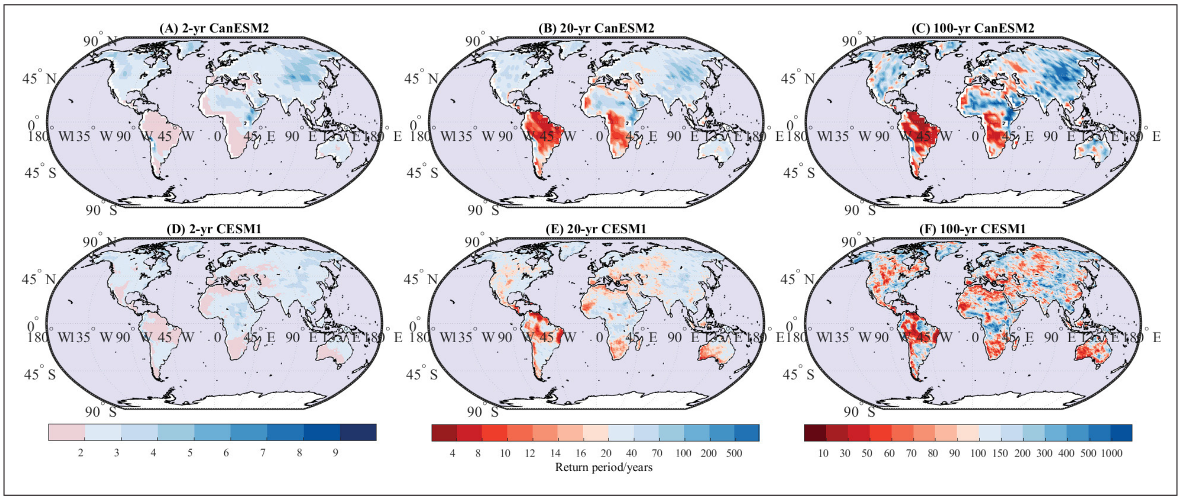

Figure 2.12 Same as Figure 2.4, but for the mean annual 1-month SPI drought frequency in the near-future period

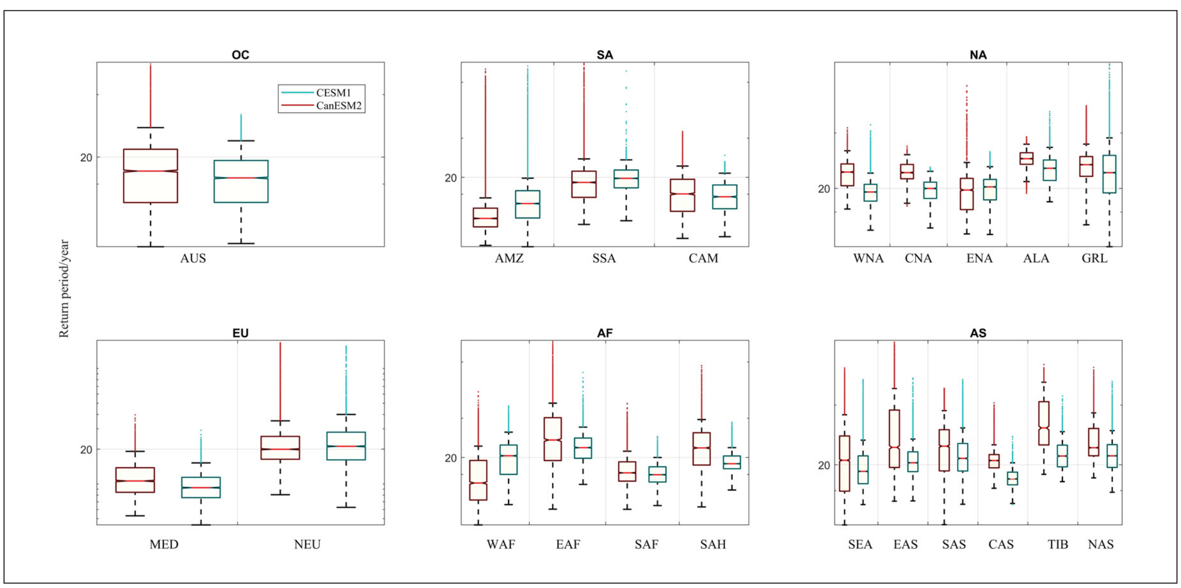

Figure 2.13 Drought frequency change of short-term severe drought over the annual scale in the far future

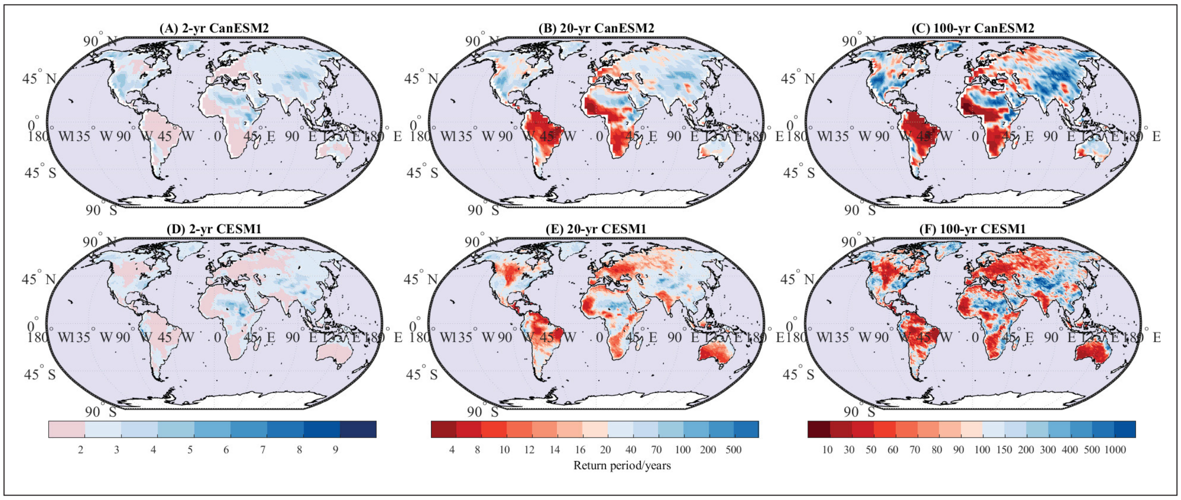

Figure 2.14　Same as Figure 2.6, but for the mean JJA 1-month SPI drought frequency in the near-future period

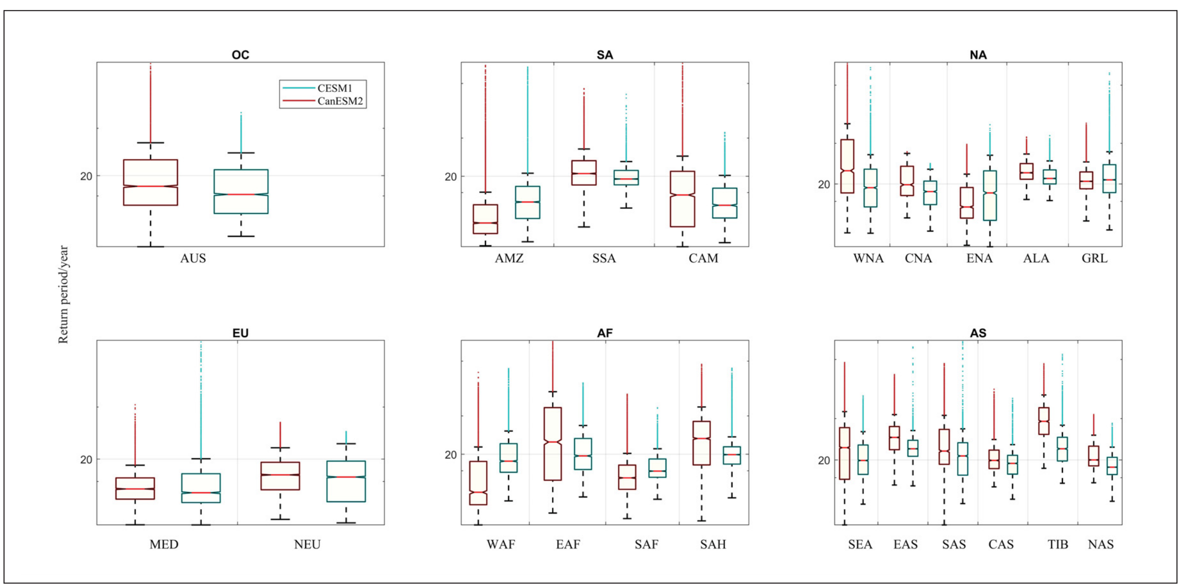

Figure 2.15　Drought frequency change of short-term severe drought in the far future JJAs

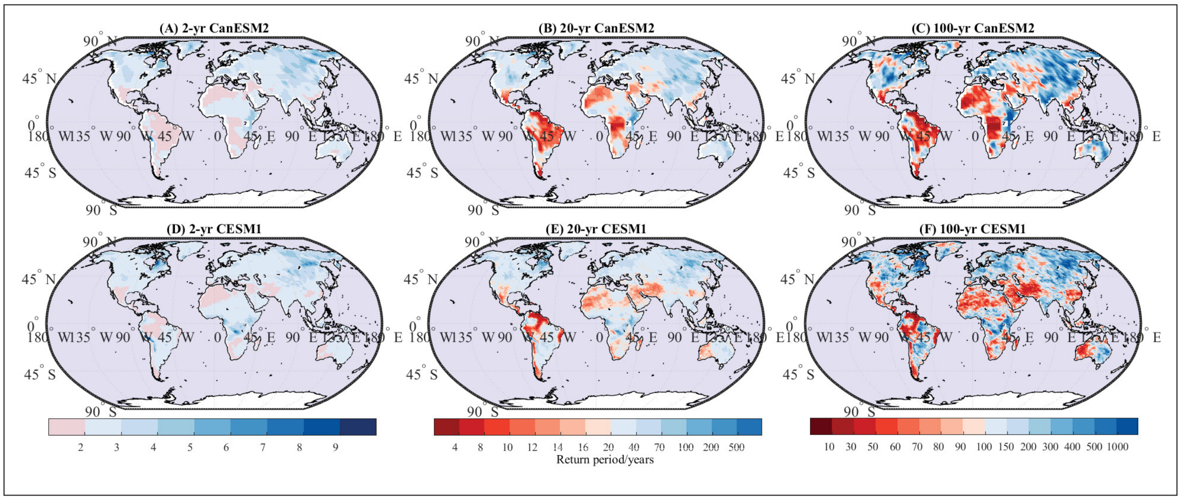

Figure 2.16 Change in the mean DJF 1-month SPI drought frequency in the near future relative to the reference period. The upper panel (A-C) is for the 2-year, 20-year, and 100-year return period change relative to the reference period in CanESM2. The bottom panel (D-F) presents changes in frequency for 2, 20 and 100-year return periods in CESM1. Red means an increase in drought frequency while cooler colors indicate a decrease. The unit of color scales is year

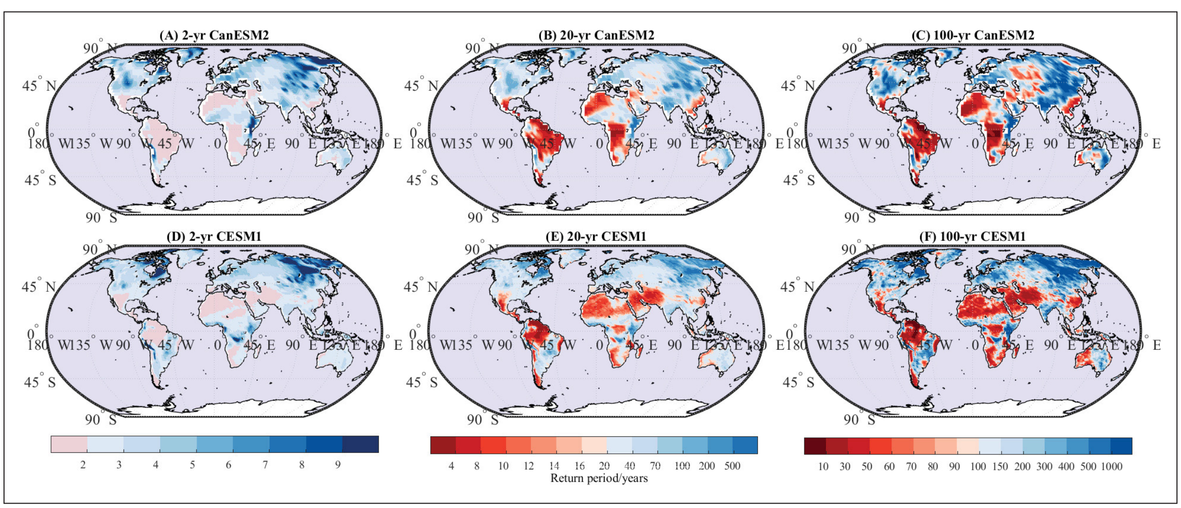

Figure 2.17 Same as Figure 2.14, but for the far-future period

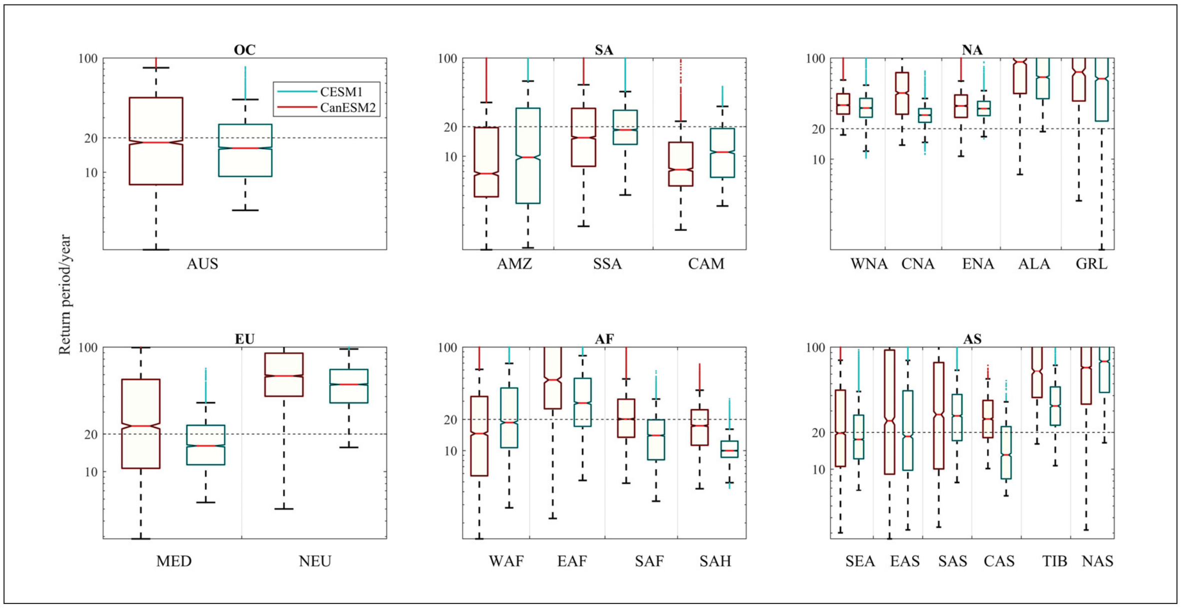

Figure 2.18 Drought frequency chagne of short-term severe drought in the far future DJFs

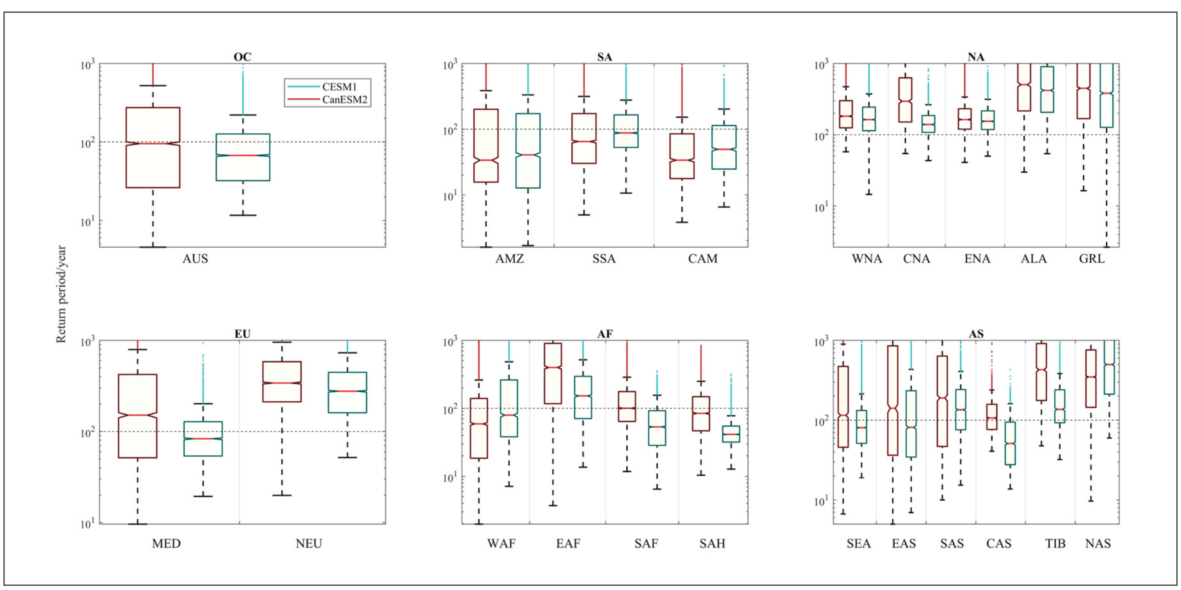

Figure 2.19 Drought frequency change of short-term extremely severe drought in the far-future DJFs

Table 2.5 Agreements and disagreements between CanESM2 and CESM1 large ensembles for short-term droughts in future DJFs

Regions with the same trend			**Regions with the different trend**	
increase	Decrease	No change in ensembles	Opposite trend	No change in one ensemble
AMZ, SSA CAM, SAH WAF	WNA, CNA ENA, ALA GRL, NEU EAF, SAS TIB, NAS		MED, EAS CAS	AUS, SAF SEA

Note:'Regions with the same trend' means that two large ensembles predicted the same change direction of extreme droughts of 3 different return periods. 'Regions with the different trend' means that two large ensembles predicted reverse trends, for example, region A was predicted to be with increasing drought frequency in CanESM2 while CESM1 projected a decreasing trend. or CanESM2 or CESM1 predicted the no change in the drought frequency

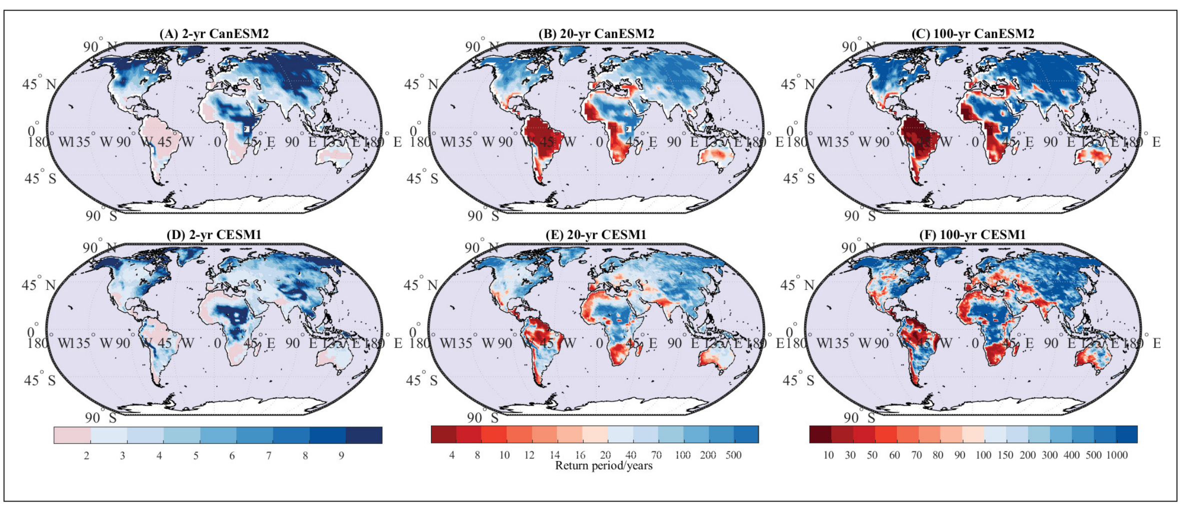

Figure 2.20 Change in the mean annual 24-month SPI drought frequency in the near future relative to the reference period. The upper panel (A-C) is for the 2-year, 20-year, and 100-year return period changes relative to the reference period in CanESM2. The bottom panel (D-F) presents changes in frequency for 2-, 20- and 100-year return periods in CESM1. Red means an increase in drought frequency while cooler colors indicate a decrease

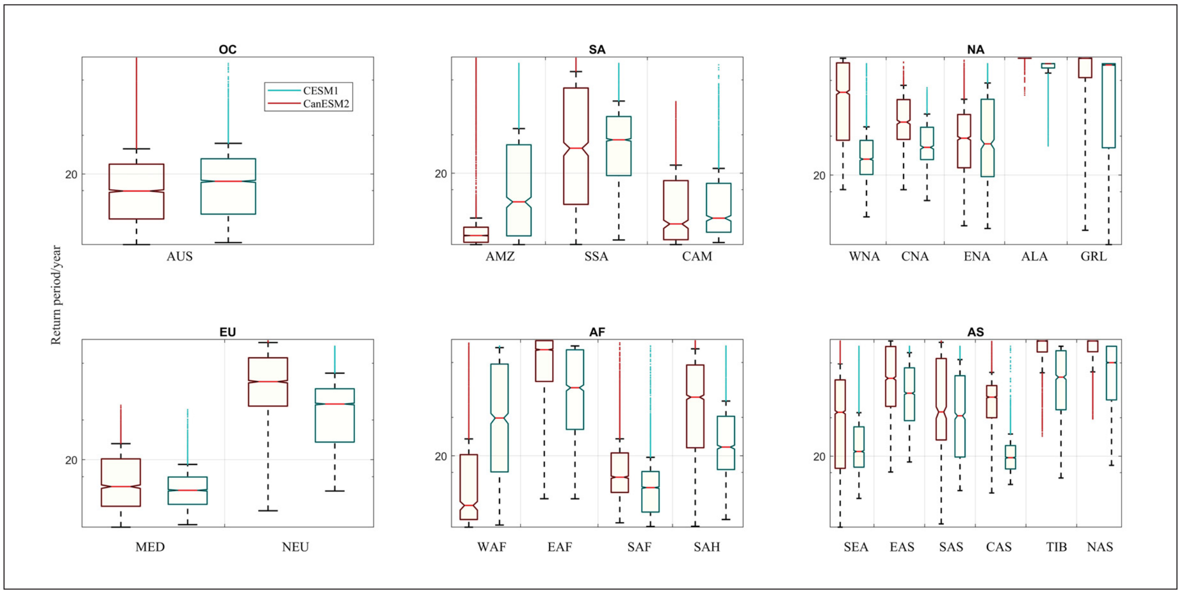

Figure 2.21 Drought frequency change of long-term severe drought over annual scale in the far future

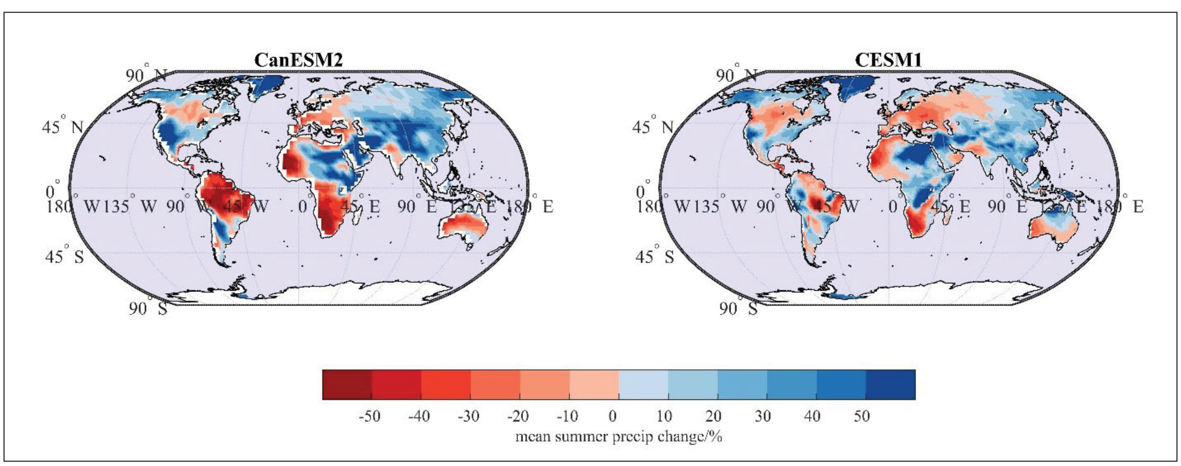

Figure 2.22 Relative change of far-future JJA precipitation in two large ensembles

CHAPTER 3

FREQUENCY CHANGE OF FUTURE EXTREME SUMMER METEOROLOGICAL AND HYDROLOGICAL DROUGHTS OVER NORTH AMERICA

Cha Zhao[1], François Brissette[1], Jie Chen[2], Jean-Luc Martel[1,3]

[1] Department of Construction Engineering, École de Technologie Supérieure,
1100 Notre-Dame West, Montreal, Quebec, Canada H3C 1K3
[2] State Key Laboratory of Water Resources & Hydropower Engineering Science,
Wuhan University,
299 Bayi Road, Wuchang Distinct, Wuhan, Hubei, China 430072
[3] Lasalle | NHC,
9620 Saint-Patrick Street, Montreal, Quebec, Canada H8R 1R8

Paper published in Journal of Hydrology, November 2019

3.1 Abstract

This paper describes projected frequency changes in extreme summer meteorological and hydrological droughts over North American catchments. It uses two large ensemble climate models (50-member CanESM2 and 40-member CESM1) under the RCP8.5 scenario to robustly assess frequency changes up to the 100-year drought, relative to the 1980-2009 reference period. Meteorological droughts, linked solely to precipitation deficit, are represented by the 1-month Standardized Precipitation Index (SPI), whereas hydrological droughts are characterized by the 1-month Streamflow Drought Index (SDI), based on hydrological simulation using a lumped hydrological model. Results show widely different patterns for future changes in extreme meteorological versus hydrological droughts. Future meteorological droughts show patterns of increasing and decreasing frequency that roughly match future expected changes of mean summer precipitation, although some regions are nonetheless projected to see more frequent extreme meteorological droughts despite increases in mean summer precipitation. The frequency changes for the 100-year meteorological droughts can be quite severe, with up to a 20-fold increase observed over some watersheds. On the other hand, hydrological droughts, which combine the effect of precipitation and temperature changes, show a mostly uniform

pattern of large to very large increases in drought frequency. This shows that the projected temperature increase is a main driver of future extreme hydrological droughts, enough to overcome the projected increase in mean summer precipitation for many North American catchments. Projected changes in both meteorological and hydrological droughts get consistently worse for the longer considered return periods. In other words, frequency changes for the 100-year droughts are more significant than those expected for the 2- and 20-year droughts. This gradual worsening toward larger extremes has potentially large societal and economic impacts. The large projected increases in the frequency of extreme hydrological drought frequency (up to 27 times) are likely to severely stress water management systems across North America.

Keywords: climate change; large ensemble climate models; extreme droughts; North America; frequency analysis

3.2 Introduction

The frequency of many extreme natural hazards, such as floods and droughts, is expected to increase as global temperatures rise due to the increasing concentration of greenhouse gases in the atmosphere (Cai, W., Wang, G., Santoso, A., McPhaden, M. J., Wu, L., Jin, F.-F., Timmermann, A., Collins, M., Vecchi, G., Lengaigne, M. et al., 2015; Fischer & Knutti, 2015; Lelieveld, J., Proestos, Y., Hadjinicolaou, P., Tanarhte, M., Tyrlis, E. & Zittis, G., 2016; Martel *et al.*, 2018; Martel, J.-L., Mailhot, A. & Brissette, F., 2020; Rupp, D. E., Li, S., Mote, P. W., Massey, N., Sparrow, S. N. & Wallom, D. C., 2017). Droughts have often been regarded as the most severe natural disaster because other catastrophes, such as floods, are typically restricted to relatively localized areas and over a well-defined time interval (Vicente-Serrano, S. M., López-Moreno, J. I., Beguería, S., Lorenzo-Lacruz, J., Azorin-Molina, C. & Morán-Tejeda, E., 2011). Droughts are responsible for land degradation, famine and epidemics in emerging nations and for large economic losses in developed regions (Nicholson, S. E., 2001). Drought is defined as a temporary and periodic natural phenomenon which is characterized by below-normal precipitation, above-normal temperature, low relative humidity, below-average cloud cover, or any combination thereof (Dai, 2011). Droughts can be classified into four primary categories: meteorological droughts, agricultural droughts, hydrological droughts, and socio-economic droughts. Meteorological droughts are characterized by a precipitation deficit, and are closely related to other types of droughts (Hannaford, J., Lloyd-Hughes, B., Keef, C., Parry, S. & Prudhomme, C., 2011). The onset of agricultural droughts depends on antecedent soil moisture conditions, and may therefore lag the start of meteorological droughts (Heim & Richard, 2002). Hydrological droughts occur when a precipitation deficit propagates to the surface or subsurface water level, resulting in difficulties supporting normal water usage (Dai, 2011; Wilhite & Glantz, 1985). Socio-economic droughts for their part occur when water shortage starts to affect people, supply and demand for economic goods (Hayes *et al.*, 2011).

There are many recent examples of severe North American droughts resulting in significant socio-economic impacts. In recent years, droughts in the United States (U.S.) have led to nearly $9 billion in annual losses (NCDC, 2013). In California, the economic impacts of droughts on agriculture led to nearly 4700 job losses, and to a $604 million gross sales deficit in 2016 alone (Medellín-Azuara, J., MacEwan, D., Howitt, R. E., Sumner, D. A., Lund, J. R., Scheer, J., Gailey, R., Hart, Q., Alexander, N. D., Arnold, B. et al., 2016). In Canada, recurrent major droughts affect the interior valley of British Columbia (BC) and the Prairies (Bonsal *et al.*, 2011; Masud *et al.*, 2015). The provincial government of BC relocated 2800 cattle and paid around $2 million to replace damaged fencing due to the droughts in 2017 (Cherneski, 2018). Eastern North American droughts typically affect smaller areas, and have a shorter duration than their Central and Western counterparts, but are nonetheless liable to have significant economic impacts (Barrie Bonsal, 2004).

Understanding the evolution of future droughts in a changing climate is of great economic importance in terms of the capacity to implement efficient adaptation measures. Anchukaitis, K., Cook, B. & Cook, E. (2016) used climate model data from the Coupled Model Intercomparison Project Phase 5 (CMIP5) ensemble (Taylor *et al.*, 2012) as well as paleoclimatic data (Last Millennium Ensemble, LME), to assess past, current and future droughts in western North America. They found that precipitation played a dominant role in controlling the occurrence and characteristics of past droughts in paleoclimate records, whereas evapotranspiration associated with the future increasing temperature would dominate the trends for future droughts. Tam *et al.* (2018) projected future changes in meteorological droughts by using 29 Global Circulation Models (GCMs) under three emission scenarios in Canada, and found that drought frequency would increase in South-west Canada and the Prairies, with larger inter-annual variability in the latter half of the 21^{st} century. Prudhomme *et al.* (2014) used 7 global impact models (GIMs), 5 GCMs under 4 Representative Concentration Pathways (RCPs) to study future hydrological droughts. They predicted a postive trend in the severity of hydrological droughts at the global scale by the end of the 21^{st} century (2070-2099). Wanders *et al.* (2015) applied a global hydrological model (PCR-GLOBEWB) forced by 5 GCMs under 4 RCPs to simulate global daily streamflow at a 0.5 grid resolution from 1971 to 2099. Droughts in this study were defined by conventional (based on the reference period) and transient (based on the previous 30 years) thresholds, respectively. Results showed that roughly half of total land surface would experience a decreasing trend in low flows.

Other studies have looked at megadroughts, which can have multi-decadal to century-long durations, and can have lasting impacts on water availability and even lead to population migrations. Using tree-ring records starting from A.D. 600, Helama, S., Meriläinen, J. & Tuomenvirta, H. (2009) explored impacts of ENSO anomalies on precipitation deficit during the medieval anomaly. Cook, E. R., Anchukaitis, K. J., Buckley, B. M., D'Arrigo, R. D., Jacoby, G. C. & Wright, W. E. (2010) also used tree rings to generate a 700-year reconstruction of monsoon patterns over Asia. This reconstruction outlined monsoon failures and megadroughts. Comparatively, much fewer studies have looked at extreme droughts, defined herein as having a longer return period ($T \geqslant 20$ years), rather than by the extreme magnitude of drought indices (Marengo & Espinoza, 2016; Roudier *et al.*, 2016). Extreme droughts, despite their low probability of occurrence, typically carry a much larger proportion of the expectancy of drought losses across the entire drought spectrum (Coumou, D. & Rahmstorf, S., 2012). This is because adaptation measures, that are typically in place to deal with those frequent droughts are largely ineffective against their more extreme counterparts. Extreme droughts are also more difficult to study due to the large statistical uncertainty related to short historical data series.

The focus of this work is therefore on the study of the evolution of future extreme summer meteorological and hydrological droughts and on comparing trends to those of more frequent droughts.

This paper is organized as follows: sections 3.3 and 3.4 respectively describe the datasets used in this work and the methodological aspects. Results are shown in section 3.5. The discussion and conclusions are respectively presented in sections 3.6 and 3.7.

3.3 Data

The watershed data used in this study comes from a combination of Canadian and U.S. databases. For Canada, hydrometeorological data and boundaries (of 532 watersheds) come from the Canadian model parameter experiment (CANOPEX) database (Arsenault, R., Bazile, R., Ouellet Dallaire, C. & Brissette, F., 2016). Observed precipitation and temperature data are basin-averaged. The Canadian watersheds are well-distributed over Canada, with the exception of the prairie areas. For the U.S., meteorological data comes from gridded dataset of Maurer, E. P., Wood, A., Adam, J., Lettenmaier, D. P. & Nijssen, B. (2002). This dataset is interpolated to a $0.125° \times 0.125°$ grid, and has been widely used in drought and climate change impact studies (Liu, C., Ikeda, K., Rasmussen, R., Barlage, M., Newman, A. J., Prein, A. F., Chen, F., Chen, L., Clark, M., Dai, A. et al., 2017; Mazrooei, A. & Sankarasubramanian, A., 2019; Sheffield, J., Goteti, G., Wen, F. & Wood, E. F., 2004). There are now several other interpolated gridded climate datasets available over the continental United States (e.g., Abatzoglou, J. T., 2013; Livneh, B., Rosenberg, E. A., Lin, C., Nijssen, B., Mishra, V., Andreadis, K. M., Maurer, E. P. & Lettenmaier, D. P., 2013). Despite minor differences between these existing datasets, Essou, G. R., Arsenault, R. & Brissette, F. P. (2016) showed that they were statistically equivalent with respect to their performance in lumped hydrological modeling over most U.S. catchments. Streamflow and watershed boundary data in the U.S. were extracted from the United States Geological Survey (USGS) database for 5265 watersheds. The combination of the Canadian and US datasets lead to a total of 5797 watersheds. Ninety percent of all watersheds have a size ranging between 536 and 35,000 km^2. The U.S. was divided into six regions (from west to east: West US, High Plains, South, Midwest, Southeast, Northeast) and Canada into 4 regions, for easier comparison. The choice of these 6 regions in the U.S. was based on the US drought monitor (https://droughtmonitor.unl.edu/). A map showing the centroid of all North American watersheds and ten regions is shown in Figure 3.1.

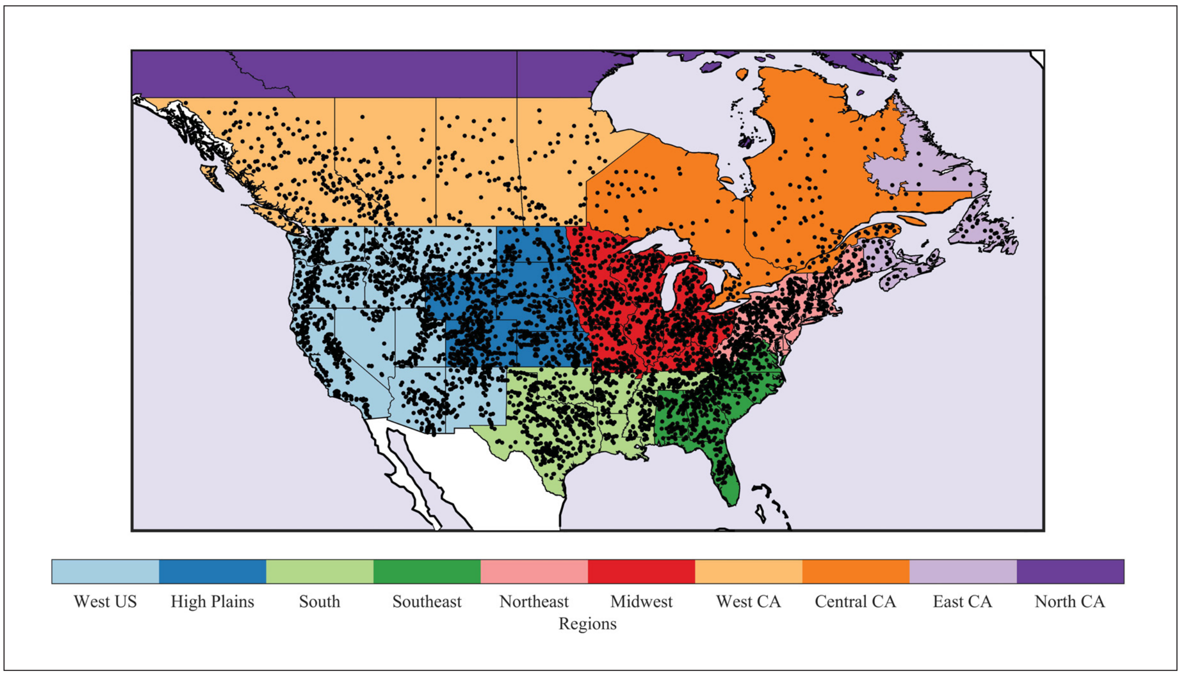

Figure 3.1 Distributions of the 5797 watersheds used in this study. The watersheds were divided into 6 regions for U.S. and 4 regions for Canada

To assess the future climate, two climate model large ensembles were used in this study. The Canadian Earth System Model (CanESM2) is a 50-member ensemble run at a spatial resolution of $2.8^\circ \times 2.8^\circ$. To produce the 50-member ensemble, historical forcing was applied to five different members to obtain different ocean states over the 1850-1950 period. Five members were perturbed 10 times, using historical forcing to 2005 and by the RCP8.5 afterward, leading to a total of 50 members over the 1950-2100 period (Arora *et al.*, 2011; Sigmond & Fyfe, 2016). The Community Earth System Model (CESM1) is a 40-member ensemble run at a spatial resolution of $1^\circ \times 1^\circ$, covering the 1920-2100 period. Each member is obtained from random atmospheric perturbations using historical forcing to 2005 and the RCP8.5 afterward until 2100. Details can be found in Kay *et al.* (2015).

3.4 Methodology

In this paper, meteorological and hydrological droughts are analyzed for 5797 North American watersheds over the 1980-2009 historical period, as well as for the near- (2036-2065) and far-future (2070-2099) periods.

The results presented in this paper for future droughts are based on climate model outputs. To evaluate the potential differences between climate model-simulated and observed drought patterns, some level of validation against observations is required. While climate models have shown their ability to simulate the current climate and its variability at the global scale (Flato, G., Marotzke, J., Abiodun, B., Braconnot, P., Chou, S. C., Collins, W. J., Cox, P., Driouech, F., Emori, S. & Eyring, V., 2013), there may be significant differences at the regional scale. Simulated meteorological outputs (precipitation, maximum and minimum daily temperature) for each watershed were averaged from a minimum of the four grid points closest to its centroid. Climate model precipitation was first compared against observation over the 1980-2009 reference period. The ensemble mean of total summer precipitation was used as a first comparison criterion. Since droughts originate from temporal variability in precipitation fields, the standard deviation of total summer precipitation was used as a second comparison criterion (standard deviation of 30×50 values).

To perform the climate change impact analysis at the watershed scale, climate model outputs were bias-corrected to account for spatial differences and model structural errors (Maraun, D., Wetterhall, F., Ireson, A., Chandler, R., Kendon, E., Widmann, M., Brienen, S., Rust, H., Sauter, T., Themeßl, M. et al., 2010; Seager, R. & Vecchi, G. A., 2010). Failing to correct for these biases may result in unrealistic streamflow simulations over the reference period, as well as over the future periods. Specifically, the daily bias correction method (DBC) of Chen et al. (2013; 2019) was adopted in this work. The DBC is a combination of the daily translation method, which is a quantile mapping approach (Mpelasoka, F. S. & Chiew, F. H., 2009), and the local intensity scaling (LOCI) approach. LOCI is used to correct the occurrence of precipitation to keep the wet-day frequencies identical to observations for the reference period (Chen *et al.*, 2013; Schmidli, J., Frei, C. & Vidale, P. L., 2006). This study was performed at the watershed scale using a lumped hydrological model (see below). All meteorological inputs were therefore averaged to the watershed scale. Bias correction factors were consequently computed between climate model- and watershed-averaged precipitation and temperature, with no prior downscaling step. The factors were kept the same for each member.

Bias-corrected climate model precipitation and temperature data were used as inputs to a hydrological model to simulate streamflows over the reference and future periods. Simulated streamflows were analyzed to assess changes in hydrological droughts. Daily streamflows were computed using the GR4J hydrological model (Perrin, C., Michel, C. & Andréassian, V., 2003), coupled with the CemaNeige snow module (Valéry, A., Andréassian, V. & Perrin, C., 2014). GR4J-CemaNeige is a reservoir-based, lumped rainfall-runoff model. The required inputs for this coupled model are temperature, precipitation, and potential evapotranspiration (PET). The PET is calculated using the Oudin, L., Hervieu, F., Michel, C., Perrin, C., Andréassian, V., Anctil, F. & Loumagne, C. (2005) formula, which is a simple, yet highly optimized, temperature-based PET model. There are several equations for calculating PET, including mass-transfer, radiation and temperature-based methods, and the relative performance of these equations has been shown to be dependent on the study area (Xu, C.-Y. & Singh, V., 2002). The Penman-Monteith equation is recommended by Food and Agriculture Organization (FAO) as its preferred and most reliable approach. In addition, it is generally agreed that a more physically-based PET formula should be preferred for climate change impact studies. However, such formulas rely on additional climate variables (such as humidity, radiation and wind speed) that are not widely available for large-scale studies such as this one. This brings significant limitations to its applicability in most areas (Rojas, J. P. & Sheffield, R. E., 2013). Oudin *et al.* (2005) assessed the impact of using various PET formulas on the outflows simulated by a daily rainfall-runoff model over 308 catchments in different climatic zones. Results showed that temperature- and radiation-based equations performed similarly with the chosen lumped hydrological model. Based on these results, the proposed Oudin *et al.* (2005) formula was found to be the most efficient for use with the GR4J hydrological model, also used in this work. This hydrological model has also been successfully used in several studies over North America (Arsenault, R., Gatien, P., Renaud, B., Brissette, F. & Martel, J.-L., 2015; Troin, M., Arsenault, R. & Brissette, F., 2015; Troin *et al.*, 2018; Velázquez, J. A., Troin, M., Caya, D. & Brissette, F., 2015). To calibrate the hydrological model, daily streamflow data over the 1950-2010 period was used, and the Kling-Gupta Efficiency (KGE, Gupta, H. V., Kling, H., Yilmaz, K. K. & Martinez, G. F., 2009) was taken as the optimal function. Following calibration, watersheds with KGE calibration value below 0.3 were removed. This cutoff resulted in 4521 watersheds being retained. The performance of GR4J-CemaNeige-Oudin is shown in Figure 3.2.

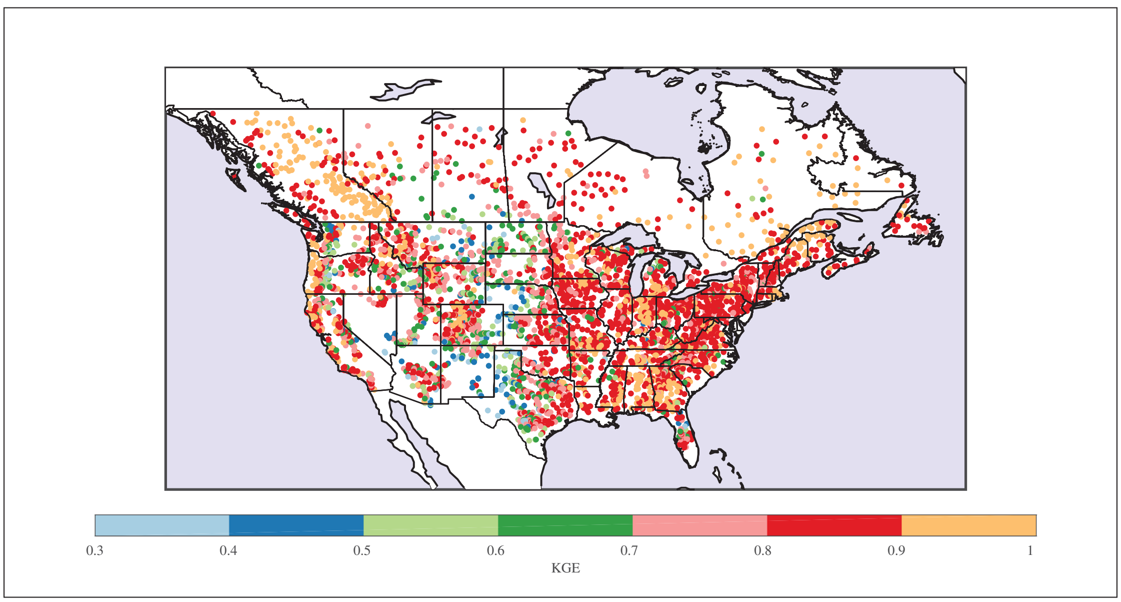

Figure 3.2 Calibration results for all 5797 watersheds over North America using the KGE as the optimal criterion

In order to study meteorological droughts over different climatological periods, drought indices must be chosen. Several drought indices are typically applied in practice to assess meteorological droughts. In this study, the Standardized Precipitation Index (SPI) was chosen based on the recommendation of the World Meteorological Organization that it could be used as a standard index for tracking meteorological droughts. It has also been widely used in many studies (Kattelus, M., Salmivaara, A., Mellin, I., Varis, O. & Kummu, M., 2016; Kumar, R., Musuuza, J. L., Loon, A. F. V., Teuling, A. J., Barthel, R., Ten Broek, J., Mai, J., Samaniego, L. & Attinger, S., 2016; Kwon, M., Kwon, H.-H. & Han, D., 2019; Preethi, B., Ramya, R., Patwardhan, S., Mujumdar, M. & Kripalani, R., 2019). It is a robust, sensitive index which can be used to monitor precipitation deficit at various temporal scales (Pai, D., Sridhar, L., Guhathakurta, P. & Hatwar, H., 2011; Stricevic, R., Djurovic, N. & Djurovic, Z., 2011). The SPI is a dimensionless indicator, which characterizes precipitation deficit relative to the long-term mean at a given location and for a given time scale (McKee, 1995; McKee *et al.*, 1993). A positive SPI index indicates above-average precipitation over a given time scale. The SPI is typically computed at time scales ranging from 1 to 24 months. This work focused on the 1-month SPI. Since the latter is computed over a short-term window, it is most often associated with meteorological droughts (Svoboda, M., Hayes, M. & Wood, D., 2012), although it can also be the end result of much longer dry sequences affecting soil moisture. In temperate climates, short-term hydrological droughts are typically the most problematic and drought durations as small as 7 days are often used to characterize their magnitude. Meteorological droughts, on the other hand, are often defined by durations of one to several months. The 1-month duration was therefore found to be a good compromise to bridge the gap between short-term hydrological and meteorological droughts. The procedure for computing SPI values consists in fitting an appropriate distribution (typically the 2-parameter gamma distribution) to precipitation data and mapping it to a normal distribution. The index represents the normal deviates of this normal distribution. More details can be found in Guttman, N. B. (1998). SPI values with return periods ranging from 2 to 100 years were estimated to assess the influence of climate change on extreme meteorological drought frequency in future periods.

A standardized drought indicator is also required for the analysis of the potential evolution of future hydrological droughts over a given time period (Vicente-Serrano *et al.*, 2011). The 1-month streamflow drought index (SDI) was chosen for hydrological droughts analysis, because it is sensitive to a wide range of drought conditions (Nalbantis, I. & Tsakiris, G., 2009). It is also region-independent, and analogous to the SPI. Similar to the SPI index computation, a distribution function is fitted to the monthly streamflow data. In this work, six potential distributions were considered: Generalized Pareto, log-logistic, lognormal, Pearson Type III, General Extreme Value (GEV) and Weibull distributions (Nalbantis, I., 2008; Vicente-Serrano *et al.*, 2011). The choice of the most appropriate distribution for each watershed was based on the best monthly fit approach (BMF) approach of Siegel, S. (1956).

This study was concerned with extreme droughts. The use of simulations from two climate model large ensembles allowed for the computation of a very large number of years for all considered 30-year periods. For each 30-year time period, CanESM2 provides a sample of 1500 equivalent years (50×30) due to the ergodic properties of the climate system. For CESM1, the number of equivalent years for each period is 1200 years (40×30). This allows for the computation of large return periods (up to 100 years) using directly obtained empirical distributions. In the real world, the analysis of extremes is typically based on a small number of years. A distribution (e.g., the GEV distribution) is fitted to this small sample, with subsequent extrapolation to larger return periods. This extrapolation results in progressively larger confidence intervals as the return period increases. In this work, the empirical return period of future drought was calculated using Cunnane's formula (1978):

$$T = \frac{N+0.2}{m-0.4} \tag{3.1}$$

where N is the number of years and m is the rank (the m^{th} smallest value). The Cunnane plotting formula provides an unbiased estimate of quantiles, and has commonly been used in hydrological studies (Ehmele, F. & Kunz, M., 2019; Wang, L., Yu, H., Yang, M., Yang, R., Gao, R. & Wang, Y., 2019b; Zhang, L. & Singh, V., 2006).

For both climate ensembles and three 30-year periods, drought return periods were calculated by picking the smallest summer SPI (or SDI) value for each of the 1500 (CanESM2) and 1200 (CESM1) years, thus allowing for the precise evaluation of rare droughts. Return periods of 2-, 20- and 100-year droughts were computed based on the reference period distribution. The 2-year drought represents a typical drought that should be exceeded every other year, on average, with a probability of exceedance of 0.5. The 20- and 100-year droughts represent extreme droughts that are only to be exceeded every 20 and 100 years, on average. This translates into a probability of exceedance respectively equal to 0.05 and 0.01.

3.5 Results

3.5.1 Climate model validation

Figure 3.3 and Figure 3.4 show the ensemble mean of total summer precipitation, as well as its standard deviation, for observation and for both climate model large ensembles over the reference period. Results are presented for each watershed (and not at the grid point scale), and as such, are consistent and comparable with the upcoming results for hydrological droughts patterns. Although there are differences between all three datasets at the local scale, both models are in agreement with respect to the representation of the spatial patterns of mean total summer precipitation and inter-annual variability over North America. CESM1 tends to be closer to observations than CanESM2, and especially over the U.S. Midwest.

As shown in Figure 3.4, CanESM2 generally underestimates the mean total summer precipitation for most watersheds over the reference period, while CESM1 performs very well for most watersheds, with the exception of the driest ones. Neither climate models shows obvious biases when simulating the standard deviation of total summer precipitation.

To further explore the models' performance in simulating the standard deviation of summer precipitation, differences between the models and observations are shown in Figure 3.5. Both models overestimate the standard deviation in the Canadian prairies and the Western U.S. (northwest and south), and underestimate the standard deviation in East Canada. In addition, CESM1 overestimates the standard deviation in the Northeast and Southest U.S., and underestimates it in the Midwest, and South. CanESM2 underestimates the standard deviation of summer precipitation in the Midwest, Northeast and Southeast, and overestimates the standard deviation in the South. In general, the difference between the observations and climate models was smaller in CESM1.

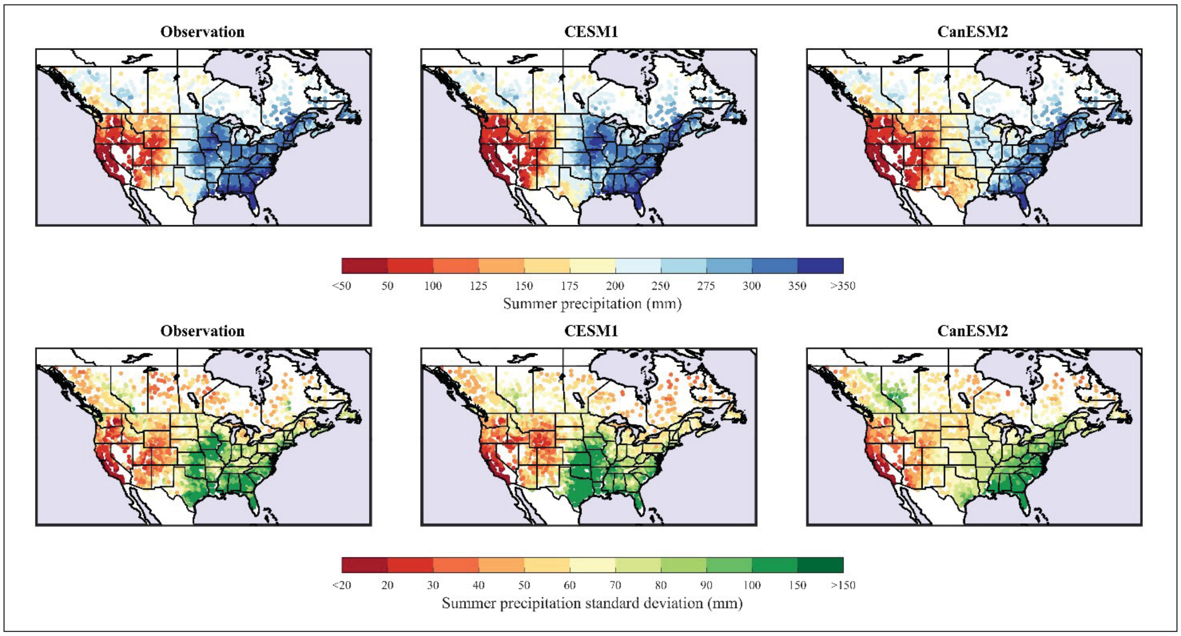

Figure 3.3 Mean summer precipitation (top) and its standard deviation (bottom) in the reference period (1980-2009) in observation (left), CESM1 (middle) and CanESM2 (right) large ensembles

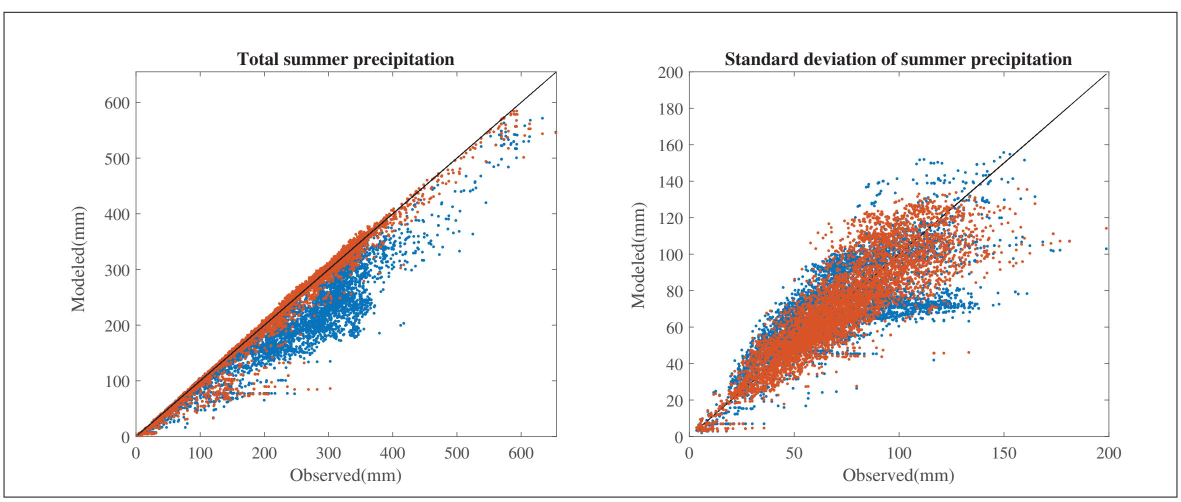

Figure 3.4 Correlation between the observation and CanESM2 (blue dots) or CESM1 (orange dots) for total summer precipitation (left) and standard deviation (right)

The climate models' temperature outputs were also validated, similarly to summer precipitation. The results are shown in Supplementary Figure 3.11 to Figure 3.13. Summer temperature is well represented by both climate model ensembles. Inter-model differences are much smaller for temperature than for precipitation. Spatial variability is reproduced slightly better by CESM1. Summer temperature is overestimated in the western part of North America and underestimated in the eastern part in CESM1, while CanESM2 overestimates the standard deviation over most of North America with the exception of Central CA.

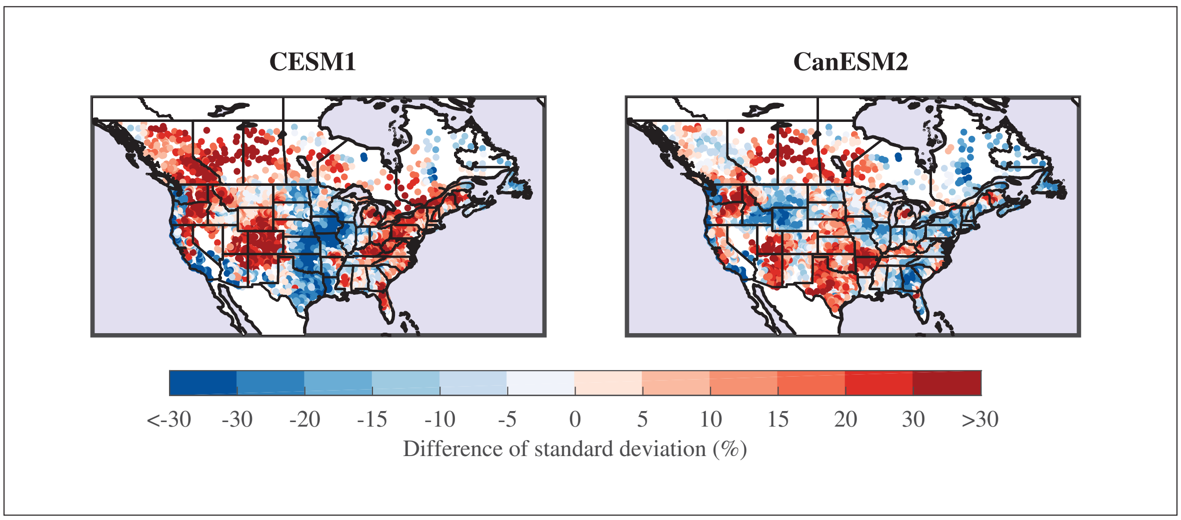

Figure 3.5 Difference in summer precipitation standard deviation between CESM1 (left) or CanESM2 (right) and observation. Blue represents underestimation while red means overestimation of the standard deviation

3.5.2 Future meteorological droughts

This paper looked at 2-, 20-, and 100-year droughts for two future time periods. Patterns were found to be very similar for both horizons and return periods, with the only difference being the change of magnitude in the more distant future. Accordingly, the main body of this paper will focus on the 100-year droughts over the more distant time horizon (2070-2099). The 2-year drought patterns are also shown to outline any potential difference between frequent and extreme drought patterns in the future. Results for the 20-year droughts and the 2036-2065 period are presented in the Supplementary Material (Figures 3.14 and 3.15).

Figure 3.6 presents the expected frequency change of future 2-year and 100-year meteorological droughts (deficit in precipitation) for both ensembles. These figures only show the relative change of future drought frequency, rather than the drought severity, similarly to what Martel *et al.* (2018) did. The spatial pattern for the 2- and 100-year droughts are very similar, indicating that changes in moderate and extreme meteorological droughts head in the same direction for each climate model. There are, however, obvious differences between the two climate models in both the direction and magnitude of the changes.

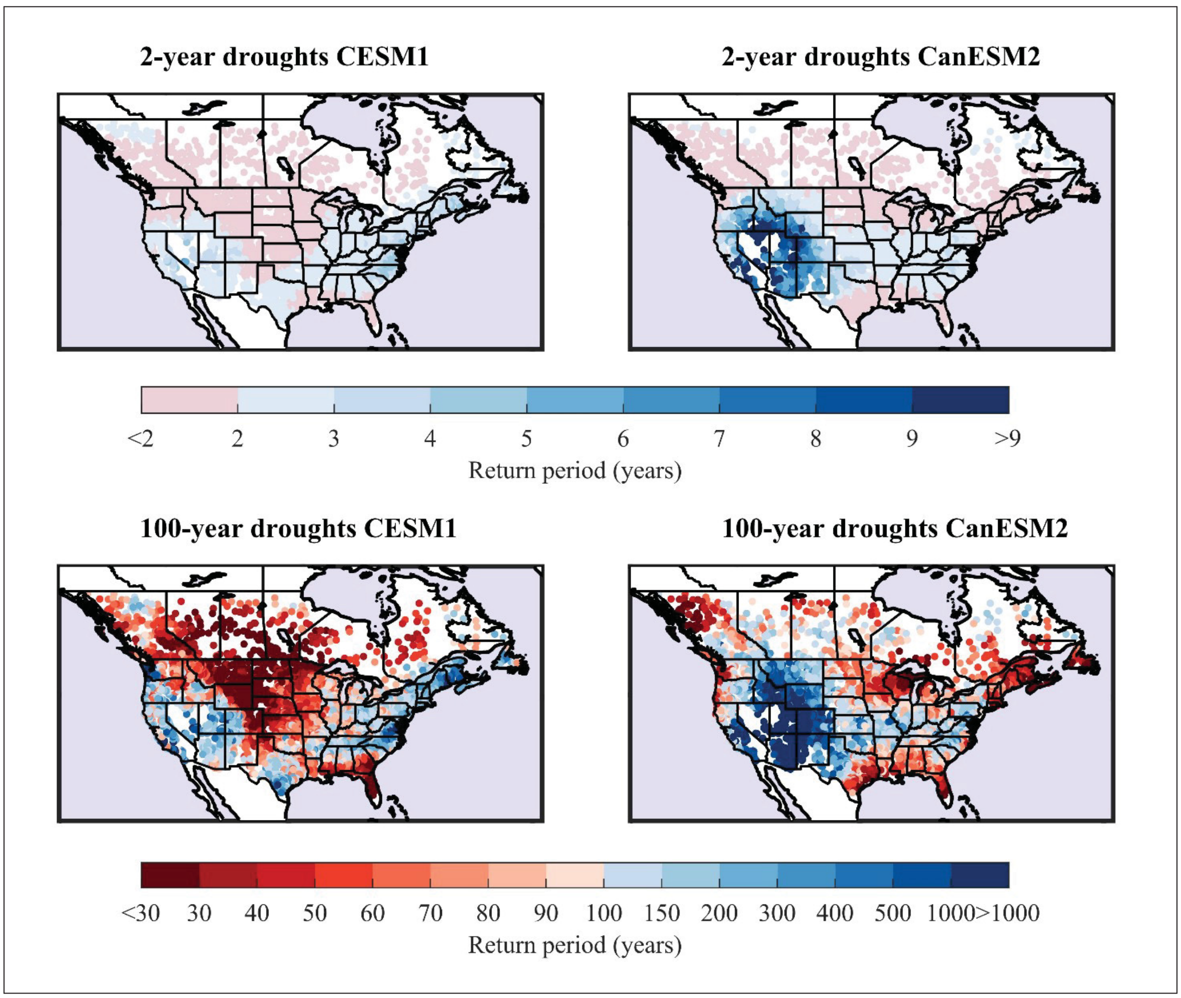

Figure 3.6 Change in the mean summer 1-month meteorological drought frequency in the far future (2070-2099) relative to the reference period (1980-2009). 2-year (top) and 100-year (bottom) droughts for the CESM1 (left) and CanESM2 (right) ensembles. Red (blue) colors indicate an increase (decrease) in the drought frequency

Both climate models predict a worsening of summer meteorological droughts over most of Canada (West and Central Canada), Midwest and over the coast in the Southeast U.S. along the Gulf of Mexico. There are large differences over the High Plains and the East Canada. CESM1 consistently predicts direr future meteorological droughts, with the exception of Southern Texas and the Northeast. The worst changes in the 100-year meteorological drought frequency are observed in Florida, with up to a ten-fold increase for CanESM2 (the current 100-year meteorological drought becoming a 10-year drought in the distant future) and a 20-fold increase for CESM1.

Since meteorological droughts were assessed based on precipitation deficit alone, it is important to assess changes in future summer precipitation to better understand the link between mean and extreme changes in droughts. Figure 3.7 presents the relative change of total summer precipitation for both climate models for the distant future relative to the historical period. The precipitation change patterns for both climate models indicate a broadly similar pattern of decreasing summer precipitation in the North, with an increasing trend in most of the U.S. A comparison of Figures 3.6 and 3.7 shows that the spatial patterns are very similar, indicating a strong correlation between changes in extreme summer meteorological drought frequency and relative changes in mean total summer precipitation. Changes in future summer precipitation explain most of the differences in meteorological drought patterns observed in Figure 3.6. There are, however, minor regional differences, such as the Western U.S. coast for CESM1, where the 100-year droughts become less frequent despite projected decreases in summer precipitation.

3.5.3 Future hydrological droughts

Meteorological droughts are due mainly to precipitation deficit, while the process leading to hydrological droughts are more complex because they are the results of the non-linear interactions between climatic variables.

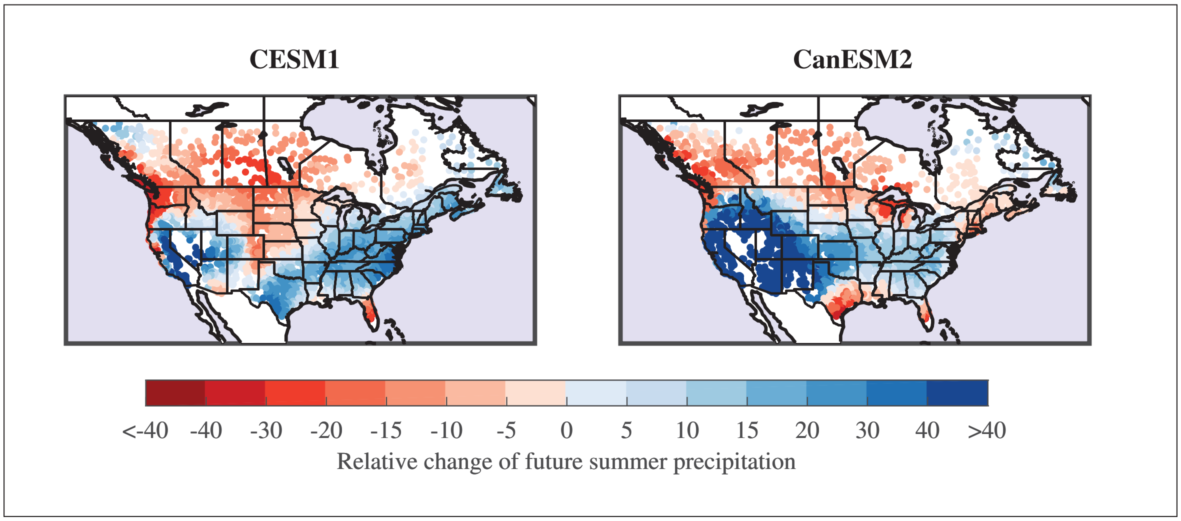

Figure 3.7 Relative change of ensemble mean future summer precipitation in the far future (2070-2099) for CESM1 (left) and CanESM2 (right)

Figure 3.8 presents changes for the 2- and 100-year hydrological droughts for the 2070-2099 period. Changes for the 20-year hydrological droughts and for the 2036-2065 period are shown in Figures 3.16 and 3.17, respectively. In comparison to meteorological droughts, results are much more consistent between climate models. Both models show large increases of frequency in hydrological droughts over almost all North American watersheds, including areas with increasing summer precipitation. The situation gets worse at the larger return periods. Increases in the 100-year drought frequencies can be as large as 22 times, in CanESM2, and 27 times, in CESM1, relative to the reference period. The Rocky Mountains (parts in West U.S and High Plains), and the Canadian West Coast are the only regions where a few watersheds do not see increases in hydrological drought frequency. The increasing frequency of future extreme hydrological droughts is clearly larger than that for future meteorological droughts.

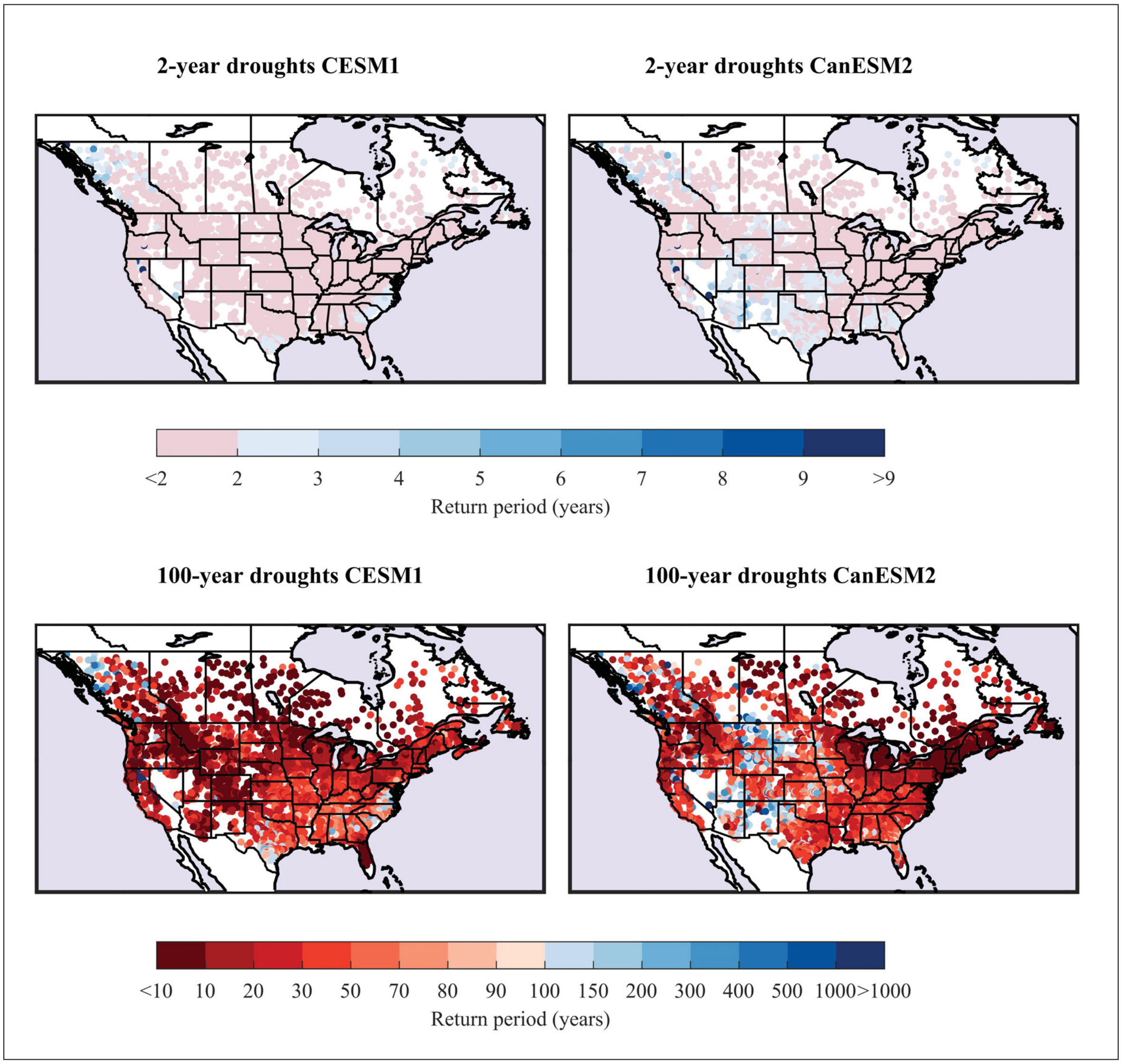

Figure 3.8 Same as Figure 3.6, but for 1-month summer hydrological droughts

3.6 Discussion

This paper assessed the climate change impacts on the change of future droughts, with 2-, 20- and 100-year return periods. Results showed that spatial patterns of changes are similar for all three return periods. However, changes in magnitude get larger for the longer return period. This progressively larger increase for longer return periods has equally been noted by others (e.g., Martel *et al.* (2020) for precipitation ranging from 1 hour to 5 days and Boo, K.-O., Kwon, W.-T. & Baek, H.-J. (2006) for temperature), and results from changes in future inter-annual climate variability. Changes for longer return periods are important since extreme events almost always lead to the largest socio-economic losses.

As has been observed in many other studies (Cook, B. I., Smerdon, J. E., Seager, R. & Coats, S., 2014; IPCC, 2013b; Lelieveld *et al.*, 2016; Tam *et al.*, 2018), projected changes are generally more important for the more distant future periods. This is especially the case in this study, where projected changes for hydrological droughts in the far future are more significant than those for meteorological droughts. This is likely because the former represents the non-linear combination of precipitation and temperature. Future changes in precipitation vary depending on the region (See Figure 3.7), sometimes helping to relieve drought problems, whereas temperature is consistently increasing over the entire North American domain (Figure 3.9). Projected mean summer temperature changes are very similar for both climate models, with a south-to-north gradient of progressively larger increases. CanESM2 projects the largest increases, and especially over Canada. Temperature changes have no direct link with meteorological droughts, but are an important driver of evapotranspiration, thus impacting soil moisture and hydrological droughts, in addition to the precipitation deficit. By the end of the century, the increase in temperature becomes the main driver of the hydrological drought process, thus resulting in larger changes, as compared to precipitation-only-driven changes for meteorological droughts. The same factors can also explain the differences in spatial areas affected by meteorological and hydrological droughts. Spatial patterns of future extreme meteorological and hydrological droughts for both future periods are shown in Figures 3.14 (3.15) and 3.16 (3.17), respectively, while the changes in magnitude are shown in Figures 3.18 and 3.19, along with Table 3.1.

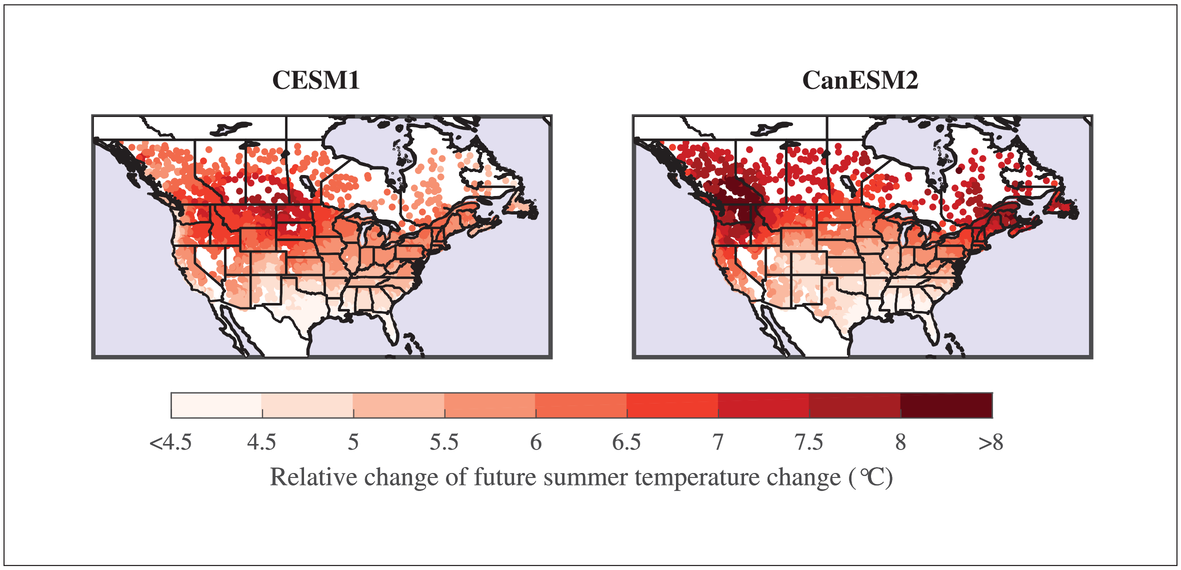

Figure 3.9 Relative change of ensemble mean future summer temperature in the far future (2070-2099) for CESM1 (left) and CanESM2 (right)

While the general conclusions apply to results of both large ensemble climate models used in this study, there are nonetheless notable differences in spatial patterns for the meteorological and hydrological droughts, and especially for meteorological droughts. Precipitation, which is the main driver of the meteorological droughts, presents larger inter-model variability than temperature, and this translates into large inter-model uncertainty. In addition, the Southern U.S. is a known region with large inter-annual variability (Wang, H., Fu, R., Kumar, A. & Li, W., 2010), and so it is expected to see large differences in spatial patterns of meteorological droughts between the two climate models. For extreme hydrological droughts, the increasing temperature is likely to be responsible for the intensified evapotranspiration, resulting in drier summer conditions. Since temperature displays less inter-model variability, the spatial patterns of extreme hydrological droughts are more consistent for both climate models. In addition, since CESM1 performed better against observed data over the reference period (for both mean summer precipitation and inter-annual variability), it could be inferred that results based on this model are more reliable, possibly in part due to its finer spatial resolution.

Since precipitation deficit is the main driver of meteorological droughts, it is perhaps intuitive to expect that more future precipitation would bring fewer droughts, and vice-versa. However, changes in variability may impact extremes differently. Figures 3.6 and 3.7 indicated that the main driver behind spatial patterns of extreme meteorological droughts appeared to result from the future changes in summer precipitation amounts. Figure 3.10 further explores this by mapping the direction of the changes between precipitation and meteorological droughts. Four patterns are therefore mapped. Regions in blue (decrease in precipitation and increase in drought, noted (P-/D+) and red (P+/D-) are consistent with this intuitive understanding of changes. Regions in green (P+/D+) show watersheds where an increase in precipitation nonetheless results in increasing meteorological drought frequencies. These watersheds are usually located in the transition area between blue and red zones, and become more common for the extreme droughts, showing how increasing inter-annual variability affecting extremes more than mean values. The number of watersheds in purple (P-/D-), indicating a decrease in extreme meteorological droughts despite a decrease in mean precipitation, is very small. Purple areas are only found in dry areas of the Southern U.S. for 2-year droughts and in the Northwestern U.S. for 100-year droughts. Northwestern U.S. is more sensitive to climate variability, and these gray regions might possibly see lower variability in future summer precipitation.

In opposition to meteorological droughts, changes in hydrological droughts result from a combination of more than one variable, and are more difficult to infer simply by looking at changes in precipitation and temperature alone. As discussed above, temperature increases appear to be the dominant factor in driving the large increases in hydrological drought frequency predicted for most of North America. The process by which these changes affect droughts have not been systematically studied, although they vary depending on watershed latitudes. The projected decrease in summer precipitation will amplify this water shortage, thus explaining the large increases in extreme drought frequency observed for those watersheds. In the South, increased evapotranspiration is somewhat overcome by the projected increase in summer precipitation, thus resulting in less severe increases in drought frequency.

The hydrological drought frequency increase predictions over North American watersheds are in line with the findings of other studies (Burke & Brown, 2008; Cook *et al.*, 2014,1; Prudhomme *et al.*, 2014; Tam *et al.*, 2018). Increases in evapotranspiration driven by higher temperatures have been shown to have pronounced effects on droughts over the Central Plains (these cover parts of south, High Plains and West Canada in this work) and Western U.S. (Anchukaitis *et al.*, 2016; Cook *et al.*, 2014).

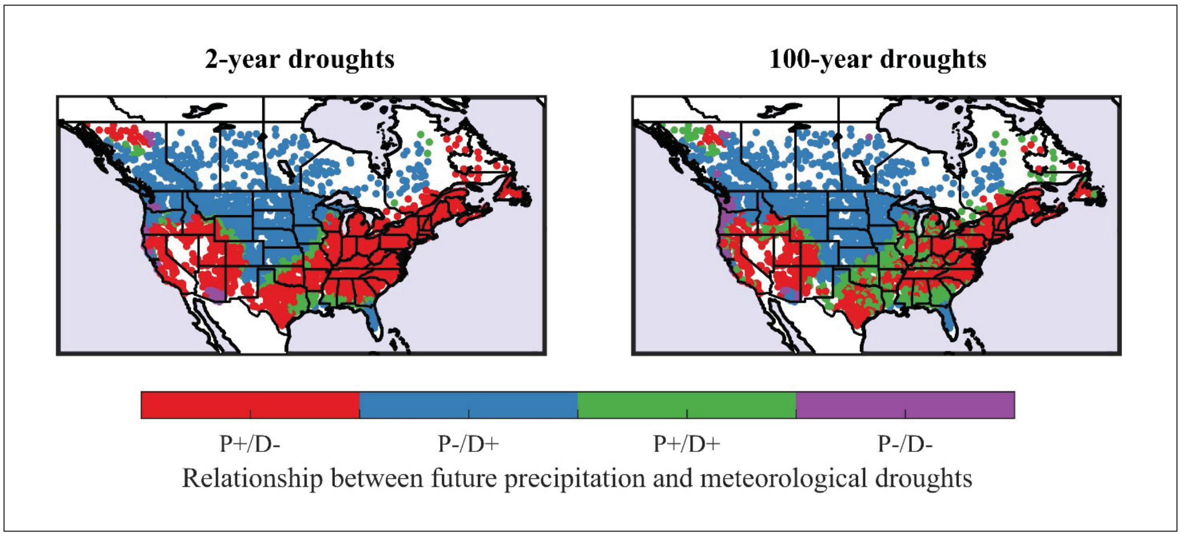

Figure 3.10 Agreement and disagreement of the change direction between far future (2070-2099) summer meteorological droughts and precipitation in CESM1. Only CESM1 was shown as it is more reliable with a better performance and finer resolution. The change direction is defined by the change of future precipitation or meteorological droughts in the more distant future compared to the reference period. 'P+/D-' means more precipitation leads to fewer droughts; 'P-/D+' means more future droughts result from less precipitation; 'P+/D+' means more precipitation but more droughts; 'P-/D-' means less future precipitation and fewer summer droughts

It is important to stress that several limitations may affect the results presented in this work. Two GCMs are likely to be insufficient to robustly assess precipitation change over the U.S., where there is large inter-model variability, and especially so in the South (Wuebbles *et al.*, 2016). This is especially true for meteorological droughts. However, by choosing these two available large ensembles, we were able to remove the uncertainty in the statistical estimation of extremes. Using many single-member GCMs would reduce the structural uncertainty, at the expense of increasing the uncertainty of extreme computation. Droughts were only assessed under the RCP8.5 emission scenario, which is a pessimistic scenario corresponding to a pathway with the higher emissions of greenhouse gases (Riahi, K., Rao, S., Krey, V., Cho, C., Chirkov, V., Fischer, G., Kindermann, G., Nakicenovic, N. & Rafaj, P., 2011), because no other RCPs were available for those large ensembles. The world is currently on an extreme scenario pathway, but this may change in the next decades. This uncertainty is therefore more important for the more distant future period. Only two drought indices were used in this study: SPI for meteorological droughts and SDI for hydrological droughts. The use of other indices may have led to different frequency increases since drought assessment is largely dependent on selection of indices (Burke & Brown, 2008; Diffenbaugh, N. S., Swain, D. L. & Touma, D., 2015). Finally, a single hydrological model was used to compute projected future streamflows. The hydrological model structure (particularly for processes driving evapotranspiration) may impact the computation of low flows (Chen *et al.*, 2011b; Troin *et al.*, 2018; Wilby, R. L. & Harris, I., 2006).

This work has not focused on the physical processes leading to the above changes and how they propagate between both types of droughts. More work should therefore focus on better understanding the factors controlling the onset, duration, and severity of agricultural and hydrological droughts. This better understanding will lead to better adaptation to changing drought conditions (Diffenbaugh *et al.*, 2015; Wanders, N. & Wada, Y., 2015; Wang, W., Ertsen, M. W., Svoboda, M. D. & Hafeez, M., 2016). The likelihood of droughts can be related to sea surface temperature anomalies (Cook *et al.*, 2007; Jiménez-Muñoz *et al.*, 2016; Wang, S., Yuan, X. & Li, Y., 2017). A full grasp of the potential linkage between the teleconnections and prolonged droughts conditions could allow for early warnings and preventive actions for water conservation and agricultural planning (Okumura, Y. M., DiNezio, P. & Deser, C., 2017). Last but not least, the uncertainty envelop related to the modeling chain (GCM/ESM, RCP, downscaling, impact model/drought index) as discussed in other studies (Chen *et al.*, 2011a,1; Minville, M., Brissette, F. & Leconte, R., 2008; Wilby & Harris, 2006) could be better delineated.

3.7 Conclusion

This work looked at future trends of extreme short-term meteorological and hydrological droughts over North America, using two climate model (CanESM2 and CESM1) large ensembles. The use of large ensembles allows for the robust estimation of 100-year droughts. Hydrological droughts were studied over 4521 watersheds by using bias-corrected climate model precipitation and temperature as inputs to the GR4J-CemaNeige-Oudin lumped hydrological model. The Standardized Precipitation Index and Standardized Drought Index were used to respectively assess meteorological and hydrological future summer droughts. The main conclusions of this work are as follows:

1) Both climate models performed well at reproducing observed mean summer precipitation and inter-annual variability over the reference period. CESM1 in particular displayed little to no bias for summer precipitation on all watersheds, with the exception of some arid watersheds. This gives confidence in the models' ability to adequately project future droughts.

2) Trends for meteorological droughts, which are mainly linked to precipitation deficit, showed varying spatial patterns, with some regions seeing increases (West and Central Canada, Midwest and Southeast coast) and others seeing decreases, in drought frequency. The evolution of meteorological drought patterns matched future expected changes for mean summer precipitation. Because of changes in variability, some regions (e.g., Southeast U.S.) will nonetheless see increasing meteorological drought frequency despite increases in mean summer precipitation. This is especially notable for the larger 100-year return period. The median increase in meteorological droughts over North America would be roughly 2-fold in the far future.

3) Hydrological droughts, which combine the effect of precipitation and temperature changes, show a very uniform pattern of worsening droughts, and that increases in temperature overcome the expected increasing mean summer precipitation in some regions. The few watersheds escaping this trend are either located in colder climates (Canadian West Coast, Rocky Mountains) or in regions with the largest projected increase in precipitation, such as

Southern Texas. The frequency changes for the 100-year hydrological drought are quite severe for several watersheds, with 4.3-fold median increase (the 100-year drought becomes a 23-year drought), but up to a 27-fold increase for the most affected watersheds.

4) Predicted changes for both meteorological and hydrological droughts get consistently worse for the longer considered return periods. In other words, frequency changes for the 100-year droughts are more significant than those expected for the 2- and 20-year droughts. This gradual worsening toward larger extremes has been noted in other studies, and is an economically important consequence of a changing climate.

3.8 Acknowledgments

This work was supported by the Natural Sciences and Engineering Research Council of Canada (Grant No. RGPIN-2015-05048). The authors acknowledge the contribution of Environment and Climate Change Canada's Canadian Centre for Climate Modelling and Analysis for making the CanESM2 Large Ensemble simulations available in this study. This large ensemble is available on the Government of Canada website (https://open.canada.ca/data/en/dataset/aa7b6823-fd1e-49ff-a6fb-68076a4a47\7c). The authors would also like to thank the Ouranos Consortium for helping with data transfer. The CESM1 large ensemble was downloaded from the Large Ensemble Community Project (LENS) website (http://www.cesm.ucar.edu/projects/community-projects/LENS/). The observed meteorological data and watershed boundaries over the Canadian part were downloaded from the CANOPEX database (http://canopex.etsmtl.net/).

3.9 Supplementary materials

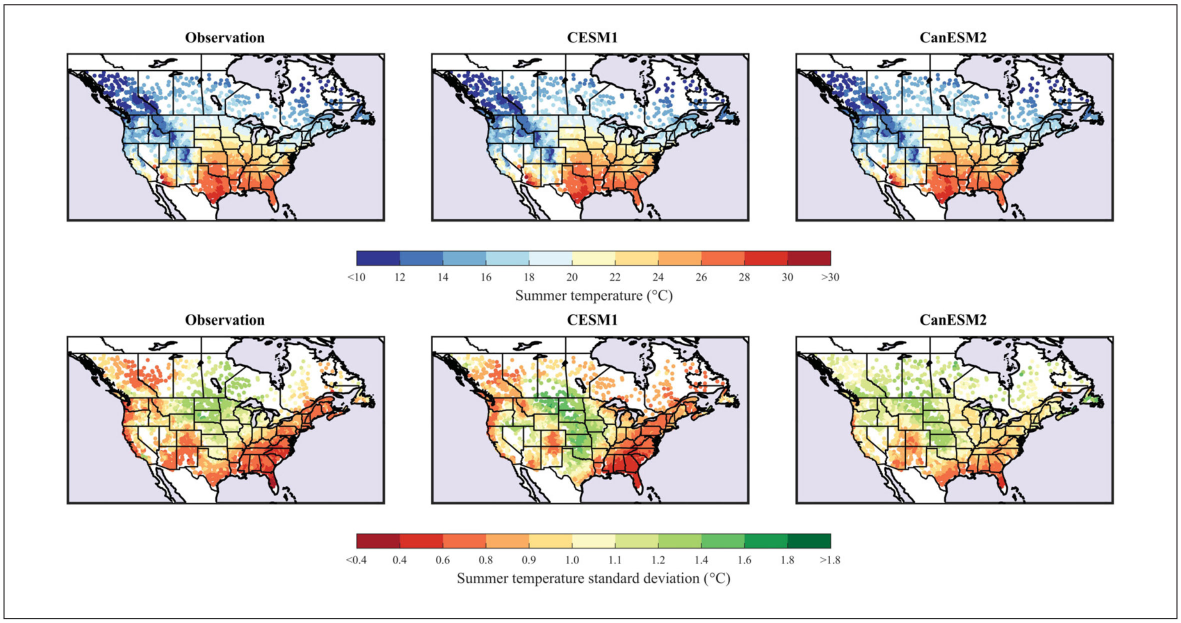

Figure 3.11 Mean summer temperature (top) and its standard deviation (bottom) in the reference period (1980-2009) in observation (left), CESM1 (middle) and CanESM2 (right) large ensembles

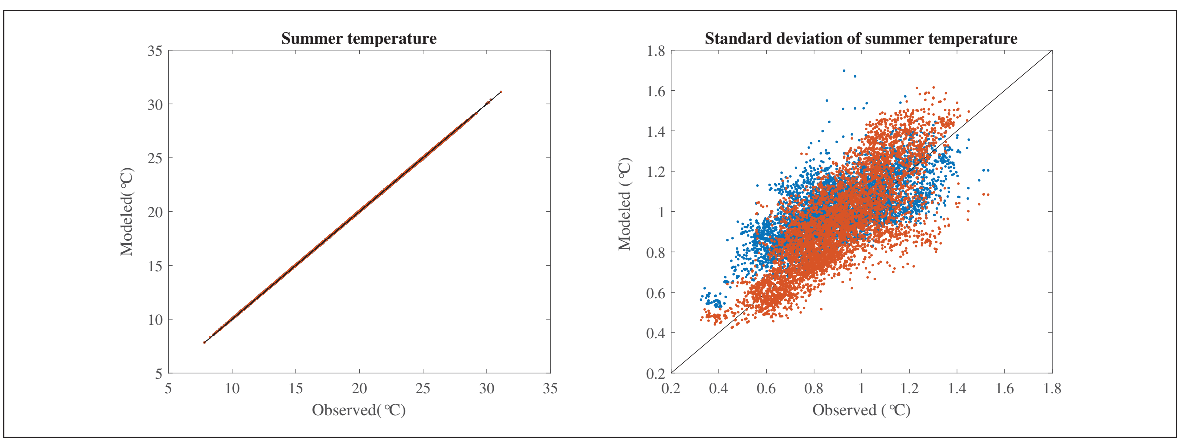

Figure 3.12 Correlation between the observation and CanESM2 (blue dots) for total summer temperature (left) and standard deviation (right)

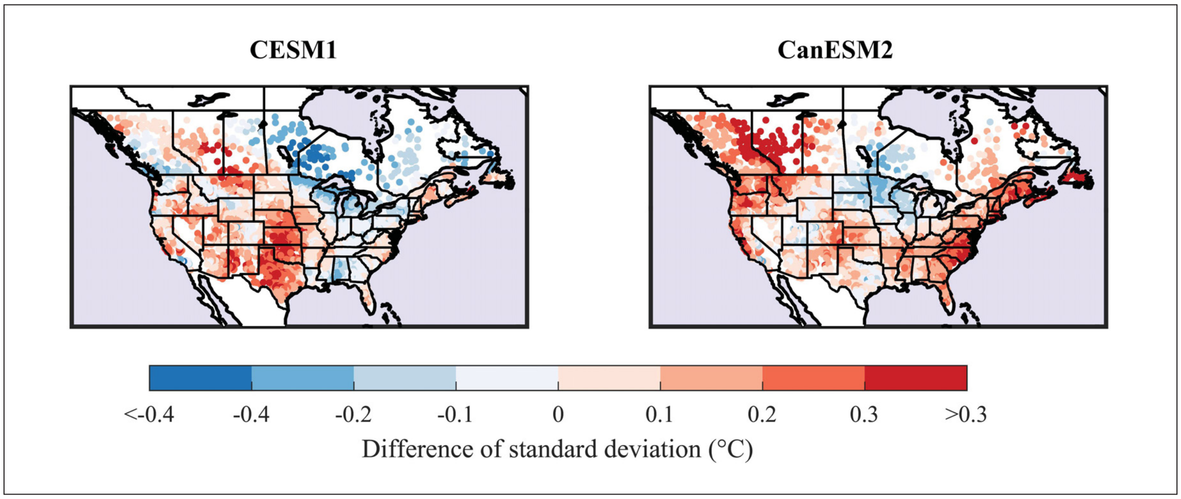

Figure 3.13 Difference in summer temperature standard deviation between CESM1 (left) or CanESM2 (right) and observation. Blue represents underestimation while red means overestimation of the standard deviation

Table 3.1 The largest change amplitude in the frequency of the extreme meteorological and hydrological droughts in two climate model large ensembles

Type	**Period**	**Meteorological droughts**				**Hydrological droughts**			
		CanESM2		CESM1		CanESM2		CESM1	
		Max	Dry range	Max	Dry range	Max	Dry range	Max	Dry range
20-year	Near future	2.8	1.0-2.1	3.0	1.0-2.0	16.5	1.3-4.0	15.1	1.1-4.4
	Far future	6.4	1.0-3.0	8.3	1.0-3.9	19.9	1.2-9.2	19.7	1.3-10.2
100-year	Near future	4.3	1.0-3.1	4.7	1.0-3.0	46.3	1.3-6.7	67.5	1.1-8.1
	Far future	9.6	1.0-4.0	20.5	1.0-7.2	90.7	1.2-21.8	97.3	1.5-26.7

Note:‘2.8’ in the table means that the 20-year droughts in the near future would be 2.8 times frequent than the reference period in CanESM2. The Dry range is calculated based on the watersheds with the increasing drought frequency trend only, 5^{th} to 95^{th} quantile.

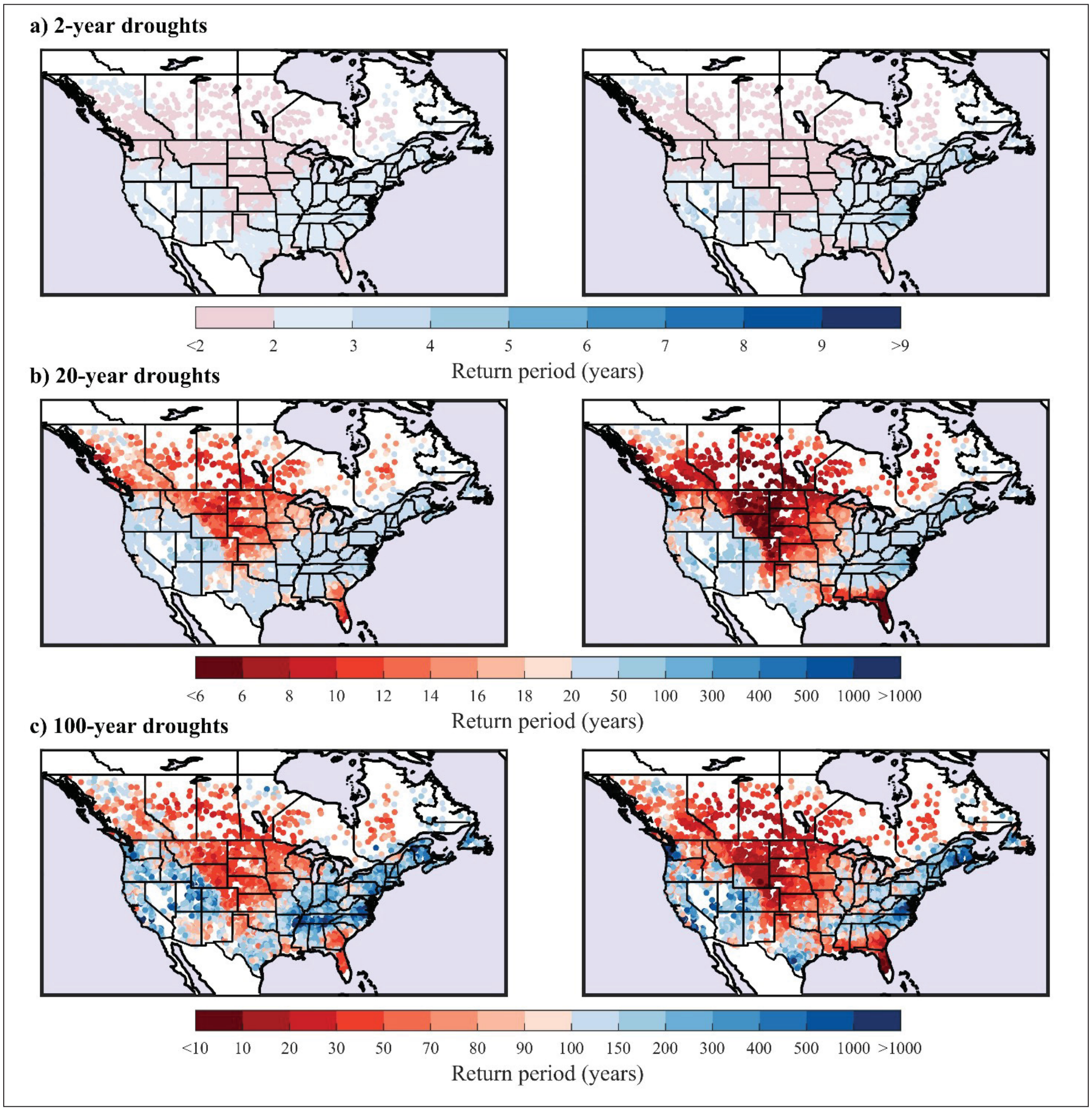

Figure 3.14 Change in the mean summer1-month SPI drought frequency in the near (left column) and far (right column) future relative to the reference period for CESM1. The upper panel is for the 2-year return period change relative to the reference period. The middle and bottom panel present changes in frequency for both the 20 and 100-year return periods. Red means an increase in drought frequency while cooler colors indicate a decrease

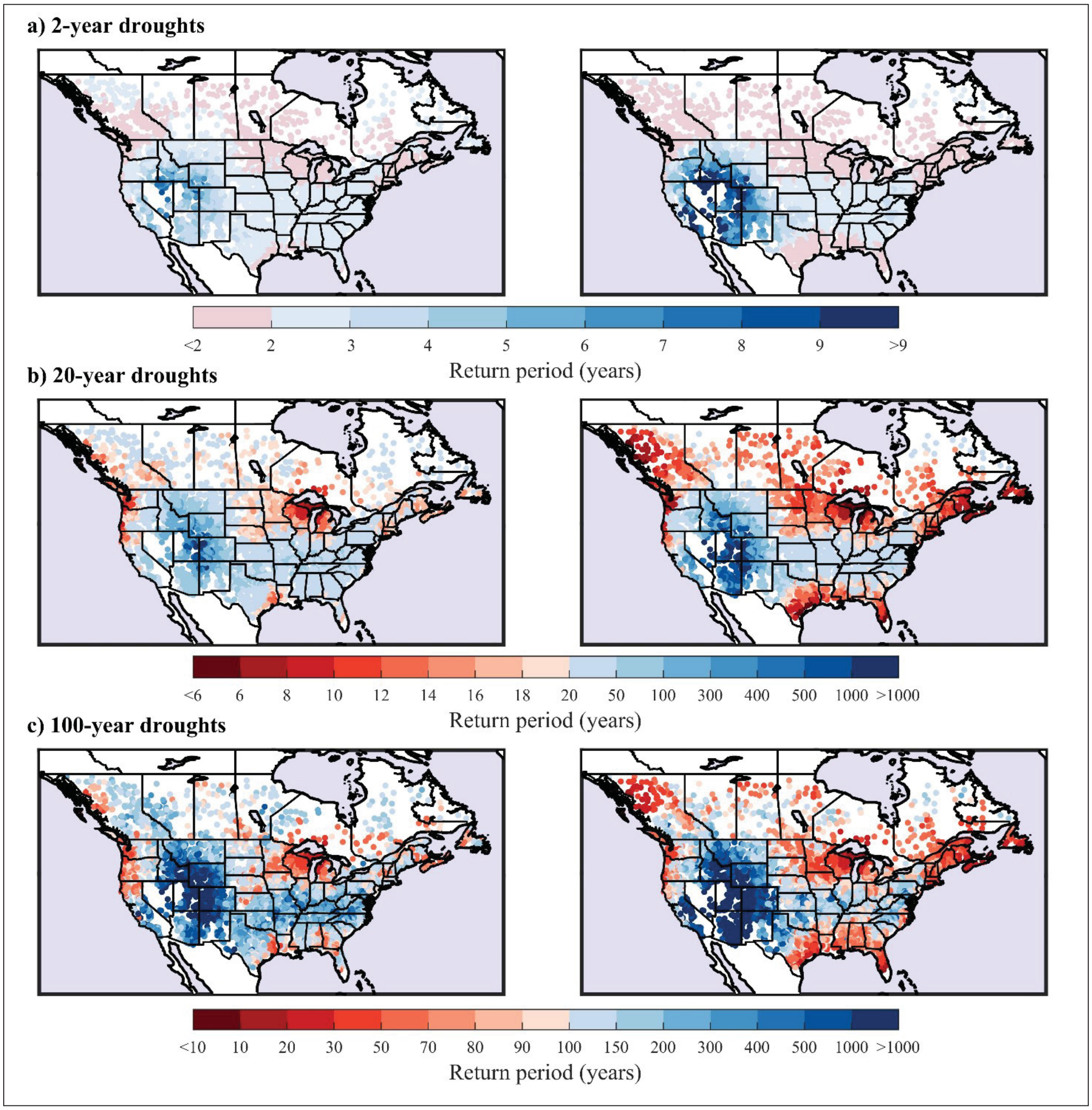

Figure 3.15 Same as Figure 3.14, but for mean summer 1-month SPI for CanESM2

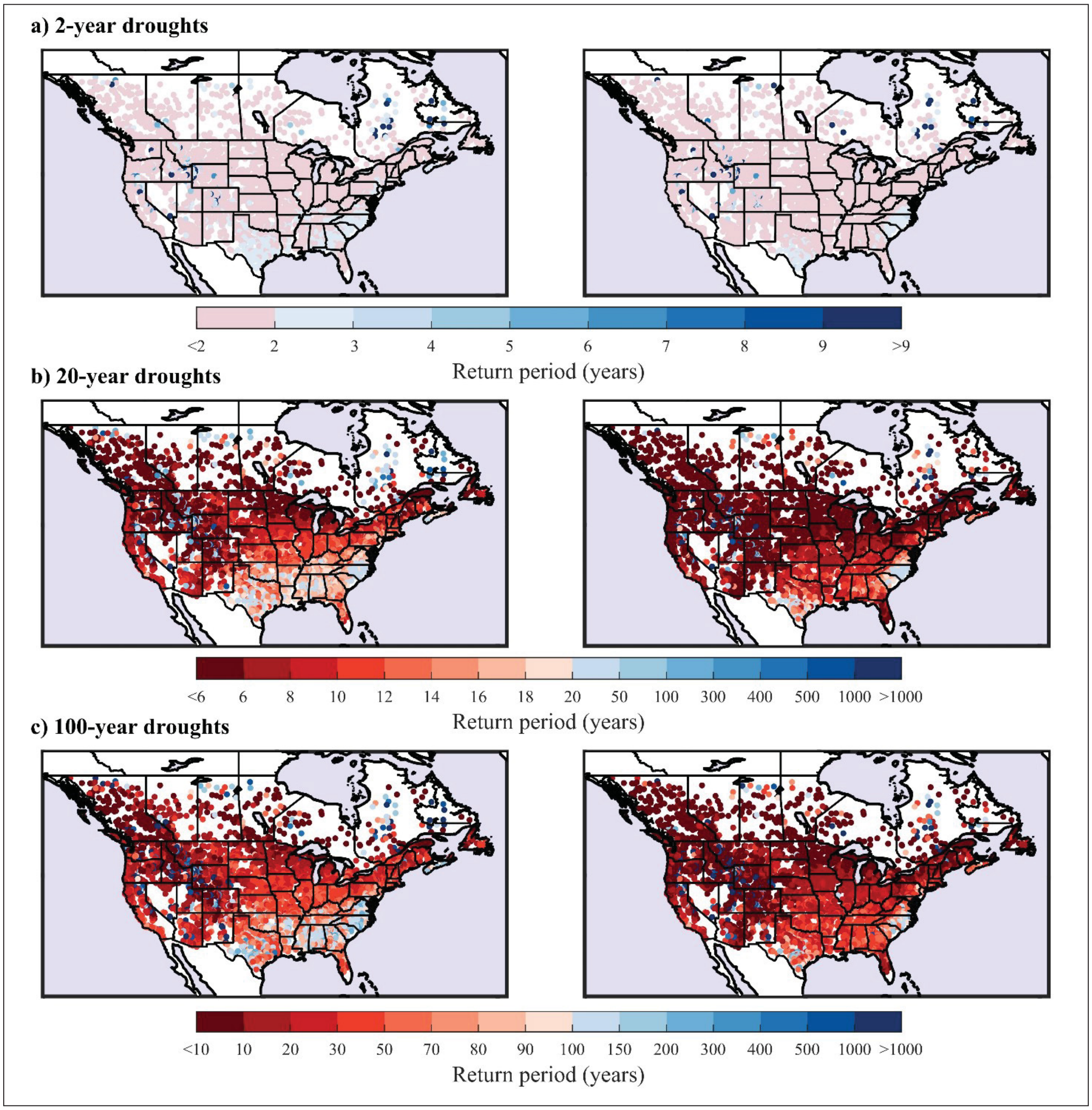

Figure 3.16 Same as Figure 3.14, but for mean summer 1-month SDI drought frequency for CESM1

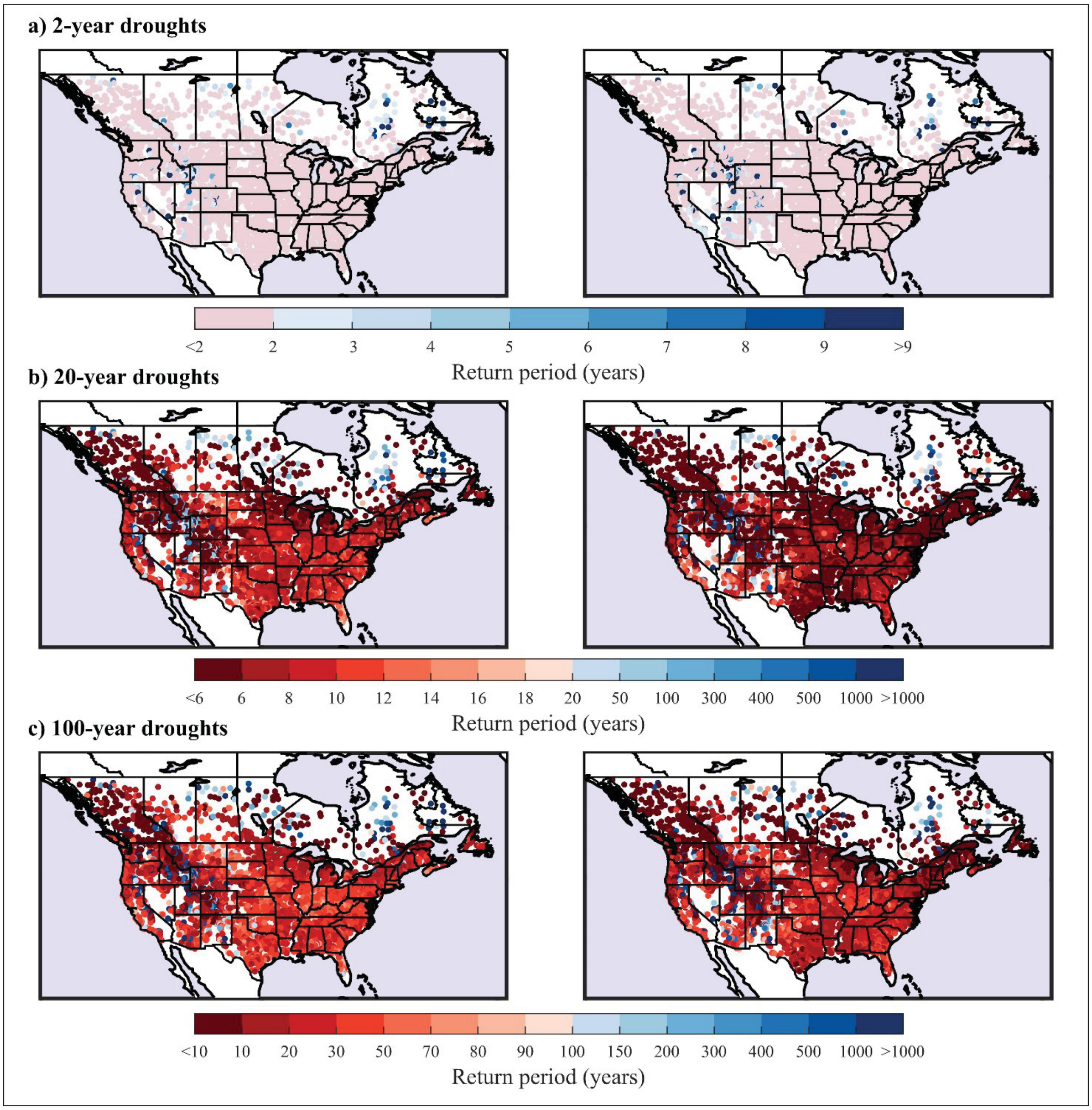

Figure 3.17 Same as Figure 3.14, but for mean summer 1-month SDI drought frequency for CanESM2

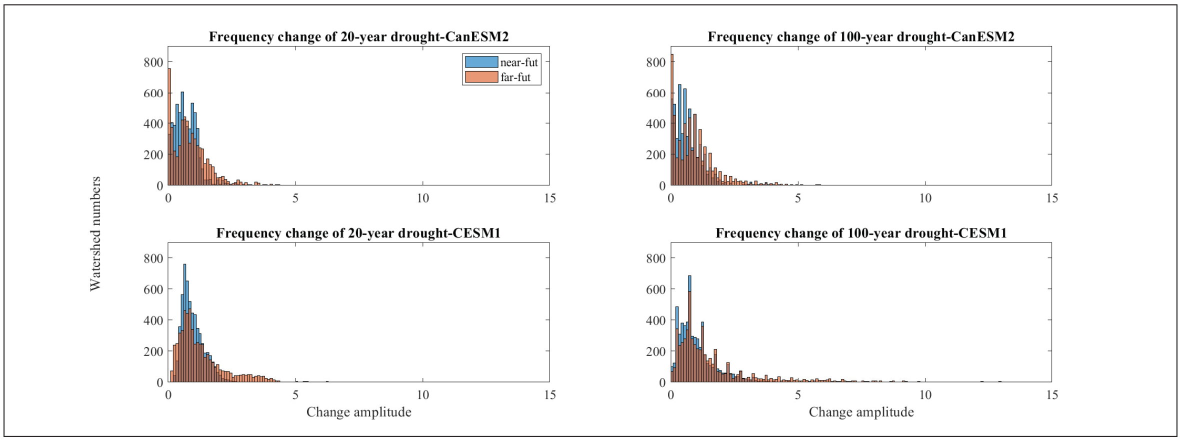

Figure 3.18 The changing amplitude in meteorological droughts in near- and far-future periods in two climate models. The largest change amplitude could reach 20.5 times in CESM1 in the far-future period, but the x-axis was limited to 15 for easier comparison

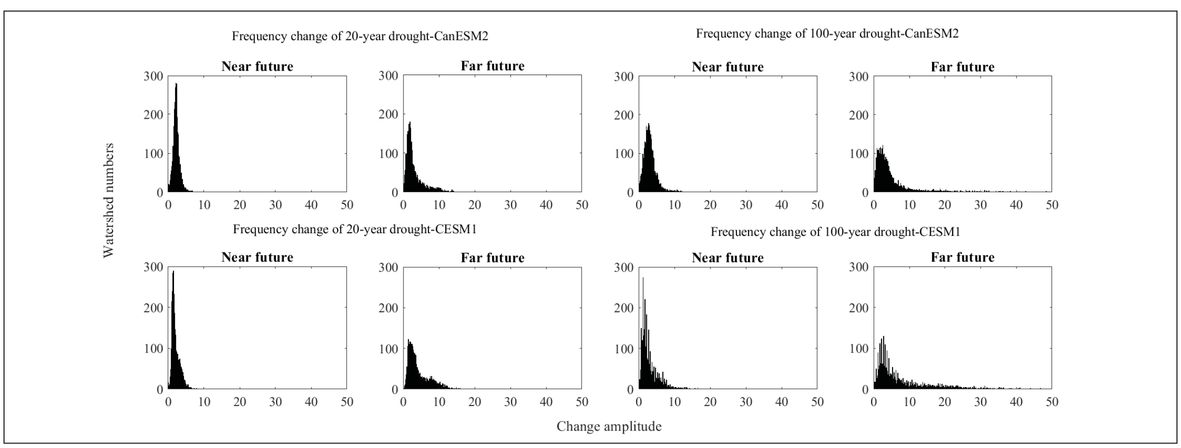

Figure 3.19 Change amplitude in hydrological droughts in near- and far- future periods in two climate models. The largest change amplitude could reach 90.7 times in CanESM2 and 97.3 times in CESM1 respectively in the far-future period, the x-axis was limited to 50 for easier comparison

CHAPTER 4

IMPACTS OF LARGE-SCALE OSCILLATIONS ON CLIMATE VARIABILITY OVER NORTH AMERICA

Cha Zhao[1], François Brissette[1]

[1] Department of Construction Engineering, École de Technologie Supérieure,
1100 Notre-Dame West, Montreal, Quebec, Canada H3C 1K3

Paper submitted for publication, February 2020

4.1 Abstract

The ocean is the main driver of internal climate variability. Therefore, a lot of work has been done to link regional hydroclimatic variability to large-scale oscillations representing the state of the combined ocean and atmosphere. However, the relatively short length of the historical record limits our ability to study the impact of these oscillations on the regional climate, and in particular, with respect to the interactions between the various ocean states represented by those oscillations. This work uses outputs from the Canadian Earth System Model large ensemble (CanESM2-LE) to study the impact of three large-scale oscillations on temperature and precipitation anomalies over 5797 North American catchments. The 50-member ensemble provides data series covering 2500 years to study the interactions between the El Niño Southern Oscillation (ENSO), Pacific Decadal Oscillation (PDO) and Atlantic Multidecadal Oscillation (AMO) over the 1961-2010 period.

The main characteristics of all three oscillations were well reproduced by CanESM2-LE. The impact of each oscillation was considered independently (with the others in their neutral phases), as well as combined with the other two (e.g., all three in non-neutral phases). The results outline a dominant role of ENSO in annual precipitation and of AMO in annual temperature over most of North America. The impact of ENSO on temperature was only significant along the West coast.

PDO does not have a significant impact on precipitation and temperature. The dominant roles of ENSO on precipitation and AMO on temperature are enhanced by interactions between these indices. These impact of interactions are consistent with their independent ones. At the regional scale, Western US was the most sensitive to variations in large-scale patterns.

Even though this study is conducted in a modeled world, the interactions are consistent with our understanding derived from observations. The results therefore extend our understanding of the relationship between large-scale oscillations and climate variability over North America and highlight the importance of considering the interactions between oscillations in order to better understand internal hydroclimatic variability.

Keywords: climate variability; teleconnection; individual effect; coupled effect; North America

4.2 Introduction

The Earth's mean average temperature increased by $0.85°C$ over the 1880 to 2012 period (IPCC, 2013b). This rate of warming, unprecedented in the geological record, has an impact on all components of the climate system (Tingley, M. P. & Huybers, P., 2013). To address the many potential effects of global warming, accurate climate projections at higher resolution are needed. However, climate change is due not only to human activities, but also to internal climate variability (Ahn, K.-H., Merwade, V., Ojha, C. & Palmer, R. N., 2016; Hulme *et al.*, 1999; IPCC, 2001). Therefore, a better understanding of the concept is crucial because the variability limits the predictability of future climate by adding additional uncertainty to that related to climate sensitivity. In addition, internal variability is unlikely to be reduced by improvements to climate models and emission scenarios (Deser *et al.*, 2012a). Patterns of internal variability are complex, and vary by location and spatial and temporal scales. Future impacts of anthropogenic forcing can be more easily evaluated in regions with lower internal variability.

Regional hydroclimatic variability is typically related to large-scale oscillations in atmospheric and oceanic patterns (Cayan, D. R., Dettinger, M. D., Pierce, D., Das, T., Knowles, N., Ralph,

F. M. & Sumargo, E., 2016). Long-term (multi-year, decadal or longer) climate anomalies can have considerable impacts on ecosystems and societies (Mantua, N. J. & Hare, S. R., 2002). A better understanding of the impact of large-scale oscillations on climate variability therefore represents an important research area. Climate indices are commonly used to characterize atmospheric and oceanic circulation patterns. Indices can be calculated as station or region average (e.g., Southern Oscillation Index) or by extracting leading patterns using the empirical orthogonal function, such as in the case of the Pacific Decadal Oscillation Index (PDO). Climatic indices are based on a single variable (e.g., sea surface temperature (SST) or sea level pressure (SLP)) or on a combination thereof (e.g., temperature and precipitation) (NCAR, 2019).

Some of these indices have been shown to influence hydroclimatic variability over North America. The main indices that are explored in the scientific literature are the El Niño-Southern Oscillation (ENSO), the Pacific/North American pattern (PNA), the North Atlantic Oscillation (NAO), the Pacific Decadal Oscillation (PDO) and the Atlantic Multi-decadal Oscillation (AMO) (Barlow *et al.*, 2001; Cayan *et al.*, 1999; Déry & Wood, 2004; Enfield *et al.*, 2001; Rogers & Coleman, 2003; Stewart *et al.*, 2005). Most of the literature focuses on these indices mostly by looking at their independent contribution to hydroclimatic variability at the watershed or state level (Cayan *et al.*, 1999; Gan, Z., Guan, X., Kong, X., Guo, R., Huang, H., Huang, W. & Xu, Y., 2019; McCabe *et al.*, 2004; Schmidt *et al.*, 2001). Kurtzman & Scanlon (2007), Schmidt *et al.* (2001), and Trenberth & Guillemot (1996) found that El Niño has a strong impact in this context, and leads to reduced precipitation in the Midwest and increased precipitation and streamflow in the Gulf of Mexico regions. PDO is the dominant pattern of decadal variability in the Northern Pacific (Mantua *et al.*, 1997). Initially, it was believed that PDO was driven by ENSO (Knutson, T. R. & Manabe, S., 1998; Newman, M., Compo, G. P. & Alexander, M. A., 2003), but other researchers suggested that they were mainly independent processes that can potentially interact with one another (Vimont, D. J., 2005). Trenberth & Guillemot (1996) found the impact of PDO on winter precipitation to be significant only in the Southern Central United States (U.S.). AMO is known to have an influence on precipitation in North

America (Enfield *et al.*, 2001; McCabe *et al.*, 2004). Precipitation and AMO have a negative correlation over the U.S., especially in the Southeast (Enfield *et al.*, 2001; Maleski & Martinez, 2018).

The coupled effect of dominant indices on hydroclimatic variability has been the focus of a much smaller number of studies (e.g., Coats, S., Smerdon, J. E., Cook, B., Seager, R., Cook, E. R. & Anchukaitis, K., 2016; Enfield *et al.*, 2001; Maleski & Martinez, 2018). These studies aim to better understand the potential constructive/destructive impact of the interactions between oscillations on the regional and local hydroclimatic variabilities. It has been found that while precipitation in North America is affected by both ENSO and AMO, a negative AMO could, however, help increase the correlation between ENSO and precipitation in the southeast (Enfield *et al.*, 2001). The North Pacific Index can interact with ENSO, resulting in a greater degree of surface temperature anomalies over North America, when they are out of phase (Yu et al., 2007). In addition, ENSO phases tend to be stronger and more stable during a positive PDO (Yu *et al.*, 2007). The combination of these two modes of variability has implications for future climate projections over North America (Gershunov & Barnett, 1998; Mantua *et al.*, 1997). For example, El Niño coupled with a positive PDO or AMO would lead to below-normal precipitation, whereas the impact of La Niña on temperature and precipitation (increased temperature and decreased precipitation) is increased during a positive AMO and PDO in the Southeast U.S. (Maleski & Martinez, 2018). Kurtzman & Scanlon (2007) used a statistical analysis of ENSO and PDO impacts on winter precipitation throughout the entire Southern U.S. at the climate-division resolution. The link between ENSO, NAO, AMO, and PDO on precipitation and temperature was evaluated by Stevens (2008), using a canonical correlation analysis. Non-parametric ranks-sum tests were used to better understand the individual and coupled impacts of ENSO, AMO and PDO on temperature and precipitation by Maleski & Martinez (2018) and on streamflows by Johnson *et al.* (2013).

The above studies consider the individual and coupled impacts of large-scale oscillations based on observations over the historical period. The length of the observation record leads to significant limitations in the exploration of the interactions between the various teleconnections, especially when considering the decadal-to-multidecadal scale of some of these indices. Theses limitations may also be overcome by using a large ensemble obtained from a single climate model. In this context, the climate model must however be able to generate sea surface temperature anomalies similar to those seen in the real world. Many of the main oscillations are reproduced by climate models, although the frequency and magnitude may differ (Flato *et al.*, 2013). More recent climate models (from the CMIP5 ensemble) have seen an improvement in the representation of ENSO, for example Bellenger, H., Guilyardi, É., Leloup, J., Lengaigne, M. & Vialard, J. (2014). Improvements have also been seen in the representation of the linkage between ENSO and observed precipitation anomalies over North America in CMIP5 (Langenbrunner, B. & Neelin, J. D., 2013). The constructive interference between ENSO and PDO is generally well reproduced in the CMIP5 ensemble (Fuentes-Franco, R., Giorgi, F., Coppola, E. & Kucharski, F., 2016). In addition, the second generation of the Canadian Earth System Model (CanESM2) skillfully represents AMO patterns at the multidecadal scale (Chylek, P., Li, J., Dubey, M., Wang, M. & Lesins, G., 2011).

A detailed and large-scale analysis of the coupled effect of the main large-scale oscillations on climate variability over North America is, however, still lacking. The aim of this study is therefore to improve the understanding of the coupled impacts of large-scale patterns on the North American climate, and how they affect temperature and precipitation. A better understanding of the interactions between ENSO, AMO and PDO may enhance the accuracy of empirical North American climate forecasts (Gershunov & Barnett, 1998; Maleski & Martinez, 2018; McCabe *et al.*, 2004). This study will also allow a comparison with other studies and lead to a more robust conclusion regarding the relationship between large-scale patterns and the North American climate.

4.3 Data

A total of 5797 watersheds are selected over North America for this work. In this corpus, 532 of the catchments are located in Canada, with the rest (5265) being in the contiguous U.S. The Canadian watershed boundaries are taken from the Canadian model parameter experiment CANOPEX database (Arsenault *et al.*, 2016) (https://sites.google.com/a/etsmtl.net/canopex/). The Canadian basins are spatially well distributed, with the exception of those in the Prairies. The boundaries of the U.S. catchments considered are extracted from the USGS database. The network of streamflow gauges is less dense over Canada and the average catchment area is larger. The median size of these watersheds is 1815km^2, and ninety percent of all of the watersheds range in size from 536 to 35,000km^2 ($min.area = 302km^2$, $max.area = 1.0741 \times 10^6 km^2$). The U.S. is divided into six regions, as presented in the United States Drought Monitor (https://droughtmonitor.unl.edu/), and from west to east, are: West US, High Plains, South, Midwest, Southeast, Northeast. Canada for its part is divided into 3 regions (no watershed data in the north in CANOPEX). Figure 4.1 presents a map showing the centroid of all North American watersheds and nine separate regions.

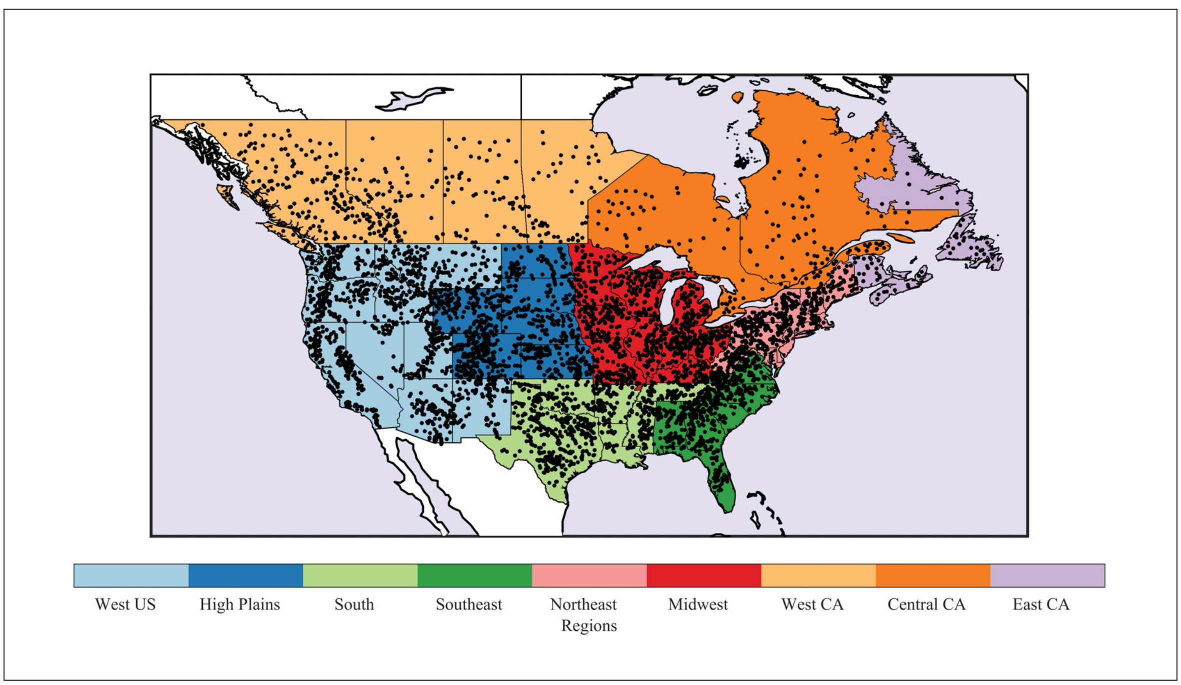

Figure 4.1 Distributions of the 5797 watersheds used in this study. The watersheds were divided into 6 regions in the U.S. and 3 regions in Canada

Precipitation, maximum and minimum temperature data, as well as sea surface temperature (SST), covering the 1961-2010 period were extracted from the Canadian Earth System Model large ensemble (CanESM2-LE). This work was conducted entirely in the context of a climate model, with the watershed boundaries representing the only real-world data. CanESM2-LE was run at a spatial resolution of $2.8^\circ \times 2.8^\circ$. Five original members derived from small atmospheric perturbations were computed over the 1850-1950 period to obtain 5 different ocean states. From 1950 to 2100, 10 random atmospheric perturbations were applied to each of the oceanic states, for a total of 50 members over the period. Historical forcing was used until 2005, and thereafter, was replaced by the Representative Concentration Pathway (RCP) 8.5 (Arora *et al.*, 2011; Sigmond & Fyfe, 2016; von Salzen *et al.*, 2013). The data for the model simulation covered the 1950-2100 period. Large ensembles generally allow the study of internal variability, and provide a better understanding of how the climate varies in the model world irrespective of any anthropogenic forcing present (Deser *et al.*, 2012a). For the 1961-2010 50-year selected period, the use of the CanESM2-LE resulted in 2500 years (50×50) to study the interactions between the different large-scale patterns. Monthly watershed precipitation and temperature were averaged from a minimum of four CanESM2 grid points closest to each watershed's centroid.

In the present study, the coupled impacts of large-scale oscillations are only analyzed in the climate world, and therefore, validation against observations is required. The characteristics of the CanESM2-LE simulated ENSO were compared with those of the computed NINO 3.4 index from the National Oceanic and Atmospheric Administration (NOAA) based on HadISST1 data (Rayner, N., Parker, D. E., Horton, E., Folland, C., Alexander, L., Rowell, D., Kent, E. & Kaplan, A., 2003). NOAA's Extended Reconstructed Sea Surface Temperature V4 database was used to validate the model performance in terms of simulating PDO and of the variability of SST in the North Atlantic (Huang, B., Banzon, V. F., Freeman, E., Lawrimore, J., Liu, W., Peterson, T. C., Smith, T. M., Thorne, P. W., Woodruff, S. D. & Zhang, H.-M., 2015a; Huang, B., Thorne, P. W., Smith, T. M., Liu, W., Lawrimore, J., Banzon, V. F., Zhang, H.-M., Peterson, T. C. & Menne, M., 2016; Liu, W., Huang, B., Thorne, P. W., Banzon, V. F., Zhang, H.-M., Freeman, E., Lawrimore, J., Peterson, T. C., Smith, T. M. & Woodruff, S. D., 2015). This dataset covers the period from 1854 to the present at the monthly time scale, with a spatial resolution of $2^\circ \times 2^\circ$.

4.4 Methodology

The NINO 3.4, AMO and PDO indices were calculated by using CanESM2 monthly SST data. The computation procedure of each index is described below.

The NINO 3.4 index is most commonly used to define El Niño and La Niña events. SST data were extracted over the NINO 3.4 region [5°N-5°S, 120°-170°W]. The mean climatology over the reference period (1981-2010) was first subtracted from monthly mean SST at the grid point scale. The SST anomaly was then area-averaged and a 5-month moving window was applied to smooth the NINO 3.4 index (Trenberth, K. E., 1997; Trenberth, K. E. & Stepaniak, D. P., 2001)

The AMO index was calculated similarly to NINO 3.4, with the difference that the global mean SST anomaly was subtracted from SST time series over the North Atlantic region [0-70°N, 0-80°W] in order to remove the global warming trend and leave internal variability untouched (Trenberth, K. E. & Shea, D. J., 2006). SST anomalies were then calculated relative to the monthly mean over the reference period and area-averaged over the North Atlantic region. Finally, the SST anomaly was smoothed with a 10-year (121-month) moving window (Enfield *et al.*, 2001).

The PDO is often regarded as a long-lived El Niño-like pattern in the North Pacific (Deser, C., Phillips, A. S. & Hurrell, J. W., 2004; Linsley, B., Wellington, G., Schrag, D., Ren, L., Salinger, M. & Tudhope, A., 2004; Mantua *et al.*, 1997; Newman *et al.*, 2003). It is represented by the leading pattern from an un-rotated Empirical Orthogonal Function (EOF) analysis of November through March monthly residual North Pacific SST anomalies (Hare, S. R., 1996; Mantua *et al.*, 1997; Zhang, Y., 1996). EOF is a statistical technique used to reduce the dimensionality of a dataset to reveal key temporal and spatial variability features (Weare, B. C. & Nasstrom, J. S., 1982). The empirical functions are often amenable to physical interpretation giving substantial insights into complex processes (Weare, B. C., 1979). The global mean SST anomaly was subtracted from the raw SST series for each North Pacific grid point [20°-70°N, 100°E-100°W] relative to the reference period. Then the seasonal cycle for each grid point was removed to obtain the regional SST anomaly. Finally, the EOF analysis was applied to find the first principal component (PC) of the SST anomaly over the North Pacific. The PDO index is the score of the first component smoothed with a 10-year moving window. The locations of Tropical Pacific (TPSST), North Pacific (NPSST) and North Atlantic (NASST) SSTs are shown in the Figure 4.2.

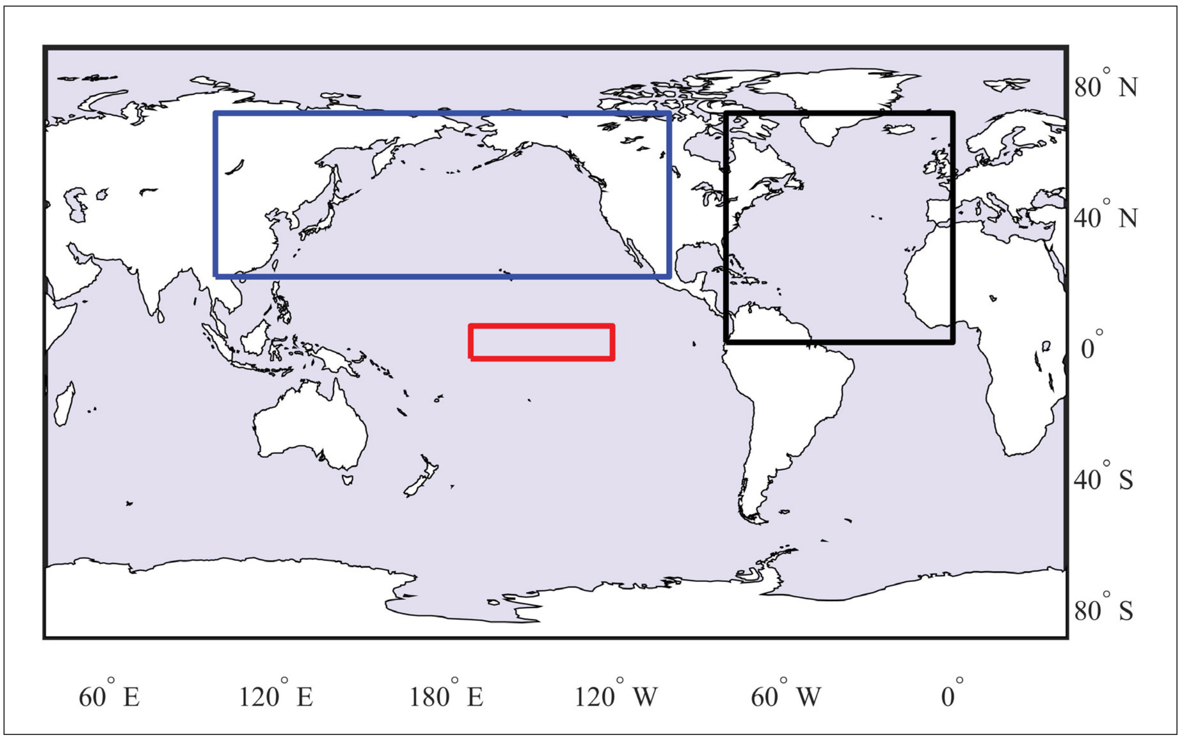

Figure 4.2 Locations of TPSST (red box), NPSST (blue box), and NASST (black box) regions

The ability of CanESM2 to reproduce the frequency and magnitude of SST anomalies must be assessed for results to be significant in the real world. In this validation step, the first member of the climate model large ensemble was used. A wavelet analysis was performed to compare ENSO characteristics. Wavelet analysis is commonly used to analyze the temporal variation of the power frequency spectrum over a given time period. It is a powerful tool for assessing the periodicity of a signal (Torrence & Compo, 1998). The wavelet validation focused on ENSO, considering that it is the only index whose frequency is significantly shorter than the chosen 50-

year study period. The validation of PDO and AMO follows a simpler graphical comparison since the 50-year segments from each member are not long enough to properly capture the periodicity of both indices.

To look at interactions between the indices, anomalies were separated into three groups using quantiles. Each index (positive, neutral or negative) was therefore considered based on this classification. The positive state was defined with an index value larger than the 75th quantile. The negative state was defined with values below the 25th quantile, while the neutral state used the 2nd tercile between the 33rd and 66th quantiles. Each index was therefore considered neutral 33 percent of the time. Based on this classification, 27 combinations in all of all three possible states for each index were obtained.

The individual and coupled effects were analyzed at the annual time scale. The individual impact consisted of years in which one index was either positive or negative, while the other two were in a neutral phase. The coupled effect looked at the 8 possible combinations of positive and negative states in order to study the constructive and destructive interactions between all 3 patterns (e.g., +++, +–, etc.). For any given combination of index states, results were presented as precipitation and temperature anomalies. The watershed baseline climate upon which anomalies were computed consists of the reference period years during which all three indices are in a neutral state.

4.5 Results

4.5.1 Climate model validation

Figure 4.3 presents the ENSO wavelet spectrum for both CanESM2 (member 1) and real-world observed data. The 50-year 1961-2010 period is used in both cases. Both wavelet spectrums are very similar indicating that CanESM2 simulates an ENSO-like oscillation similar to the observed one. Both spectrums are characterized by a prominent 2- to 7-year power band.

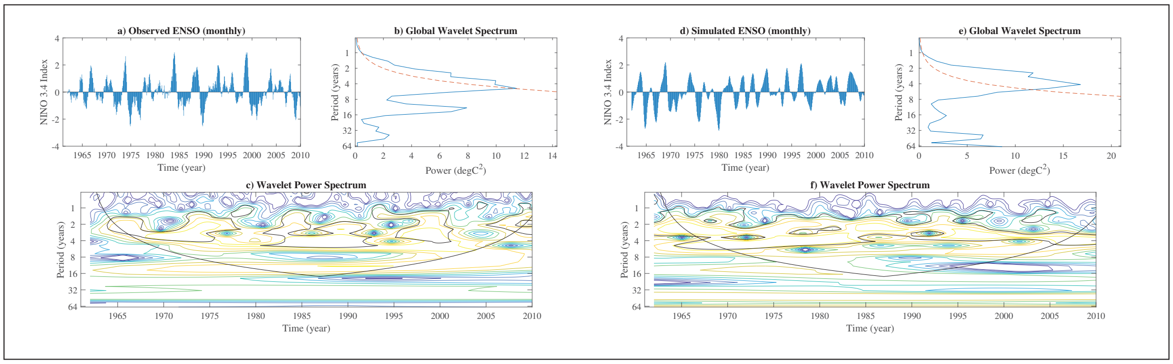

Figure 4.3 Comparison between observed and simulated monthly NINO 3.4 index. c) and f) are the wavelet power spectrums of observed and simulated ENSO

Figure 4.4 presents the PDO pattern corresponding to the first principal component for both observation and CanESM2. The spatial patterns are very similar, with only some minor differences in the western North Pacific. The percentage of explained variance is nearly identical. The sea surface temperature contrast between cold and warm regions is however slightly stronger in CanESM2.

Because of the long-term periodicity of SST in the North Atlantic Ocean, the validation of the characteristics of AMO is difficult with only 50 continuous years. A comparison of interannual variability was chosen to provide some degree of validation of the climate model's ability in the North Atlantic. Figure 4.5 presents the standard deviations of SST in the North Atlantic over the 1961-2010 period for observations and CanESM2. The spatial pattern of SST variability in the North Atlantic, with the increasing variance from the equator toward higher latitudes, is generally well represented by CanESM2. There are, however, some regional differences. The high-variability region along the eastern coast of North America exists in both datasets, but differs in magnitude and location.

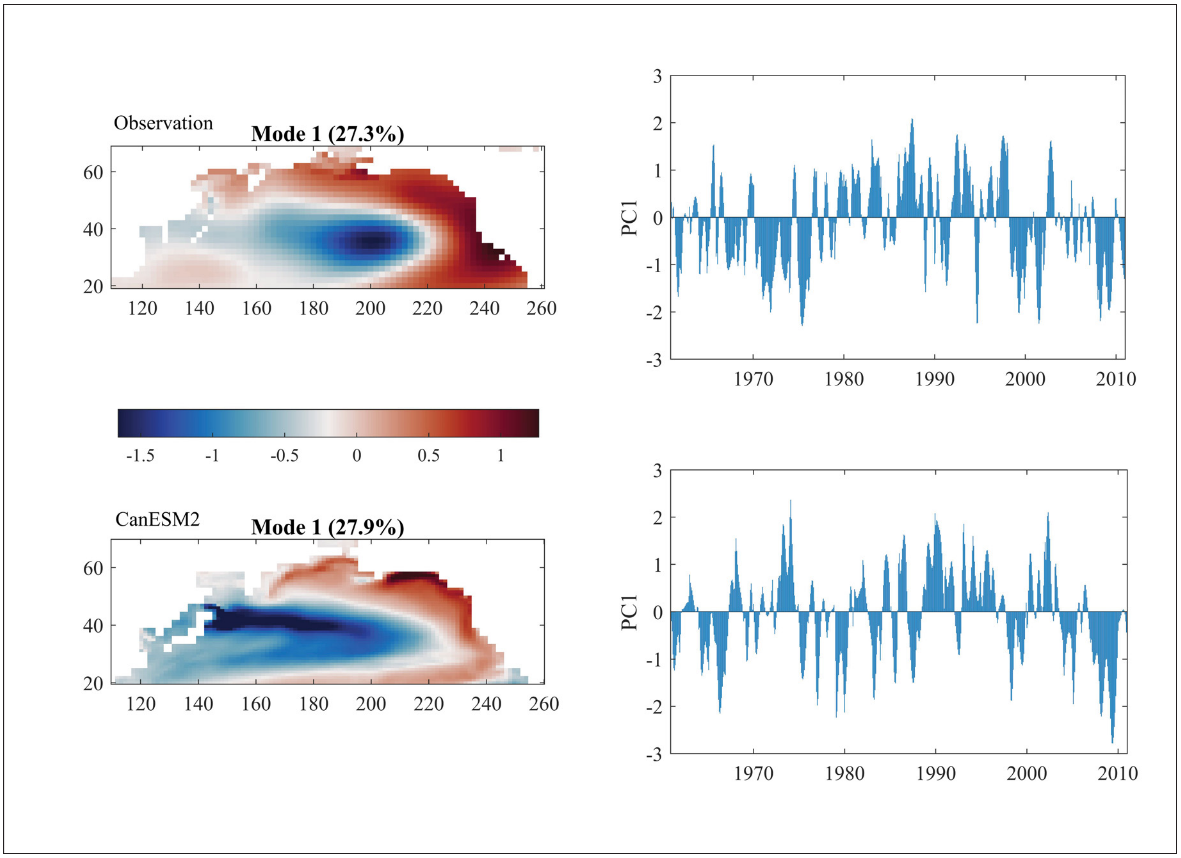

Figure 4.4 EOF map (left) and its corresponding principal component (right) of the first mode of North Pacific SST in observation (upper row) and CanESM2 (lower row). The percentage is the explained variance of the first leading pattern

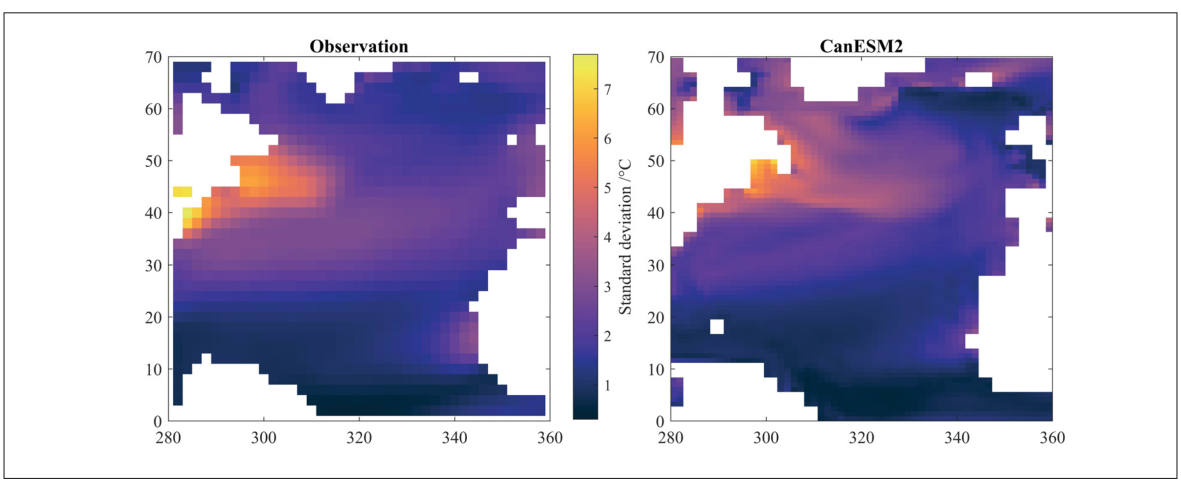

Figure 4.5 Standard deviation of sea surface temperature in North Atlantic during the 1961-2010 analysis period

4.5.2 Individual impact of large-scale oscillations

The individual impact of each oscillation is first examined. As earlier discussed, the individual impact is defined based on each index being in a positive or negative phase with the other two in a neutral state. The number of years selected (out of 2500 years) for each index is presented in Table 4.1.

Table 4.1 Number of years used for the individual effect of ENSO, AMO and PDO

ENSO or AMO or PDO	Number of years
PDO+	95
PDO-	69
AMO+	77
AMO-	94
ENSO+	33
ENSO-	61

Figure 4.6 presents the CanESM2 precipitation anomalies associated with each oscillation, with the other two being in a neutral phase. The figure shows a strong impact of ENSO on annual precipitation over North America, and particularly over the U.S. Annual precipitation is below average during La Niña events and above normal during El Niño years over a large part of North America. The influence of ENSO is most prominent over the Southern West US and Western High Plains. The impact over British Columbia and Washington State is reversed, but weaker. Most of Eastern Canada is only very weekly affected by ENSO. The impact of AMO is comparatively weaker. It controls part of the precipitation variability in West and East Canada. Over the U.S., the spatial pattern is roughly similar to that of ENSO, but reversed, with the potential for destructive interference. PDO has the weakest impact of all on precipitation. A positive PDO matches the ENSO pattern quite well, showing the potential for a constructive effect with ENSO in some regions.

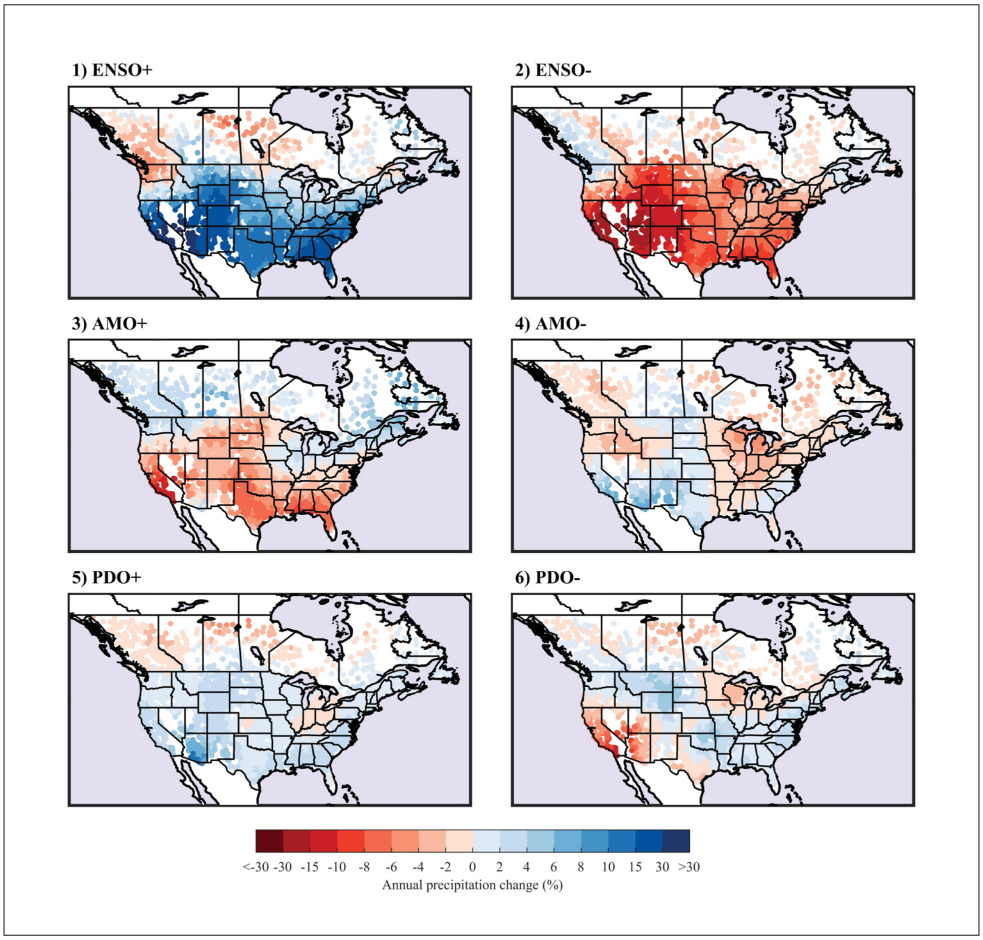

Figure 4.6 Individual effects of ENSO, AMO, and PDO in different phase on the change of annual precipitation in CanESM2. Blue means an increase in annual precipitation, while red means a decrease in annual precipitation at the scale of each studied watershed

Figure 4.7 presents the individual impact of each index on annual temperature anomalies. It shows a very strong influence of AMO at modulating temperatures over all of North America. A positive AMO correlates with higher temperature across the continent. The opposite is observed for the negative phase, albeit with a slightly weaker magnitude. The impact of both phases is stronger on the eastern half of North America and weaker on the West Coast. The impact of ENSO on temperature anomalies is only felt on the Northwestern part of North America, and especially during an El Niño phase. PDO exerts minimal influence on temperature anomalies, and only along the Northwestern coast.

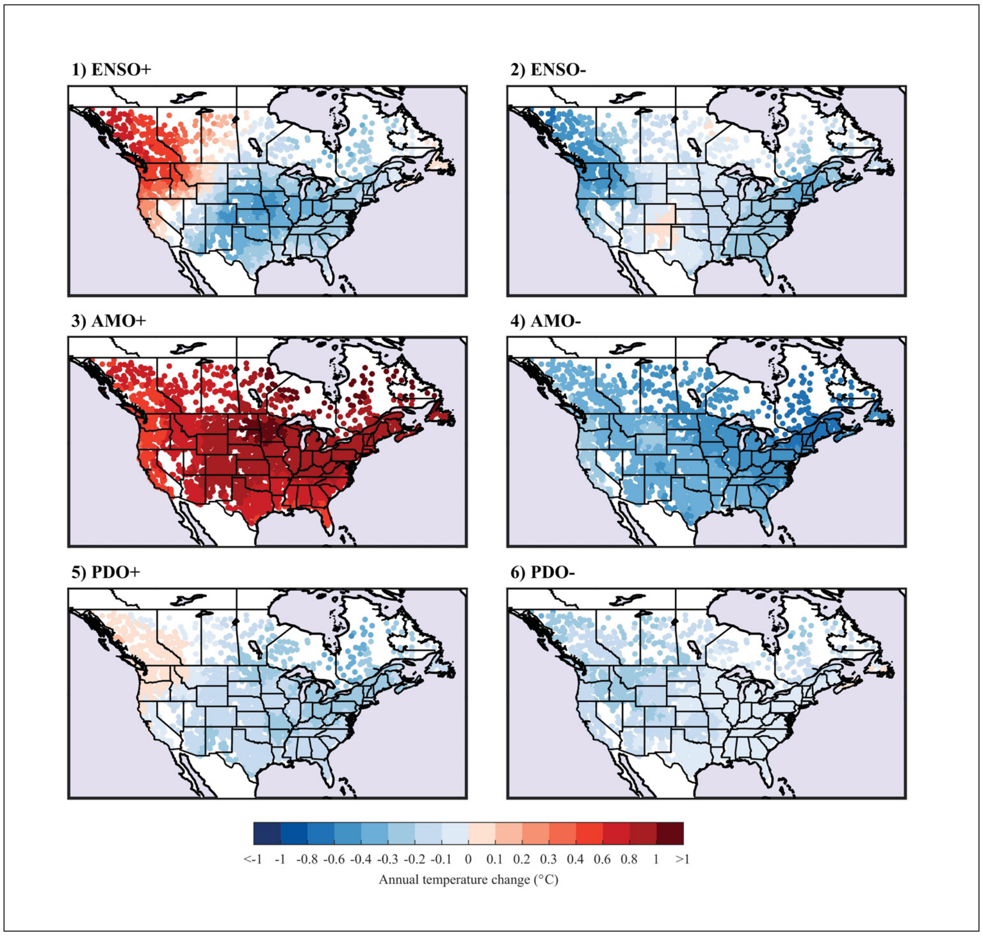

Figure 4.7 Same as Figure 4.6, but for annual temperature. Blue means a decrease, while red indicates an increase at the scale of each studied watershed

4.5.3 Coupled impact of large-scale oscillations

The number of years for the combinations of non-neutral states for the three patterns is shown in Table 4.2. The coupled impacts of ENSO, AMO and PDO on annual precipitation anomalies are shown in Figure 4.8. The eight graphs represent the eight possible combinations of the three indices in their non-neutral phases. Figure 4.8 clearly shows that ENSO remains the main source of precipitation variability over most of North America. As was the case for the individual impact, El Niño is largely associated with a precipitation increase whereas the La Niña phase comes with decreased precipitation. However, the interactions with PDO and AMO create more complex regional patterns especially in Northwestern North America. The magnitude of the precipitation anomalies increases, as compared to Figure 4.6, thus showing a clear constructive interference consistent with the individual impacts. For example, La Niña is clearly enhanced by a positive AMO, whereas the impact of El Niño in the U.S. is emphasized by a negative AMO. The influence of oscillations in Northwestern N.A. is the greatest when an out-of-phase AMO encounters the in-phase ENSO and PDO (Figure 4.8.3 and Figure 4.8.6). The constructive impact of an out-of-phase ENSO and AMO plays an important role in controlling precipitation in this area, while precipitation in Central Canada primarily follows the change patterns of AMO.

Table 4.2 Number of years used for the coupled effect of ENSO, AMO and PDO

Coupled effect	**Number of years**
ENSO+ & AMO+ & PDO+	54
ENSO- & AMO+ & PDO+	10
ENSO+ & AMO- & PDO+	20
ENSO- & AMO- & PDO+	31
ENSO+ & AMO+ & PDO-	53
ENSO- & AMO+ & PDO-	23
ENSO+ & AMO- & PDO-	8
ENSO- & AMO- & PDO-	62

In order to better summarize the variability at the regional scale, Figure 4.9 presents boxplots of the annual precipitation anomalies for the eight combinations of the three indices. All watersheds within a region are represented by a boxplot, showing the median and interquartile range, largest and smallest values. Figure 4.9 shows that the interactions at the regional scale are especially significant over the U.S. domain. The western U.S. is the most sensitive region to interactions, followed by the High Plains region.

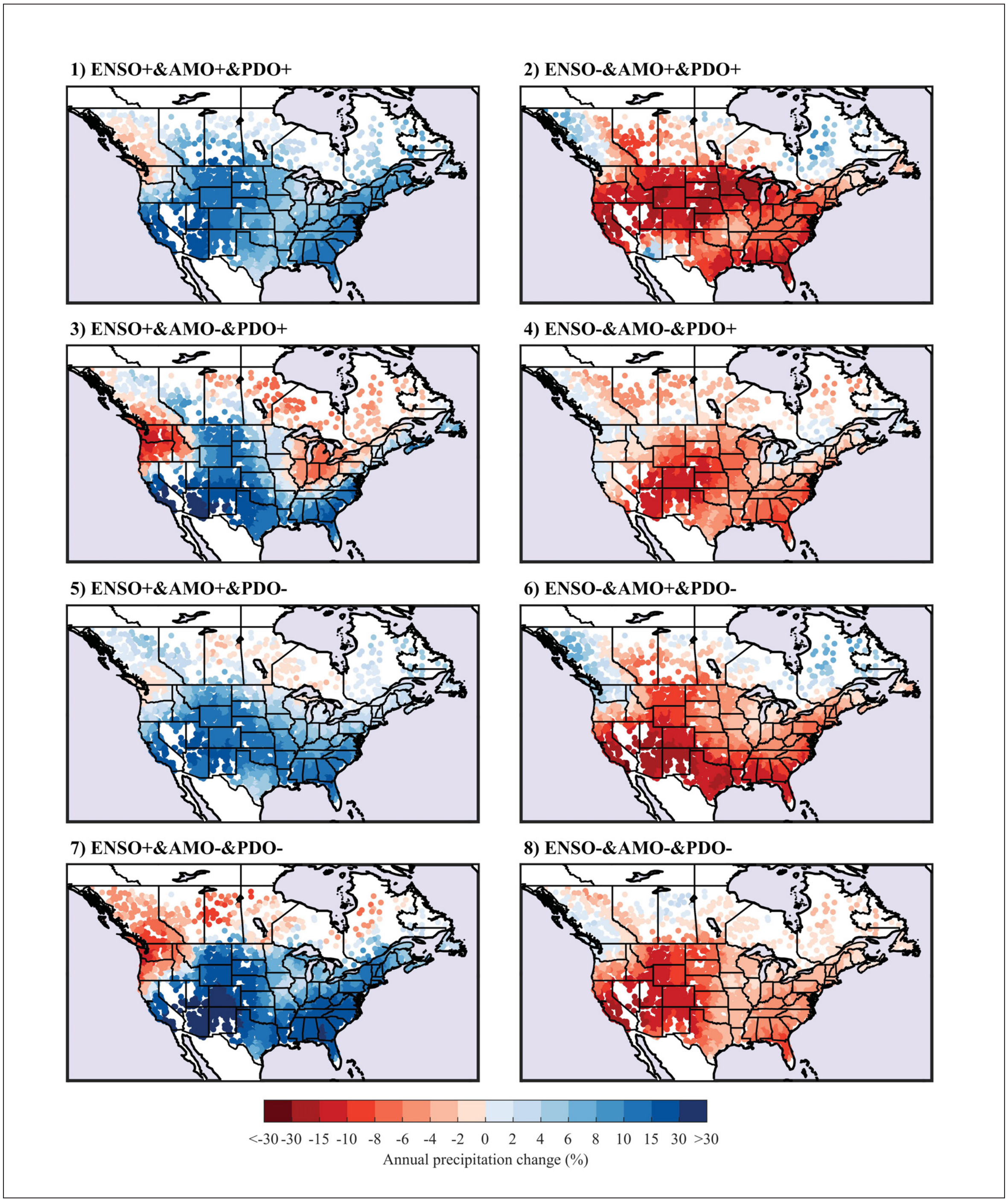

Figure 4.8 Coupled effect of the PDO, AMO and ENSO on annual precipitation in CanESM2

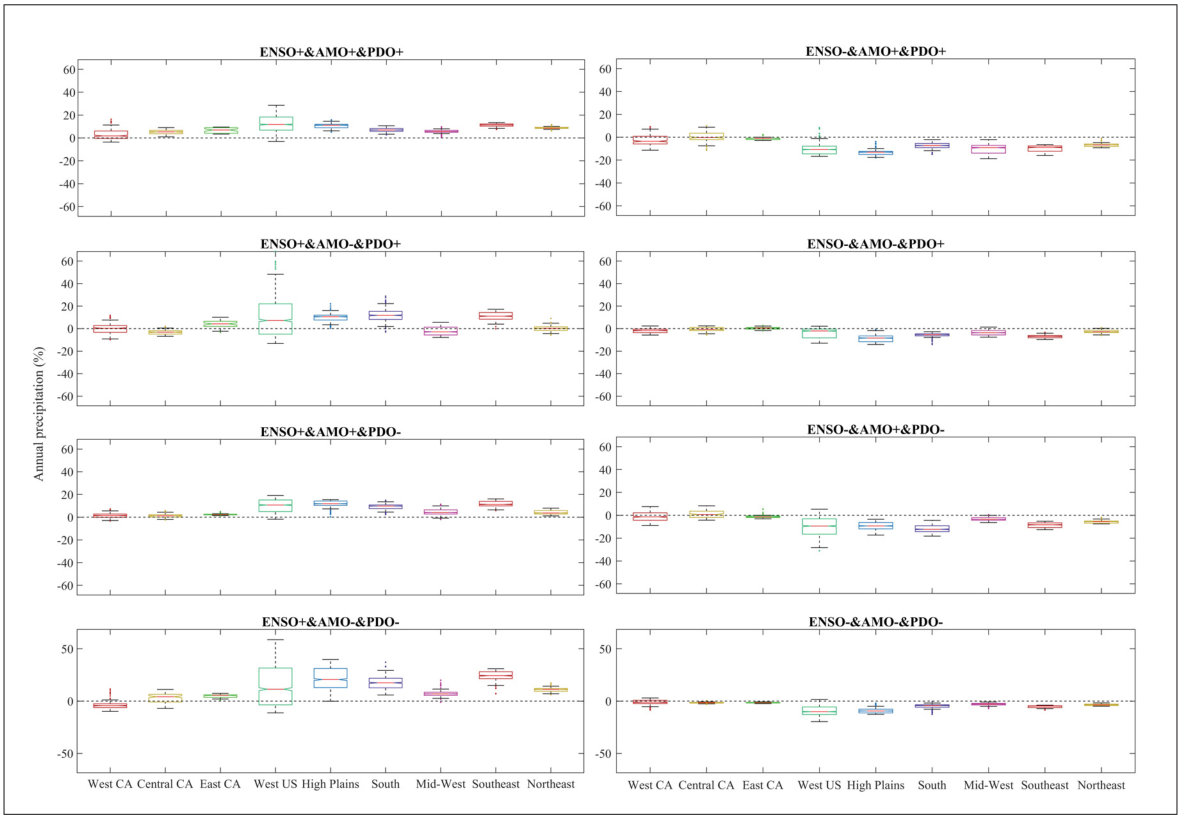

Figure 4.9 Regional variance of annual precipitation under the coupled effect of large-scale oscillations

Figure 4.10 presents the coupled effect of ENSO, AMO and PDO on annual temperature anomalies. The spatial patterns are much more homogenous than for precipitation. The role of AMO is still prominent over contiguous North America, but the magnitude of the temperature anomalies is amplified or damped as a result of the interactions with ENSO and PDO. These interactions can be largely inferred from individual impacts. For example, positive temperature anomalies are maximal over Northwestern North America when all three indices are in their positive phase. Negative anomalies are strongest in the Central U.S., where the impact of a negative AMO is amplified by El Niño. The impact of PDO is mostly seen in the Western regions (West Canada, West US). This is made clearer in Figure 4.11, which shows the regional variance of temperature anomalies.

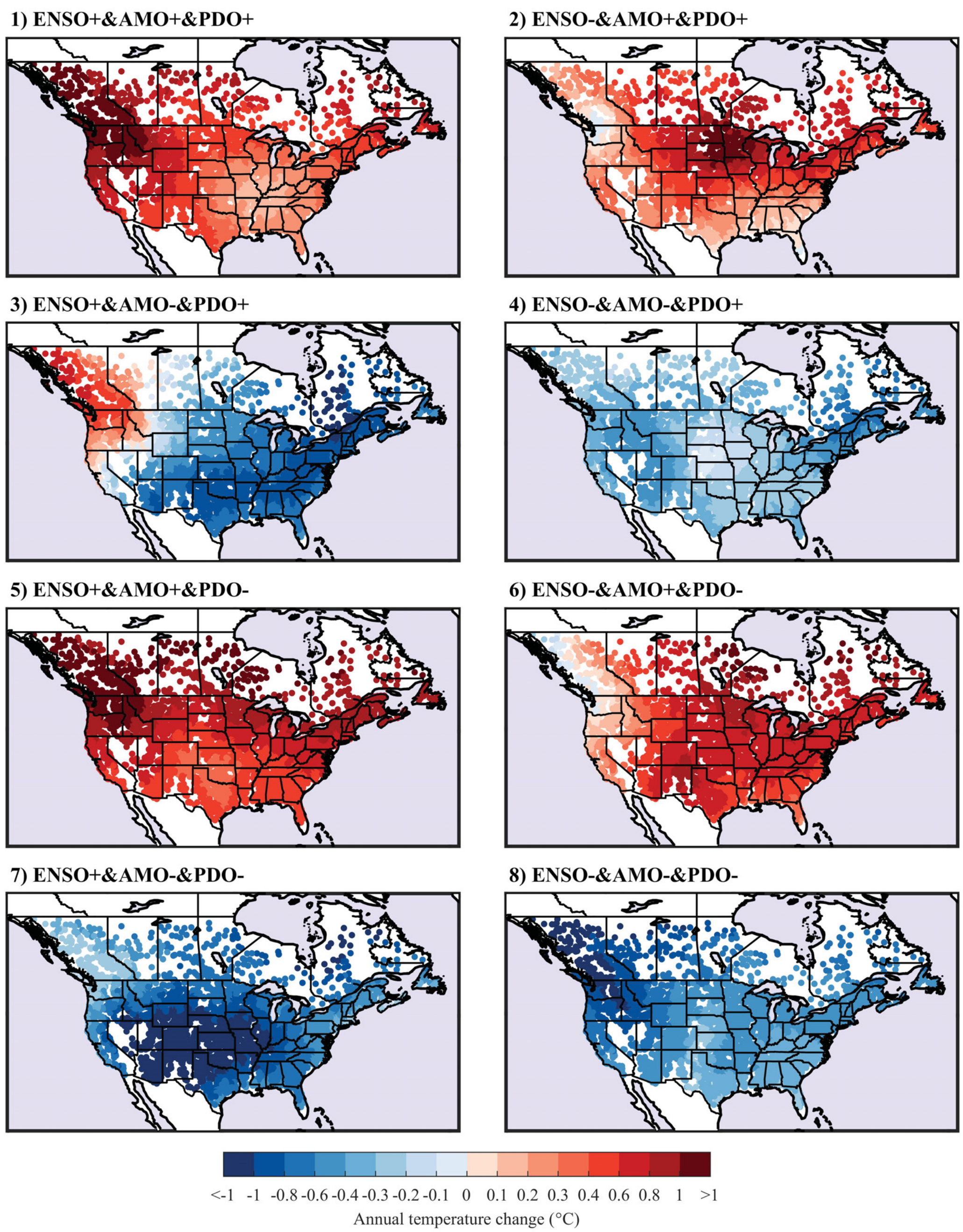

Figure 4.10 Coupled effect of ENSO, AMO and PDO on the annual temperature in CanESM2. Blue means a decrease in annual temperature, while red indicates an increase in annual temperature at the scale of each studied watershed

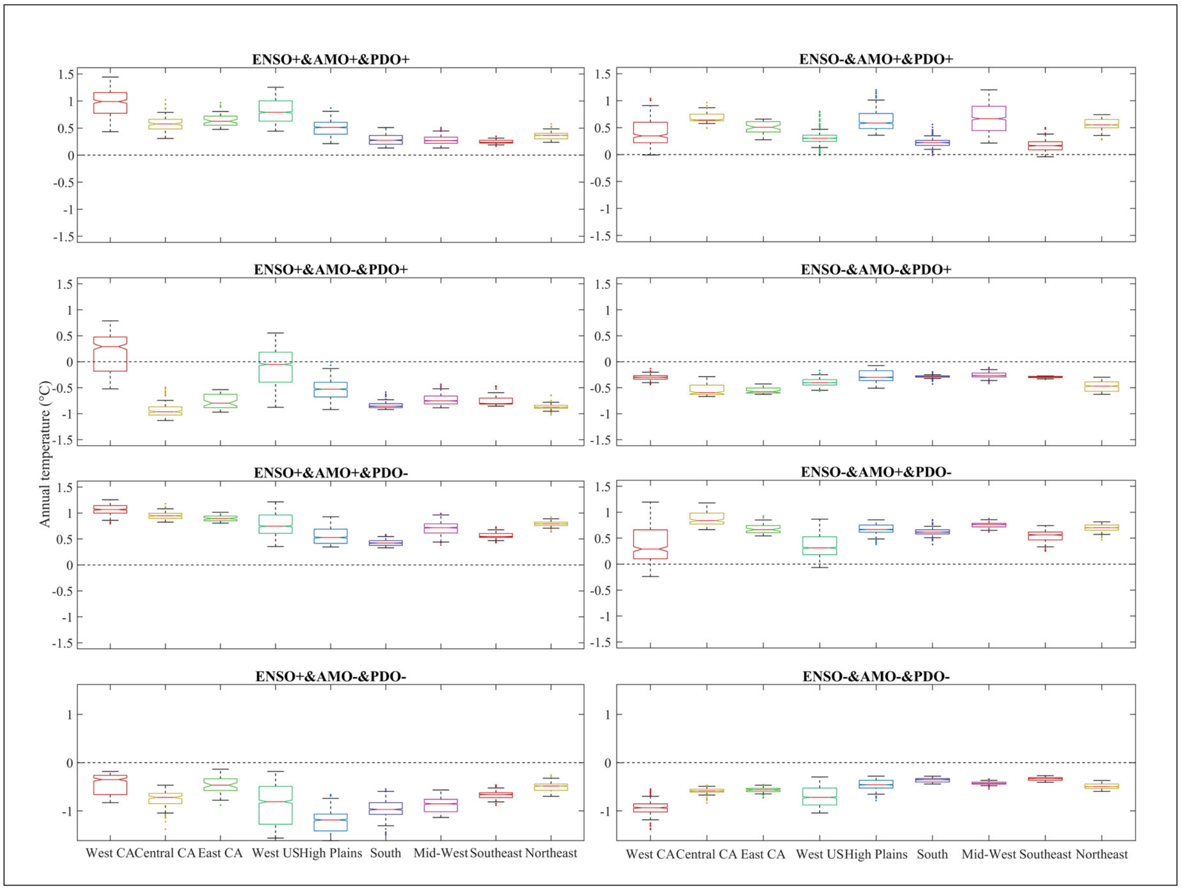

Figure 4.11 Regional variance of annual temperature under the coupled effect of large-scale oscillations

4.6 Discussion

This paper assessed the individual and coupled impacts of three large-scale oscillations on temperature and precipitation anomalies over North America, using climate model data from the CanESM2 large ensemble. Results showed a dominant impact of ENSO on mean annual precipitation, and of AMO, on mean annual temperature.

Since this study was performed entirely with outputs from a single climate model, it is important to compare our results with those of real-world studies. The significant dominant impact of ENSO on annual precipitation and AMO on annual temperature have been shown by other studies using observations (Goly, A. & Teegavarapu, R. S., 2014; Maleski & Martinez, 2018;

McCabe *et al.*, 2004; Stevens, K. A. & Ruscher, P. H., 2014). The Northern Hemisphere mean surface temperature warmed over the 20$^{\text{th}}$ century, and a departure from the monotonic increasing trend was found to be associated with variability in the Atlantic (Zhang, R., Delworth, T. L. & Held, I. M., 2007), which suggests that AMO plays an important role in temperature variation. The minimal impact of PDO on precipitation is also in line with the findings of Kurtzman & Scanlon (2007), Johnson *et al.* (2013) and Maleski & Martinez (2018).

The constructive interference of in-phase ENSO and PDO documented by Hu, Z.-Z. & Huang, B. (2009) is well preserved by CanESM2 (Figure 4.8.6), while the destructive effect is not as well simulated (Figures 4.8.3 and 4.8.7). These findings are in line with the conclusion of Fuentes-Franco *et al.* (2016), drawn from 11 CMIP5 GCMs.

Maleski & Martinez (2018) studied the impact of the interactions of ENSO, AMO and PDO on climate in the Southeastern US. They found that a positive AMO leads to decreased precipitation, while its negative counterpart was associated with increased precipitation, in line with our results. However, our results on the impact of ENSO on temperature are different from what Maleski & Martinez (2018) found. In our study, the individual impact of ENSO on temperature is not clear in this region although it amplifies the effect of AMO on temperature. Some of the differences seen may be attributed to different definitions of ENSO (based on the October to September water year) and AMO (leading pattern of detrended North Atlantic SST anomaly). Furthermore, although the authors explored the impact of all three oscillations, the combined effect was only based on the combination of two modes, versus three in the present work.

To further explore the validity of the results presented in this paper, we looked at the 2011-2015 California droughts. The Southern West US has been proven to be particularly sensitive to the studied oscillations. The fall 2011 to fall 2015 period was the driest on record since monitoring started in 1895 in California (Ellen, H., Jeffrey, M. & Caitrin, C., 2015). During that span, California mostly experienced negative ENSO, negative PDO and positive AMO (ENSO- & AMO+ & PDO-). Based on our results (Figures 4.8.6 and 4.9.6), this combination simultaneously leads to less precipitation and higher temperature, which are the two key elements leading to droughts. Since 2014, there have been a few El Niño events, which relieved drought conditions to a certain extent.

As is the case for all studies, this work comes with several limitations and uncertainties. The mean climate was defined based on the 1981-2010 period and no post-processing was performed on the climate model data over the 1961-2010 analysis period. No detrending was performed, even though some variables, especially temperature, do have significant trends at the catchment scale. Detrending is not a simple task, especially when it should be done at the regional scale to overcome the local impact of internal variability. As well, it may introduce significant uncertainty. Linear and polynomial trends have been suggested to represent the human-induced climate warming trend (Meehl, G. A., Hu, A., Santer, B. D. & Xie, S.-P., 2016; Messié, M. & Chavez, F., 2011; Messié & Chavez, 2011). A more intrinsic trend, decomposed from the signal itself, rather than pre-determined, was also produced by using ensemble empirical mode decomposition (EEMD, Huang, N. E., Shen, Z., Long, S. R., Wu, M. C., Shih, H. H., Zheng, Q., Yen, N.-C., Tung, C. C. & Liu, H. H., 1998). There is no scientific consensus on how this should be done, on how to take into account internal variability at the local and regional scales, and on how much an uncertainty introduced by trend removal in climate change impact studies. Even though CanESM2 data was available until 2100, we restricted our analysis to the 1961-2010 period to avoid the detrending issue, while still keeping our data sample large enough. Our results are also constrained by CanESM2 SST data. While a validation was performed on its ability, it was far from exhaustive. Although recent climate models have shown significant improvement in SST modeling, there are still large errors in the mid- and high-latitude regions (Flato *et al.*, 2013). A cold bias of more than 1°C in the zonal mean near-surface ocean temperature was found in the high latitudes of the North Hemisphere. A cold tongue error in the tropical Pacific was reduced by 30% in CMIP5 and the cold bias in the Atlantic was found to be related to errors in the thermocline depth (Flato *et al.*, 2013).

The time period considered in hydroclimatological studies is also important because it determines the potential number of warm and cold phases of oscillations within the analysis period (Kurtzman & Scanlon, 2007). The time-period selection also constrains comparisons with other studies. The analysis period in this study is from 1961 to 2010, a 50-year period. This is not long enough to capture a full cycle of multi-decadal scale oscillations such as AMO. While this is not necessarily a problem with a climate model large ensemble, it is however an important limitation in observations. In the limited observational records, El Niño often shares common periods with non-neutral AMO and/or PDO, making it hard to distinguish the individual effect of each mode of variability (Maleski & Martinez, 2018). There are strong interactions between the oscillations. If these three indices were truly individual, there should be roughly 70 years for combinations in Table 4.1 (individual effect, $0.33 \times 0.33 \times 0.25 \times 2500$) and 39 years for those in Table 4.2 (coupled effect, $0.25 \times 0.25 \times 0.25 \times 2500$). However, the number of common years (Tables 4.1 and 4.2) suggests that the three indices are somewhat correlated. ENSO and PDO are often in phase, resulting in a larger number of common years. Analyses based on short time series can lead to an overconfident estimation of the role of oscillations (McCabe, G. J. & Dettinger, M. D., 1999). Furthermore, our work only focused on 14 out of 27 possible combinations. The two-by-two combinations were not looked at in this work. The thresholds used to define negative, neutral and positive phases are somewhat arbitrary, and may influence the results. Moreover, only three oscillations were selected in this study, chosen because of their documented impact on the North American climate.

Finally, this study focused solely on precipitation and temperature anomalies. Future work should look at streamflow and droughts resulting from non-linear interactions between precipitation and temperature. ENSO has been shown to impact flooding, for example, although its role is quite complex (Emerton, R., Cloke, H., Stephens, E., Zsoter, E., Woolnough, S. & Pappenberger, F., 2017). The large sample provided by CanESM2-LE may help clarify the impact of SSTs on droughts and floods. Another interesting avenue would be to look at climate model millennium simulations, which consist of continuous pre-industrial simulations, and thus allow an examination of complete low-frequency oscillation cycles.

4.7 Conclusions

This study explored the individual and coupled impacts of the El Niño-Southern Oscillation, Pacific Decadal Oscillation, and Atlantic Multidecadal Oscillation on North American climate variability at the watershed scale, using sea surface temperature data from the CanESM2 large ensemble. The use of a climate model large ensemble allows the sampling of a very large number of years in order to study the interactions between the three oscillations. The main conclusions of this work are as follows:

1) The CanESM2 climate model performed well in representing the main characteristics of the chosen climate oscillations. The 2- to 7-year periodicity of ENSO, the spatial pattern of PDO and SST variability in the North Atlantic were well reproduced by the model. This provides confidence in our ability to draw conclusions applicable to the real world.

2) The individual impact of each oscillation was assessed by selecting years during which the other two oscillations were in their neutral phases. Results indicate that annual precipitation anomalies are mainly controlled by ENSO, while AMO plays the dominant role in temperature variability over most of North America. ENSO only affects the temperature anomalies along the Canadian and US West coasts. PDO only had a minimal impact on precipitation and temperature.

3) Regarding interactions, the dominant role of ENSO in driving precipitation anomalies remains. El Niño is stronger when PDO is in-phase and AMO is out-of-phase, and vice versa. The role of AMO in driving temperature anomalies remains fundamental even when considering interactions. A positive AMO is reinforced by El Niño on the West Coast and a negative PDO, in the East. The impact of a negative AMO is enhanced by a negative PDO mainly over the Central and Southern U.S., and damped by El Niño along the Canadian and US West coasts.

4) Results demonstrate the constructive and destructive impacts of interactions between oscillations and outline the complexity of the processes controlling internal climate variability at the regional scale.

We believe that this work demonstrates the potential of using climate model simulations to investigate the role of sea surface temperature in driving the regional climate under the absence of anthropogenic forcing.

4.8 Acknowledgments

The authors acknowledge the contribution of the Canadian Centre for Climate Modelling and Analysis (CCMA) for making the CanESM2 Large Ensemble simulations available for this study. The authors would also like to thank the Ouranos Consortium for helping with the data transfer. The data is now available for the 1950-2100 period from the CCMA website (http://collaboration.cmc.ec.gc.ca/cmc/cccma/CanSISE/output/CCCma/CanESM2/). The historical NINO 3.4 index and the SST reanalysis data were obtained from the National Oceanic and Atmospheric Administration (NOAA) (https://www.esrl.noaa.gov/psd/gcos_wgsp/Times -eries/Nino34/;https://www.esrl.noaa.gov/psd/data/gridded/data.noaa.ersst.v4.html).

GENERAL DISCUSSION

In this chapter, the main results of this thesis are synthesized in light of the main objective of this work which was to explore the impacts of climate change on meteorological and hydrological droughts, globally, but with an emphasis over North America. Following the discussion, some limitations of this work and some recommendations for further researches are outlined.

5.1 Frequency change of future extreme droughts

The frequency change of meteorological droughts at the global scale, and hydrological droughts over 5797 North American watersheds was projected for 2, 20, and 100-year return periods. This work was performed using two climate model large ensembles.

Annual and seasonal extreme meteorological droughts were first assessed at the global scale for both short-term (1-month) and long-term (24-month) durations. The results showed a worsening pattern of extreme meteorological droughts largely associated to the projected change in mean annual precipitation. This is particularly striking in tropical and subtropical areas. Future summer (JJA) extreme meteorological droughts are projected to get worse compared to their winter (DJF) counterpart. The spatial distribution of affected areas is consistent with other studies (e.g., Dai, 2011; IPCC, 2013b; Sheffield & Wood, 2008), with the exception of Western Africa. Some of those studies projected even larger increases, with differences likely related to drought type and chosen drought indices. Climate change affects the temporal variability of precipitation, which may lead to increases in extreme meteorological drought frequency, even in regions with increasing mean annual precipitation. This is especially the case for droughts with larger return periods. The results obtained from the two large ensembles are fairly consistent with differences typically originating in regions where the internal variability of precipitation is large. These regions were also identified by the IPCC as having low inter-model agreement.

Over North America, the frequency change of future hydrological droughts is consistently more severe compared to meteorological droughts. This is because hydrological droughts combine the effect of precipitation deficit and increased temperature which pushes evapotranspiration toward larger rates. The intensified evapotranspiration creates additional stress in regions with decreased mean annual precipitation, and even offsets the projected increase of mean annual precipitation over some watersheds. It therefore suggests that increased evapotranspiration is the key driver in the evolution of future hydrological droughts over North America. Spatial trends are similar for both studied periods, with the more distant future experiencing more severe changes of extreme droughts.

5.2 Limitations of droughts assessment in this work

There are however many uncertainties related to our work, which partly limit our conclusions on the frequency evolution of future meteorological and hydrological droughts. As is the case for most scientific studies, methodological choices may affect the results of this work. The main limitations of this study can be separated as follows: drought definitions, evaluation envelope and representation of physical processes. These limitations are discussed separately in the following paragraphs.

Different drought definitions may result in slightly different conclusions about the impact of climate change on droughts. In our study, meteorological droughts were assessed using the SPI, which is solely driven by precipitation. Some drought indices (e.g., PDSI and SPEI), also categorized as meteorological drought indices (Svoboda *et al.*, 2016), consider water supply and demand simultaneously, thus showing more severe drought conditions under a warming climate (Burke & Brown, 2008; Sheffield & Wood, 2008). Since surface moisture/water balance is related to agricultural droughts, some researches have explored the characteristics of agricultural droughts based on those same indices (Dai, 2011; Keyantash, J. & Dracup, J. A., 2002; Touma *et al.*, 2015). Different drought indices projected for the near future showed small but consistent drying trends in the future. However, for the more distant future, larger differences were found to emerge (Feng, S., Trnka, M., Hayes, M. & Zhang, Y., 2017) depending on drought definition.

A different selection of duration, frequency and intensity of droughts can also lead to slightly different projections of change and limit the inter-comparison between researches. Drought indices can be calculated at 1-, 3-, 6-, 12-month or even longer time intervals. As we know that changes in future climate variability are dependent on both spatial and temporal scales, this also renders the intercomparison between different studies more difficult. In our work, short-term meteorological and hydrological droughts were defined with a 1-month duration. This was a compromise between the full spectrum of droughts which can be as short as 7 days for hydrological droughts in a temperate climate all the way to the seasonal or annual scales in drier or strongly seasonal climates. In other studies, short-term droughts are often defined at the seasonal scale. In addition, hydrological and meteorological droughts typically have a different response time. It has been shown that streamflows respond rapidly to short-term meteorological droughts whereas reservoir storage deficit is associated with meteorological droughts of a much longer duration (Vicente-Serrano, S. M. & López-Moreno, J. I., 2005). Three levels of droughts frequency (2, 20 and 100-year return periods) were assessed in this work. Even though this work covers a wide range of return periods, it is possible that looking at more return periods could yield somewhat different results. Our results indicate a worsening of droughts for shorter durations and longer return periods, which is in line with some other studies for precipitation, meteorological and hydrological droughts (Feyen, L. & Dankers, R., 2009; Leng *et al.*, 2015; Martel *et al.*, 2020; Sheffield & Wood, 2008).

The experiment design in this Thesis offers a narrow window into future hydrological droughts conditions. Only two climate models (CanESM2 and CESM1) were used to analyze the frequency change of future droughts. The focus of this work was extreme droughts, and large-ensemble are especially well suited for this task. At the beginning of this work, these were the only two climate models for which large-ensemble was available, and it is still the case today although climate model runs with limited ensembles (3 to 10 members) are becoming more and more available. It would therefore be important to compare the climate sensitivity of these two climate models against other IPCC climate models. For the same reasons of availability, the RCP8.5 was the only scenario analyzed. The RCP8.5 combines assumptions about high population and relatively slow income growth with modest rates of technological change and energy intensity improvements (Riahi *et al.*, 2011). It is considered a pessimistic scenario, but it has the advantage of emphasizing the climate change signal with respect to internal variability which is an important asset when looking at precipitation which has a weak anthropogenic forcing to internal variability ratio (e.g., Martel *et al.*, 2018). A single bias correction method was used for the hydrological drought climate scenarios and the impact of this source of uncertainty was therefore not studied.

The representation of physical processes also brings limitations to droughts assessments. Different climate models have different model structures and parameter sets that lead to different realizations of the future climate system. Hydrological droughts result from the complex combination of dynamical processes, with only some of which represented in the impact models, and sometimes in a very simplified way. In this study, only one hydrological model was adopted to simulate streamflows over North American watersheds. Most simple hydrological models like the one used in this work depend on the estimation of potential evapotranspiration. Due to limitations in data availability, temperature-based formulas are often used, many of which have a high sensitivity to changes in temperature. While physically-based formula may be better suited for a study like this one, the input data to calibrate the evapotranspiration equation over the reference period are generally unavailable.

Finally, this work only took climate change impacts into consideration. The spatial extent and/or frequency change of future droughts may be underestimated because future water use was not considered. With increasing population and water demand, future droughts may become more severe.

5.3 The impacts of natural climate variability

In the first part, we used large ensembles to create large samples to explore the future frequency of extreme droughts. In Chapter 4, we explicitly looked at the impacts of natural climate variability on precipitation and temperature by using three climatic indices (ENSO, AMO and PDO). ENSO was used to represent the tropical Pacific Ocean, PDO for the North Pacific, and AMO for the North Atlantic.

The contributions of natural climate variability to the North American climate was assessed in term of large-scale oscillations at the interannual and multidecadal scales over the 1961-2010 period. Because of the large sample size provided by the CanESM2 large ensemble, specific attention was given to the interactions between the oscillations, something that is not possible to do in the real world. Our results confirmed the dominant role of ENSO in controlling the variability of precipitation, and the important impact of AMO on annual temperature. These were also observed by Goly & Teegavarapu (2014), Maleski & Martinez (2018) and McCabe *et al.* (2004).

The constructive effect of ENSO and PDO is well simulated by the climate model while the destructive effect is less accurately represented, a finding in line with the work of Fuentes-Franco *et al.* (2016). The influence of PDO is not significant compared with the other two patterns, which is the main difference between this work and other studies which only considered the single pattern or the combination of two patterns over the Pacific Ocean (Kurtzman & Scanlon, 2007; Maleski & Martinez, 2018).

There are several other limitations affecting this work. In this study, the selected three oscillations are all coupled modes of variability. Climate variability should also be affected by other atmospheric or oceanic circulations. The selected indices only range from annual to the multidecadal time scale, but there are many other oscillations having local or global impacts on climate over different time scales (a couple of weeks to a few months, to decades). This study used climate model outputs without any post-processing. This implies the possible presence of trends in the data, and especially so for temperature. The 1960-2010 period is the only one analyzed to limit the impact of trends. The anthropogenic climate change is often removed through detrending in recent researches (Cai, W., Borlace, S., Lengaigne, M., Van Rensch, P., Collins, M., Vecchi, G., Timmermann, A., Santoso, A., McPhaden, M. J., Wu, L. et al., 2014; Lim, Y.-K., Schubert, S. D., Kovach, R., Molod, A. M. & Pawson, S., 2018). However, the detrending process itself has large uncertainties. In current scientific communities, linear and polynomial trends are suggested to represent the human-induced climate warming trend (Meehl *et al.*, 2016; van Oldenborgh, G. J., Doblas-Reyes, F. J., Wouters, B. & Hazeleger, W., 2012). A more intrinsic trend is also produced by using ensemble empirical mode decomposition (EEMD) method (Huang *et al.*, 1998). But there's not enough evidence to show which trend is the most realistic and how much uncertainty it introduces to climate studies and how internal variability affects the trend removal process. There are also additional concerns with respect to detrending ensembles. All members of the ensemble should be detrended identically since subject to the same forcing. This implies pooling all members together prior to the detrending process, similarly to what has been suggested for bias correction (e.g., Chen *et al.*, 2019).

In addition, the results are also constrained by the quality of model-simulated SST data. There are still large SST errors in mid- and high-latitude regions in climate model outputs. Although the basic spatial structure is well captured by climate models, persistent biases with large local impacts may remain in the mean state of the tropical Pacific Ocean (Ackerley, D., Highwood, E. J. & Frame, D. J., 2009; Brown, A., Milton, S., Cullen, M., Golding, B., Mitchell, J. & Shelly, A., 2012; Guilyardi, E., Wittenberg, A., Fedorov, A., Collins, M., Wang, C., Capotondi, A., Van Oldenborgh, G. J. & Stockdale, T., 2009; Randall, D. A., Wood, R. A., Bony, S., Colman, R., Fichefet, T., Fyfe, J., Kattsov, V., Pitman, A., Shukla, J., Srinivasan, J. et al., 2007). A cold tongue error still exists in the tropical Pacific in CMIP5, and there are still some important SST errors in the Atlantic (Flato *et al.*, 2013). The spatial pattern of observed teleconnections in the Pacific are well represented in some GCMs when ENSO and PDO are in phase, but the out-of-phase variance is less accurate (Fuentes-Franco *et al.*, 2016).

Finally, the time period considered in hydroclimatological studies is of importance because it determines the number of warm and cold phases within the analysis period (Kurtzman & Scanlon, 2007). The analysis period for this study is from 1961 to 2010, and only covers a 50-year period. The length of the analysis period is too short to capture a full cycle of the multi-decadal ocean-atmospheric oscillations. Even though the climate model large ensemble provides 50 members (leading to $50 \times 50 = 2500$ years), the number of common years under different combinations of phases for each index is still limited to less than 50 years. Analysis based on short time series could lead to an overconfident estimation of the role of oscillations (McCabe & Dettinger, 1999).

5.4 Recommendations for future work

Many of the limitations discussed above can be addressed in future work. This would extend and strengthen the results obtained through this thesis, and help further the body of knowledge required for future droughts adaptation.

5.4.1 Climate change impacts on droughts

The frequency changes of meteorological and hydrological droughts were projected separately in this thesis with no consideration on the propagation from one type to the other. Drought propagation in the current and future climate should be studied to further our understanding of future impacts and current vulnerability. In addition to future frequency, future work should concentrate on the onset and duration of droughts, since minor meteorological droughts can develop into comparatively much more severe hydrological droughts (Van Lanen, H. A., 2006). The droughts durations considered in this thesis started at the monthly time scale. In temperate climate catchments, hydrological droughts duration is commonly smaller than 1-month, and especially so on small catchments. However, simulating smaller catchments using climate models brings additional challenges, including the ability to accurately simulate sub-daily precipitation.

The evolution of the combined role of precipitation deficit and increased potential evapotranspiration in the development and propagation of hydrological droughts is also an area that should be further explored. Precipitation deficit is the main driver of all types of droughts, but potential evapotranspiration will play an increasingly significant role in a warmer climate. Consequently, in the future, changes in hydrological droughts frequency may be mostly driven by temperature increases, although the change in mean precipitation and precipitation variability are also likely to remain important.

A complete uncertainty envelop should be assessed for hydrological droughts in future researches. As mentioned in the literature review section, hydrological drought uncertainty comes from six main sources: GGES, GCM, natural climate variability, downscaling methods, impact models, and impact model parametric uncertainty. This uncertainty should be assessed for each studied drought index. The need to evaluate GCM uncertainty requires the use of multiple GCMs and this implies that extreme droughts would be limited to smaller return periods than the one considered in this study, since large ensembles are not available for multiple climate models. Additional climate model large ensembles should be added when they become available. The upcoming CMIP6 ensemble will in principle provide 5-member ensembles for most GCMs which would allow a much better delineation of uncertainty. Other emission scenarios should also be added to the analysis. If a complete uncertainty study is expected or deemed necessary, other downscaling methods would also need to be added. The use of additional hydrological models should be considered to learn about the uncertainties introduced by the impact model, since model structure, underlying physics and dynamical process, as well as spatial configuration which are all important (Clark *et al.*, 2016). This is especially important for droughts that are often not well simulated by hydrological models. This last point underlines the important point that most hydrological models struggle at representing low flows compared to floods for example. It is therefore likely that inter-model variability, and therefore contribution to uncertainty is large.

5.4.2 Natural climate variability

The final aim of this thesis was to assess the influence of natural climate variability on the future climate and variability of future droughts. Results showed that some regions will experience increasing extreme droughts even though the mean annual precipitation is projected to increase. Such changes are not in contradiction and originate from changes in internal variability. This should be studied further.

Many long-duration droughts which occurred before the mid-20th century (e.g., the 1930s Dust Bowl), are not well documented because weather stations were not widely available. A better understanding of the past may yield significant clues as to the future of our planet. Reconstructed paleoclimatic data can preserve the signal of internal variability and allow for the exploration of how the climate system changes across various time scales. This data should be of a long enough duration to capture the characteristics of internal variability, without the anthropogenic forcing. There is a large ensemble that could be used for that purpose. The CESM1 Last Millennium Ensemble, covers a 1156-year period from 850 to 2006. The ensemble has 36 members, reconstructed by using the transient evolution of solar intensity, volcanic emissions, greenhouse gases, aerosols, land use conditions, and orbital parameters. The data is available at the monthly, daily and 6-hourly time scales (Otto-Bliesner, B. L., Brady, E. C., Fasullo, J., Jahn, A., Landrum, L., Stevenson, S., Rosenbloom, N., Mai, A. & Strand, G., 2016). This ensemble would be very well suited to the study of low-frequency patterns of natural climate variability. Such work would help us better understand the linkage between high and low-frequency components of internal variability and how they impact regional and local climates.

CONCLUSION

The impact of climate change on future extreme droughts was explored in this work. Two GCMs with a large ensemble (CanESM2 and CESM1) were used to assess the impact of climate change on droughts. The future frequency change of meteorological droughts was assessed by using the SPI while future change of hydrological droughts was assessed by using the SDI. The impacts of large-scale oscillations on North American climate variability were also studied to try to link conditions leading to droughts with indices of internal climate variability. The large sample size of GCM large ensembles allows for the direct calculation of droughts with very large return periods. It also allows the study of climatic anomalies linked to the rare combination of distinct phases of various climatic indices. The main conclusions of this work are summarized as follows:

Both climate models project increases of extreme meteorological drought frequency over many of the world's regions, including Central America, Northern South America, Northern and southern Africa, the Mediterranean region, and parts of Australia. The spatial pattern of areas affected by an increasing frequency of extreme meteorological droughts generally matches the change patterns of future annual mean precipitation. Short-term (1-month) droughts would be at least 2 times more frequent for most low- to mid-latitude regions, while long-term (24-month) droughts would be at least 3 times more frequent in future periods. Changes in future extreme meteorological drought frequency are more significant for short-term summer (June-July-August) droughts and get progressively worse for larger return periods.

Over North America, the evolution of future summer meteorological drought patterns generally match the expected changes in mean summer precipitation. Trends for meteorological droughts display a complex spatial pattern with some regions seeing increases (West and Central Canada, Mid-west and Southeast coast) and others seeing decreases in drought frequency. Because of changes in variability, some regions (e.g., Southeast U.S.) will nonetheless see increasing meteorological drought frequency despite increases in mean summer precipitation.

Changes of future extreme hydrological droughts are significantly more severe than their meteorological counterparts, showing a very uniform pattern across North America. This suggests that increases in temperature overcome the expected increasing mean summer precipitation observed in many regions. The few watersheds escaping this trend are either located in colder climates (North of West Canada, Rocky Mountains) or in regions with the largest projected increase in precipitation, like Southern Texas. Predicted changes for both meteorological and hydrological droughts get consistently worse for the longer considered return periods.

The CanESM2-LE is able to represent characteristics of the three studied climate oscillations during the 1961-2010 analysis period. The 2 to 7-year periodicity of ENSO, the spatial pattern of PDO and the variability of SST in the North Atlantic are all well reproduced by CanESM2. This provides a confidence in the ability of using the model to better understand the individual and combined impacts of large-scale oscillations on climate variability. Results show that annual precipitation anomalies are mostly influenced by ENSO whereas temperature anomalies are mostly controlled by AMO over most of North America. El Niño only has a minor impact on temperature anomalies along the eastern coast. A positive AMO is associated with higher temperatures over most of North America and increased precipitation in northern watersheds. The effect of PDO on climate variability is comparatively weaker than ENSO and AMO. The results indicate that North American climate variability is mainly affected by the tropical Pacific Ocean and the Northern Atlantic Ocean. The regions most affected by large-scale variability are mostly close to the Pacific Ocean, including the Western US, High Plains and Western Canada. The patterns of constructive and destructive interference between the three studied indices outline the need to take into account these interactions to better understand internal climate variability and its impact on precipitation and temperature anomalies.

APPENDIX I

CALCULATION RECIPE FOR STANDARDIZED PRECIPITATION INDEX IN MATLAB

```
function [Index]=SPI(data,scale,nm)
% Input data
  % data : Monthly precipitation in 'mm' (column vector)
  % scale : Accumulation period,e.g.,1,3,12,48, in months
  % nm : Number of months (1-month SPI, nm=12; 3-month SPI, nm=4)
% Output data
  % Index: SPI Index, starts from the second year of analysis period

data1=[];
for i=1:scale
    data1=[data1,data(i:length(data)-scale+i)];
end            %each row is the accumulation months

data2=sum(data1,2);
if(scale>1)
    data2(1:nm*ceil(scale/12)-scale+1)=[];
end            %exclude the first year

for i=1:nm
    Data=data2(i:nm:length(data2));
    [zeroa]=find(Data==0);
    Data_nozero=Data;
    Data_nozero(zero)=[];
    q=length(zero)/length(Data);
    p=gamfit(Data_nozero);
    Gam=q+(1-q)*gamcdf(Data,p(1),p(2));
    Index(Xn)=norminv(Gam);
end
```

APPENDIX II

CALCULATION RECIPE FOR LARGE-SCALE OSCILLATIONS INDICES IN MATLAB

```
%% This function is used to extract the SST data and calculate the ...
    NINO 3.4 index

function [NINO_index]=NINO_34_Calculation(lat,lon,sst,analysis_sta,...
analysis_fin,base_sta, base_fin,dates)
%Input data
  % lat (lon): latitude (longitude), column vector
  % dates: monthly calendar
  % sst: sea surface temperature, 3-D matrix (lon*lat*months)
  % analysis_sta: the start year of analysis period
  % analysis_fin: the end year of analysis period
  % base_sta: the start year of reference period
  % base_fin: the end year of reference period

   a1=find(dates(:,1)==analysis_sta&dates(:,2)==1);
   b1=find(dates(:,1)==analysis_fin&dates(:,2)==12);
   ny=analysis_fin-analysis_sta+1;
   year=analysis_sta:analysis_fin;
   dates1=dates(a1:b1,:);

   %extract sst data in NINO 3.4 region [5N-5S 120-170W]
   [X,Y]=meshgrid(lat,lon);
   a=find(lat>-5&lat<5);
   b=find(lon>190&lon<240);
   Region_Nino_lat=X(b,a);
   Region_Nino_lon=Y(b,a);
   sst1=sst(b,a,a1:b1);%sea surface temperature in NINO 3.4 region ...
       in selected analysis period

```

```
    a2=find(dates1(:,1)==base_sta&dates1(:,2)==1);
    b2=find(dates1(:,1)==base_fin&dates1(:,2)==12);

    for ii=1:length(b)
        for jj=1:length(a)
            sst_anomaly(ii,jj,:)=anomaly_making(squeeze(sst1(ii,jj,:)),...
            year,base_sta,base_fin,ny,12,1);
        end
    end %SST anomaly in grid scale

    %area-averaged SST anomaly in NINO 3.4 region
    X=area_average(sst_anomaly,dates1,lon(b),lat(a));

    %5-month running mean
    NINO_index=zscore(moving_average_extend(X));
end
```

```
% SST anomalies averaged over field [0-70N, 0-80W] with the global ...
    mean SST was removed.
% This function was used to calculate the PDO index
function [Index, expv]= PDO_Calculation(lat, lon, sst, analysis_sta, ...
    analysis_fin, base_sta, base_fin, dates)
% Input data
    % lat (lon): latitude (longitude), column vector
    % dates: monthly calendar
    % sst: sea surface temperature, 3D matrix (lon*lat*months)
    % analysis_sta: the start year of analysis period
    % analysis_fin: the end year of analysis period
    % base_sta: the start year of reference period
    % base_fin: the end year of reference period
% Output data
    % Index: monthly Pacific Decadal Index
    % expv: the explained variance by the first EOF

% Extend the period to minimize the effect of 10-year moving average
    analysis_sta=analysis_sta-10;
    analysis_fin=analysis_fin+10;

    year=analysis_sta:analysis_fin;
    ny=length(year);
    a1=find(dates(:,1)==analysis_sta&dates(:,2)==1);
    b1=find(dates(:,1)==analysis_fin&dates(:,2)==12);
    dates1=dates(a1:b1,:);
    [X,Y]=meshgrid(lat,lon);
    a=find(lat≥20&lat<70);
    b=find(lon>110&lon<260);
    Region_PDO_lat=X(b,a);
    Region_PDO_lon=Y(b,a);
    sst1=sst(b,a,a1:b1);
```

```
% Calculate the global mean SST anomalies
    sst_global_average=area_average(sst(:,:,a1:b1),dates1,lon,lat);
    b1=find(dates1(:,1)==base_sta&dates1(:,2)==1);
    b2=find(dates1(:,1)==base_fin&dates1(:,2)==12);

    sst_global_anomaly=anomaly_making(sst_global_average,analysis_sta:
    analysis_fin,base_sta,base_fin,ny,12,1);

% Remove the global mean SST anomaly from SST series
    for ii=1:length(b)
        for jj=1:length(a)
            data=squeeze(sst1(ii,jj,:));
            A=isnan(data);
            if numel(data(A))==length(dates1)
                sst2(ii,jj,:)=NaN(length(dates1),1);
                continue
            else
            sst2(ii,jj,:)=data-sst_global_anomaly;
            end
        end
    end

% Calculate the anomaly over the reference period
    for ii=1:length(b)
       for jj=1:length(a)
           sst_anomaly(ii,jj,:)=anomaly_making(squeeze(sst2(ii,jj,:)),
           year,base_sta,base_fin,ny,12,1);
       end
    end

% Pick the data in November through March
    c1=find(dates1(:,2)==11|dates1(:,2)==12|dates1(:,2)==1|      ...
        dates1(:,2)==2|dates1(:,2)==3);
    sst_anomaly_Win=sst_anomaly(:,:,c1);
```

```
    dates2=dates1(c1,:);

    sst_anomaly_win=permute(sst_anomaly_Win,[2,1,3]);
    Region_PDO_lat=Region_PDO_lat';
    Region_PDO_lon=Region_PDO_lon';

% Calculate the EOFs
   [eof_maps,pc,expvar] = eof(sst_anomaly_win);

% Find the index of the maximum value in the time series:
   [maxval,ind] = max(abs(pc(1,:)));

% Divide the time series by its maximum value:
   PC = pc(1,:)/maxval;

% Multiply the corresponding EOF map:
   eof_maps = eof_maps(:,:,1)*maxval;

   T1=analysis_sta:1/12:analysis_fin+1;
   T1(length(T1))=[];
   T2=T1(1,c1);
   Z=interp1(T2,PC,T1);
   S=moving_average_extend(Z,121);
   clear Z

   Z=S(12*10+1:12*60);
% Standize the amplitude
   T3=analysis_sta+10:1/12:analysis_fin-9;
   T3(length(T3))=[];
   c1=find(T3==analysis_sta+10);
   c2=length(T3);

   Index=(Z-mean(Z(c1:c2,1)))/std(Z(c1:c2,1));
   expv=expvar(1,1);
end
```

```
% This function is used to calculate the Atlantic Multidecadal ...
    Oscillation Index
% SST anomalies averaged over field [0-70N, 0-80W] with the global ...
    mean SST was removed.

function [Index]=AMO_Calculation(date_sta, date_fin, analysis_sta, ...
    analysis_fin, lat, lon, sst, base_sta, base_fin )
% Input:
   %date_sta/date_fin: start/end year of sst data
   %analysis_sta/analysis_fin: start/end year of analysis period
   %base_sta/base_fin: start/end year of reference period

   month=date_sta:1/12:date_fin+1;
   month(:,length(month))=[];

% Extend the length of analysis period to minimize the effect of ...
    10-year moving average
    cal_sta=analysis_sta-10;
    cal_fin=analysis_fin+10;
    a1=find(month==cal_sta);
    a2=find(month==cal_fin+1)-1;
    dates=Calendar_making(cal_sta,cal_fin,2);
    ny=cal_fin-cal_sta+1;

    [X,Y]=meshgrid(lat,lon);
    a=find(lat≥0&lat≤70);
    b=find(lon≥280&lon≤360);

    Region_AMO_lat=X(b,a);
    Region_AMO_lon=Y(b,a);
    sst_region=sst(b,a,a1:a2);%original regional series
    lat1=lat(a);
```

```
    lon1=lon(b);

% Calculate the global mean SST anomalies
    sst_global_average=area_average(sst(:,:,a1:a2),dates,lon,lat);
    b1=find(dates(:,1)==base_sta&dates(:,2)==1);
    b2=find(dates(:,1)==base_fin&dates(:,2)==12);

    sst_global_anomaly=anomaly_making(sst_global_average,cal_sta:cal_fin,
    base_sta,base_fin,ny,12,1);

% Remove the global mean SST anomaly from SST series
    for ii=1:length(b)
        for jj=1:length(a)
            data=squeeze(sst_region(ii,jj,:));
            A=isnan(data);
            if numel(data(A))==length(dates)
                sst2(ii,jj,:)=NaN(length(dates),1);
                continue
            else
            sst2(ii,jj,:)=data-sst_global_anomaly;
            end
        end
    end

% Compute the area average
    sst_area_average=area_average(sst2,dates,lon1,lat1);

% Calculate the anomaly over the reference period
    sst_AMO_anomaly=anomaly_making(sst_area_average,cal_sta:cal_fin,...
    base_sta,base_fin,ny,12,1);

% 10-year (121-month) moving average
    sst_anomaly_smooth=moving_average_extend(sst_AMO_anomaly,121);
    Index=sst_anomaly_smooth(12*10+1:12*60);
end
```

REFERENCES

Abatzoglou, J. T. (2013). Development of gridded surface meteorological data for ecological applications and modelling. *International Journal of Climatology*, 33(1), 121–131.

Ackerley, D., Highwood, E. J. & Frame, D. J. (2009). Quantifying the effects of perturbing the physics of an interactive sulfur scheme using an ensemble of GCMs on the climatepre-diction. net platform. *Journal of Geophysical Research: Atmospheres*, 114(D1).

Ahmed, K., Shahid, S., bin Harun, S. & Wang, X.-j. (2016). Characterization of seasonal droughts in Balochistan Province, Pakistan. *Stochastic environmental research and risk assessment*, 30(2), 747–762.

Ahn, K.-H., Merwade, V., Ojha, C. & Palmer, R. N. (2016). Quantifying relative uncertainties in the detection and attribution of human-induced climate change on winter streamflow. *Journal of hydrology*, 542, 304–316.

Alahdin, S., Ghafouri, H. & Haghighi, A. (2018). Derivation of conflict resolution rule-curves in multi-purpose multi-reservoir system for inter-basin water transfer during drought. *Environmental Resources Research*, 6(1), 51–68.

Alamgir, M., Shahid, S., Mohsenipour, M. & Ahmed, K. (2015). Return periods of extreme meteorological droughts during monsoon in Bangladesh. *Applied Mechanics and Materials*, 735, 186–189.

Allen, R. G., Pruitt, W. O., Wright, J. L., Howell, T. A., Ventura, F., Snyder, R., Itenfisu, D., Steduto, P., Berengena, J., Yrisarry, J. B. et al. (2006). A recommendation on standardized surface resistance for hourly calculation of reference ETo by the FAO56 Penman-Monteith method. *Agricultural Water Management*, 81(1-2), 1–22.

Alley, W. M. (1984). The Palmer drought severity index: limitations and assumptions. *Journal of climate and applied meteorology*, 23(7), 1100–1109.

Anchukaitis, K., Cook, B. & Cook, E. (2016). Past, present, and future western North American drought in models and paleoclimate data. *AGU Fall Meeting Abstracts*.

Arnell, N. W. (2003). Relative effects of multi-decadal climatic variability and changes in the mean and variability of climate due to global warming: future streamflows in Britain. *Journal of Hydrology*, 270(3-4), 195–213.

Arnell, N. W. & Gosling, S. N. (2016). The impacts of climate change on river flood risk at the global scale. *Climatic Change*, 134(3), 387–401.

Arnell, N., Grabs, W., Mimikou, M., Schumann, A., Reynard, N., Kaczmarek, Z., Oancea, V., Buchtele, J., Kasparek, L., Blazoka, S. et al. (2000). Effect of climate change on hydrological regimes and water resources in Europe. *Summary Report of Projects EV5V-CT93-0293 and EV5V-CT94-0114. University of Southampton, UK*.

Arora, V. K. & Boer, G. J. (2001). Effects of simulated climate change on the hydrology of major river basins. *Journal of Geophysical Research: Atmospheres*, 106(D4), 3335–3348.

Arora, V., Scinocca, J., Boer, G., Christian, J., Denman, K., Flato, G., Kharin, V., Lee, W. & Merryfield, W. (2011). Carbon emission limits required to satisfy future representative concentration pathways of greenhouse gases. *Geophysical Research Letters*, 38(5).

Arsenault, R., Gatien, P., Renaud, B., Brissette, F. & Martel, J.-L. (2015). A comparative analysis of 9 multi-model averaging approaches in hydrological continuous streamflow simulation. *Journal of Hydrology*, 529, 754–767.

Arsenault, R., Bazile, R., Ouellet Dallaire, C. & Brissette, F. (2016). CANOPEX: A Canadian hydrometeorological watershed database. *Hydrological Processes*, 30(15), 2734–2736.

Asong, Z. E., Wheater, H. S., Bonsal, B., Razavi, S. & Kurkute, S. (2018). Historical drought patterns over Canada and their teleconnections with large-scale climate signals. *Hydrology and Earth System Sciences*, 22(6), 3105–3124.

Ault, T. R., Mankin, J. S., Cook, B. I. & Smerdon, J. E. (2016). Relative impacts of mitigation, temperature, and precipitation on 21st-century megadrought risk in the American Southwest. *Science Advances*, 2(10), e1600873.

Aut, M. F. (2015). STI: Calculation of the Standardized Temperature Index. *Physica Status Solidi*.

Ayala, J. J. H. & Heslar, M. (2019). Examining the spatiotemporal characteristics of droughts in the Caribbean using the standardized precipitation index (SPI). *Climate Research*, 78(2), 103–116.

Bader, D. C., Covey, C., Gutowski Jr, W. J., Held, I. M., Miller, R. L., Tokmakian, R. T., Zhang, M. H. et al. (2008). Climate models: an assessment of strengths and limitations.

Barlow, M., Nigam, S. & Berbery, E. H. (2001). ENSO, Pacific decadal variability, and US summertime precipitation, drought, and stream flow. *Journal of climate*, 14(9), 2105–2128.

Barnett, T. P., Adam, J. C. & Lettenmaier, D. P. (2005). Potential impacts of a warming climate on water availability in snow-dominated regions. *Nature*, 438(7066), 303.

Barrie Bonsal,Grace Koshida, E. T. O. E. W. (2004). *Chapter 3. Droughts. In Threats to Water Availability in Canada. Environment Canada*.

Bellenger, H., Guilyardi, É., Leloup, J., Lengaigne, M. & Vialard, J. (2014). ENSO representation in climate models: from CMIP3 to CMIP5. *Climate Dynamics*, 42(7-8), 1999–2018.

Bonsal, B. R., Wheaton, E. E., Chipanshi, A. C., Lin, C., Sauchyn, D. J. & Wen, L. (2011). Drought research in Canada: A review. *Atmosphere-Ocean*, 49(4), 303–319.

Bonsal, B. R., Aider, R., Gachon, P. & Lapp, S. (2013). An assessment of Canadian prairie drought: past, present, and future. *Climate Dynamics*, 41(2), 501–516.

Bonsal,B.R., P. D. S. F. R. A. & Berg, A. (2019). *Changes in freshwater availability across Canada; Chapter 6 in Canada's Changing Climate Report* (Report n°p. 261-342). Ottwa, Ontario.

Boo, K.-O., Kwon, W.-T. & Baek, H.-J. (2006). Change of extreme events of temperature and precipitation over Korea using regional projection of future climate change. *Geophysical Research Letters*, 33(1).

Boyer, C., Chaumont, D., Chartier, I. & Roy, A. G. (2010). Impact of climate change on the hydrology of St. Lawrence tributaries. *Journal of hydrology*, 384(1-2), 65–83.

Braun, M., Caya, D., Frigon, A. & Slivitzky, M. (2012). Internal variability of the Canadian RCM's hydrological variables at the basin scale in Quebec and Labrador. *Journal of Hydrometeorology*, 13(2), 443–462.

Brito, S., Cunha, A., Cunningham, C., Alvalá, R., Marengo, J. & Carvalho, M. (2018). Frequency, duration and severity of drought in the Semiarid Northeast Brazil region. *International Journal of Climatology*, 38(2), 517–529.

Brown, A., Milton, S., Cullen, M., Golding, B., Mitchell, J. & Shelly, A. (2012). Unified modeling and prediction of weather and climate: A 25-year journey. *Bulletin of the American Meteorological Society*, 93(12), 1865–1877.

Burke, E. J. & Brown, S. J. (2008). Evaluating uncertainties in the projection of future drought. *Journal of Hydrometeorology*, 9(2), 292–299.

Burke, E. J., Brown, S. J. & Christidis, N. (2006). Modeling the recent evolution of global drought and projections for the twenty-first century with the Hadley Centre climate model. *Journal of Hydrometeorology*, 7(5), 1113–1125.

Burrows, K. & Kinney, P. (2016). Exploring the climate change, migration and conflict nexus. *International journal of environmental research and public health*, 13(4), 443.

Cai, W., Borlace, S., Lengaigne, M., Van Rensch, P., Collins, M., Vecchi, G., Timmermann, A., Santoso, A., McPhaden, M. J., Wu, L. et al. (2014). Increasing frequency of extreme El Niño events due to greenhouse warming. *Nature climate change*, 4(2), 111.

Cai, W., Wang, G., Santoso, A., McPhaden, M. J., Wu, L., Jin, F.-F., Timmermann, A., Collins, M., Vecchi, G., Lengaigne, M. et al. (2015). Increased frequency of extreme La Niña events under greenhouse warming. *Nature Climate Change*, 5(2), 132.

Cayan, D. R., Dettinger, M. D., Diaz, H. F. & Graham, N. E. (1998). Decadal variability of precipitation over western North America. *Journal of Climate*, 11(12), 3148–3166.

Cayan, D. R., Redmond, K. T. & Riddle, L. G. (1999). ENSO and hydrologic extremes in the western United States. *Journal of Climate*, 12(9), 2881–2893.

Cayan, D. R., Dettinger, M. D., Pierce, D., Das, T., Knowles, N., Ralph, F. M. & Sumargo, E. (2016). Natural variability, anthropogenic climate change, and impacts on water availability and flood extremes in the Western United States. *Water Policy and Planning in a Variable and Changing Climate*, 17.

Chen, J. & Brissette, F. P. (2018). Reliability of climate model multi-member ensembles in estimating internal precipitation and temperature variability at the multi-decadal scale. *International journal of climatology*.

Chen, J., Brissette, F. P. & Leconte, R. (2011a). Uncertainty of downscaling method in quantifying the impact of climate change on hydrology. *Journal of hydrology*, 401(3-4), 190–202.

Chen, J., Brissette, F. P., Poulin, A. & Leconte, R. (2011b). Overall uncertainty study of the hydrological impacts of climate change for a Canadian watershed. *Water Resources Research*, 47(12).

Chen, J., Brissette, F. P., Chaumont, D. & Braun, M. (2013). Performance and uncertainty evaluation of empirical downscaling methods in quantifying the climate change impacts on hydrology over two North American river basins. *Journal of Hydrology*, 479, 200–214.

Chen, J., Brissette, F. P., Zhang, X. J., Chen, H., Guo, S. & Zhao, Y. (2019). Bias correcting climate model multi-member ensembles to assess climate change impacts on hydrology. *Climatic Change*, 1–17.

Cherneski, P. (2018). *The Impacts and Costs of Drought to the Canadian Agriculture Sector*.

Church, J., Clark, P., Cazenave, A., Gregory, J., Jevrejeva, S., Levermann, A., Merrifield, M., Milne, G., Nerem, R., Nunn, P. et al. (2013). Climate change 2013: the physical science basis. Contribution of Working Group I to the Fifth Assessment Report of the Intergovernmental Panel on Climate Change. *Sea level change*, 1137–1216.

Chylek, P., Li, J., Dubey, M., Wang, M. & Lesins, G. (2011). Observed and model simulated 20th century Arctic temperature variability: Canadian earth system model CanESM2. *Atmospheric Chemistry and Physics Discussions*, 11(8), 22893–22907.

Clark, M. P., Wilby, R. L., Gutmann, E. D., Vano, J. A., Gangopadhyay, S., Wood, A. W., Fowler, H. J., Prudhomme, C., Arnold, J. R. & Brekke, L. D. (2016). Characterizing uncertainty of the hydrologic impacts of climate change. *Current Climate Change Reports*, 2(2), 55–64.

Clarvis, M. H., Fatichi, S., Allan, A., Fuhrer, J., Stoffel, M., Romerio, F., Gaudard, L., Burlando, P., Beniston, M., Xoplaki, E. et al. (2014). Governing and managing water resources under changing hydro-climatic contexts: The case of the upper Rhone basin. *Environmental science & policy*, 43, 56–67.

Clausen, B. & Pearson, C. (1995). Regional frequency analysis of annual maximum streamflow drought. *Journal of Hydrology*, 173(1-4), 111–130.

Coats, S., Smerdon, J. E., Cook, B., Seager, R., Cook, E. R. & Anchukaitis, K. (2016). Internal ocean-atmosphere variability drives megadroughts in Western North America. *Geophysical research letters*, 43(18), 9886–9894.

Cook, B. I., Smerdon, J. E., Seager, R. & Coats, S. (2014). Global warming and 21 st century drying. *Climate Dynamics*, 43(9-10), 2607–2627.

Cook, B. I., Ault, T. R. & Smerdon, J. E. (2015). Unprecedented 21st century drought risk in the American Southwest and Central Plains. *Science Advances*, 1(1), e1400082.

Cook, E. R., Seager, R., Cane, M. A. & Stahle, D. W. (2007). North American drought: Reconstructions, causes, and consequences. *Earth-Science Reviews*, 81(1-2), 93–134.

Cook, E. R., Anchukaitis, K. J., Buckley, B. M., D'Arrigo, R. D., Jacoby, G. C. & Wright, W. E. (2010). Asian monsoon failure and megadrought during the last millennium. *Science*, 328(5977), 486–489.

Coumou, D. & Rahmstorf, S. (2012). A decade of weather extremes. *Nature climate change*, 2(7), 491.

Craen, S. d., Commandeur, J. J., Frank, L. E. & Heiser, W. J. (2006). Effects of group size and lack of sphericity on the recovery of clusters in K-means cluster analysis. *Multivariate Behavioral Research*, 41(2), 127–145.

Cunnane, C. (1978). Unbiased plotting positions—a review. *Journal of Hydrology*, 37(3-4), 205–222.

Dai, A. (2011). Drought under global warming: a review. *Wiley Interdisciplinary Reviews: Climate Change*, 2(1), 45–65.

Dai, A. (2013a). Increasing drought under global warming in observations and models. *Nature Climate Change*, 3(1), 52.

Dai, A. (2013b). The influence of the inter-decadal Pacific oscillation on US precipitation during 1923–2010. *Climate dynamics*, 41(3-4), 633–646.

Dai, A. & Bloecker, C. E. (2019). Impacts of internal variability on temperature and precipitation trends in large ensemble simulations by two climate models. *Climate dynamics*, 52(1-2), 289–306.

Dai, A. & Zhao, T. (2017). Uncertainties in historical changes and future projections of drought. Part I: estimates of historical drought changes. *Climatic Change*, 144(3), 519–533.

Dai, A., Trenberth, K. E. & Qian, T. (2004). A global dataset of Palmer Drought Severity Index for 1870–2002: Relationship with soil moisture and effects of surface warming. *Journal of Hydrometeorology*, 5(6), 1117–1130.

Dai, A., Fyfe, J. C., Xie, S.-P. & Dai, X. (2015). Decadal modulation of global surface temperature by internal climate variability. *Nature Climate Change*, 5(6), 555.

Dai, A., Zhao, T. & Chen, J. (2018). Climate Change and Drought: a Precipitation and Evaporation Perspective. *Current Climate Change Reports*, 4(3), 301–312.

Déry, S. J. & Wood, E. F. (2004). Teleconnection between the Arctic Oscillation and Hudson Bay river discharge. *Geophysical Research Letters*, 31(18).

Deser, C., Phillips, A. S. & Hurrell, J. W. (2004). Pacific interdecadal climate variability: Linkages between the tropics and the North Pacific during boreal winter since 1900. *Journal of Climate*, 17(16), 3109–3124.

Deser, C., Knutti, R., Solomon, S. & Phillips, A. S. (2012a). Communication of the role of natural variability in future North American climate. *Nature Climate Change*, 2(11), 775.

Deser, C., Phillips, A., Bourdette, V. & Teng, H. (2012b). Uncertainty in climate change projections: the role of internal variability. *Climate dynamics*, 38(3-4), 527–546.

Dibike, Y., Prowse, T., Bonsal, B. & O'Neil, H. (2017). Implications of future climate on water availability in the western Canadian river basins. *International Journal of Climatology*, 37(7), 3247–3263.

Diffenbaugh, N. S., Swain, D. L. & Touma, D. (2015). Anthropogenic warming has increased drought risk in California. *Proceedings of the National Academy of Sciences*, 112(13), 3931–3936.

Donat, M. G., Lowry, A. L., Alexander, L. V., O'Gorman, P. A. & Maher, N. (2016). More extreme precipitation in the world's dry and wet regions. *Nature Climate Change*, 6(5), 508.

Dong, B.-W. & Sutton, R. (2002). Adjustment of the coupled ocean–atmosphere system to a sudden change in the thermohaline circulation. *Geophysical Research Letters*, 29(15), 18–1.

Dracup, J. A., Lee, K. S. & Paulson Jr, E. G. (1980). On the definition of droughts. *Water resources research*, 16(2), 297–302.

Ehmele, F. & Kunz, M. (2019). Flood-related extreme precipitation in southwestern Germany: development of a two-dimensional stochastic precipitation model. *Hydrology and Earth System Sciences*, 23(2), 1083–1102.

Ehret, U., Zehe, E., Wulfmeyer, V., Warrach-Sagi, K. & Liebert, J. (2012). HESS Opinions" Should we apply bias correction to global and regional climate model data?". *Hydrology and Earth System Sciences*, 16(9), 3391–3404.

Ellen, H., Jeffrey, M. & Caitrin, C. (2015). California's Latest Drought. *PPIC*.

Emerton, R., Cloke, H., Stephens, E., Zsoter, E., Woolnough, S. & Pappenberger, F. (2017). Complex picture for likelihood of ENSO-driven flood hazard. *Nature communications*, 8(1), 1–9.

Enfield, D. B., Mestas-Nuñez, A. M. & Trimble, P. J. (2001). The Atlantic multidecadal oscillation and its relation to rainfall and river flows in the continental US. *Geophysical Research Letters*, 28(10), 2077–2080.

Environment-Canada. (2004). Threats to water availability in Canada. National Water Research Institute Burlington.

Espinoza, J. C., Ronchail, J., Guyot, J. L., Junquas, C., Vauchel, P., Lavado, W., Drapeau, G. & Pombosa, R. (2011). Climate variability and extreme drought in the upper Solimões River (western Amazon Basin): Understanding the exceptional 2010 drought. *Geophysical Research Letters*, 38(13).

Essou, G. R., Arsenault, R. & Brissette, F. P. (2016). Comparison of climate datasets for lumped hydrological modeling over the continental United States. *Journal of hydrology*, 537, 334–345.

Everitt, B. & Rabehesketh, S. (1980). Cluster Analysis. *Quality & Quantity*, 14(1), 75-100.

Everitt, B. S. & Dunn, G. (2013). *Applied Multivariate Data Analysis, Second Edition*.

Eyring, V., Bony, S., Meehl, G. A., Senior, C. A., Stevens, B., Stouffer, R. J. & Taylor, K. E. (2016). Overview of the Coupled Model Intercomparison Project Phase 6 (CMIP6) experimental design and organization. *Geoscientific Model Development*, 9(5), 1937–1958.

Fatichi, S., Rimkus, S., Burlando, P. & Bordoy, R. (2014). Does internal climate variability overwhelm climate change signals in streamflow? The upper Po and Rhone basin case studies. *Science of the Total Environment*, 493, 1171–1182.

Feng, D., Beighley, E., Raoufi, R., Melack, J., Zhao, Y., Iacobellis, S. & Cayan, D. (2019). Propagation of future climate conditions into hydrologic response from coastal southern California watersheds. *Climatic Change*, 1–20.

Feng, S., Trnka, M., Hayes, M. & Zhang, Y. (2017). Why do different drought indices show distinct future drought risk outcomes in the US Great Plains? *Journal of Climate*, 30(1), 265–278.

Feyen, L. & Dankers, R. (2009). Impact of global warming on streamflow drought in Europe. *Journal of Geophysical Research: Atmospheres*, 114(D17).

Field, C. B., Barros, V., Stocker, T. F. & Dahe, Q. (2012). *Managing the risks of extreme events and disasters to advance climate change adaptation: special report of the intergovernmental panel on climate change*. Cambridge University Press.

Fischer, E. M. & Knutti, R. (2015). Anthropogenic contribution to global occurrence of heavy-precipitation and high-temperature extremes. *Nature Climate Change*, 5(6), 560.

Flato, G., Marotzke, J., Abiodun, B., Braconnot, P., Chou, S. C., Collins, W. J., Cox, P., Driouech, F., Emori, S. & Eyring, V. (2013). Evaluation of climate models. In: climate change 2013: the physical science basis. Contribution of working group I to the fifth assessment report of the intergovernmental panel on climate change [Stocker, T.F., D. Qin, G.-K. Plattner, M. Tignor, S.K. Allen, J. Boschung, A. Nauels, Y. Xia, V. Bex and P.M. Midgley (eds.)]. Cambridge, United Kingdom and New York, NY, USA: Cambridge University Press.

Forootan, E., Khaki, M., Schumacher, M., Wulfmeyer, V., Mehrnegar, N., van Dijk, A., Brocca, L., Farzaneh, S., Akinluyi, F., Ramillien, G. et al. (2019). Understanding the global hydrological droughts of 2003–2016 and their relationships with teleconnections. *Science of the Total Environment*, 650, 2587–2604.

Fowler, H. J., Blenkinsop, S. & Tebaldi, C. (2007). Linking climate change modelling to impacts studies: recent advances in downscaling techniques for hydrological modelling. *International journal of climatology*, 27(12), 1547–1578.

Fu, Q. & Feng, S. (2014). Responses of terrestrial aridity to global warming. *Journal of Geophysical Research: Atmospheres*, 119(13), 7863–7875.

Fuentes-Franco, R., Giorgi, F., Coppola, E. & Kucharski, F. (2016). The role of ENSO and PDO in variability of winter precipitation over North America from twenty first century CMIP5 projections. *Climate dynamics*, 46(9-10), 3259–3277.

Fuhrer, J., Beniston, M., Fischlin, A., Frei, C., Goyette, S., Jasper, K. & Pfister, C. (2006). Climate risks and their impact on agriculture and forests in Switzerland. In *Climate Variability, Predictability and Climate Risks* (pp. 79–102). Springer.

Gan, T. Y. (2000). Reducing vulnerability of water resources of Canadian prairies to potential droughts and possible climatic warming. *Water Resources Management*, 14(2), 111–135.

Gan, Z., Guan, X., Kong, X., Guo, R., Huang, H., Huang, W. & Xu, Y. (2019). The Key Role of Atlantic Multidecadal Oscillation in Minimum Temperature Over North America During Global Warming Slowdown. *Earth and Space Science*, 6(3), 387–397.

Gershunov, A. & Barnett, T. P. (1998). Interdecadal modulation of ENSO teleconnections. *Bulletin of the American Meteorological Society*, 79(12), 2715–2726.

Giorgi, F. & Francisco, R. (2000). Uncertainties in regional climate change prediction: a regional analysis of ensemble simulations with the HADCM2 coupled AOGCM. *Climate Dynamics*, 16(2-3), 169–182.

Giuntoli, I., Villarini, G., Prudhomme, C. & Hannah, D. M. (2018). Uncertainties in projected runoff over the conterminous United States. *Climatic Change*, 150(3), 149–162. doi: 10.1007/s10584-018-2280-5.

Golian, S., Mazdiyasni, O. & AghaKouchak, A. (2015). Trends in meteorological and agricultural droughts in Iran. *Theoretical and applied climatology*, 119(3-4), 679–688.

Goly, A. & Teegavarapu, R. S. (2014). Individual and coupled influences of AMO and ENSO on regional precipitation characteristics and extremes. *Water Resources Research*, 50(6), 4686–4709.

Gosling, S. N. & Arnell, N. W. (2016). A global assessment of the impact of climate change on water scarcity. *Climatic Change*, 134(3), 371–385.

Gray, S. T., Betancourt, J. L., Fastie, C. L. & Jackson, S. T. (2003). Patterns and sources of multidecadal oscillations in drought-sensitive tree-ring records from the central and southern Rocky Mountains. *Geophysical Research Letters*, 30(6).

Grillakis, M. G. (2019). Increase in severe and extreme soil moisture droughts for Europe under climate change. *Science of The Total Environment*, 660, 1245–1255.

Guilyardi, E., Wittenberg, A., Fedorov, A., Collins, M., Wang, C., Capotondi, A., Van Oldenborgh, G. J. & Stockdale, T. (2009). Understanding El Niño in ocean–atmosphere general circulation models: Progress and challenges. *Bulletin of the American Meteorological Society*, 90(3), 325–340.

Gupta, H. V., Kling, H., Yilmaz, K. K. & Martinez, G. F. (2009). Decomposition of the mean squared error and NSE performance criteria: Implications for improving hydrological modelling. *Journal of hydrology*, 377(1-2), 80–91.

Guttman, N. B. (1998). Comparing the palmer drought index and the standardized precipitation index 1. *JAWRA Journal of the American Water Resources Association*, 34(1), 113–121.

Guttman, N. B. (1999). Accepting the standardized precipitation index: a calculation algorithm 1. *JAWRA Journal of the American Water Resources Association*, 35(2), 311–322.

Haddeland, I., Heinke, J., Biemans, H., Eisner, S., Flörke, M., Hanasaki, N., Konzmann, M., Ludwig, F., Masaki, Y., Schewe, J. et al. (2014). Global water resources affected by human interventions and climate change. *Proceedings of the National Academy of Sciences*, 111(9), 3251–3256.

Hagemann, S., Chen, C., Haerter, J. O., Heinke, J., Gerten, D. & Piani, C. (2011). Impact of a statistical bias correction on the projected hydrological changes obtained from three GCMs and two hydrology models. *Journal of Hydrometeorology*, 12(4), 556–578.

Ham, Y.-G. & Kug, J.-S. (2014). Effects of Pacific Intertropical Convergence Zone precipitation bias on ENSO phase transition. *Environmental Research Letters*, 9(6), 064008.

Hamed, K. & Rao, A. R. (2019). *Flood frequency analysis*. CRC press.

Hanesiak, J., Stewart, R., Bonsal, B., Harder, P., Lawford, R., Aider, R., Amiro, B., Atallah, E., Barr, A., Black, T. et al. (2011). Characterization and summary of the 1999–2005 Canadian Prairie drought. *Atmosphere-Ocean*, 49(4), 421–452.

Hannaford, J., Lloyd-Hughes, B., Keef, C., Parry, S. & Prudhomme, C. (2011). Examining the large-scale spatial coherence of European drought using regional indicators of precipitation and streamflow deficit. *Hydrological Processes*, 25(7), 1146–1162.

Hare, S. R. (1996). *Low frequency climate variability and salmon production*. (Ph.D. thesis, University of Washington).

Harris, I., Jones, P. D., Osborn, T. J. & Lister, D. H. (2014). Updated high-resolution grids of monthly climatic observations–the CRU TS3. 10 Dataset. *International journal of climatology*, 34(3), 623–642.

Hawkins, E. & Sutton, R. (2009). The potential to narrow uncertainty in regional climate predictions. *Bulletin of the American Meteorological Society*, 90(8), 1095–1108.

Hayes, M., Svoboda, M., Wall, N. & Widhalm, M. (2011). The Lincoln declaration on drought indices: universal meteorological drought index recommended. *Bulletin of the American Meteorological Society*, 92(4), 485–488.

Hayes, M. J., Svoboda, M. D., Wiihite, D. A. & Vanyarkho, O. V. (1999). Monitoring the 1996 drought using the standardized precipitation index. *Bulletin of the American meteorological society*, 80(3), 429–438.

He, J., Valeo, C. & Bouchart, F.-C. (2006). Enhancing urban infrastructure investment planning practices for a changing climate. *Water science and technology*, 53(10), 13–20.

Hegerl, G. C., Black, E., Allan, R. P., Ingram, W. J., Polson, D., Trenberth, K. E., Chadwick, R. S., Arkin, P. A., Sarojini, B. B., Becker, A. et al. (2018). Challenges in quantifying changes in the global water cycle. *Bulletin of the American Meteorological Society*, 99(1).

Heim, J. & Richard, R. (2002). A review of twentieth-century drought indices used in the United States. *Bulletin of the American Meteorological Society*, 83(8), 1149–1165.

Heim, R. et al. (2000). Drought indices: a review. *Drought: a global assessment*, 159–167.

Helama, S., Meriläinen, J. & Tuomenvirta, H. (2009). Multicentennial megadrought in northern Europe coincided with a global El Niño–Southern Oscillation drought pattern during the Medieval Climate Anomaly. *Geology*, 37(2), 175–178.

Hirabayashi, Y., Kanae, S., Emori, S., Oki, T. & Kimoto, M. (2008). Global projections of changing risks of floods and droughts in a changing climate. *Hydrological Sciences Journal*, 53(4), 754–772.

Hisdal, H. & Tallaksen, L. (2000). Assessment of the regional impact of droughts in Europe. *Drought event definition technical report to the ARIDE project*, (6).

Hoerling, M., Eischeid, J., Kumar, A., Leung, R., Mariotti, A., Mo, K., Schubert, S. & Seager, R. (2014). Causes and predictability of the 2012 Great Plains drought. *Bulletin of the American Meteorological Society*, 95(2), 269–282.

Howitt, R., MacEwan, D., Medellín-Azuara, J., Lund, J. R. & Sumner, D. (2015). *Economic analysis of the 2015 drought for California agriculture*. Center for Watershed Sciences University of California, Davis, CA.

Hu, Q. & Feng, S. (2012). AMO-and ENSO-driven summertime circulation and precipitation variations in North America. *Journal of Climate*, 25(19), 6477–6495.

Hu, Z.-Z. & Huang, B. (2009). Interferential impact of ENSO and PDO on dry and wet conditions in the US Great Plains. *Journal of Climate*, 22(22), 6047–6065.

Hu, Z.-Z., Kumar, A., Jha, B. & Huang, B. (2012). An analysis of forced and internal variability in a warmer climate in CCSM3. *Journal of Climate*, 25(7), 2356–2373.

Huang, B., Banzon, V. F., Freeman, E., Lawrimore, J., Liu, W., Peterson, T. C., Smith, T. M., Thorne, P. W., Woodruff, S. D. & Zhang, H.-M. (2015a). Extended reconstructed sea surface temperature version 4 (ERSST. v4). Part I: Upgrades and intercomparisons. *Journal of climate*, 28(3), 911–930.

Huang, B., Thorne, P. W., Smith, T. M., Liu, W., Lawrimore, J., Banzon, V. F., Zhang, H.-M., Peterson, T. C. & Menne, M. (2016). Further exploring and quantifying uncertainties for extended reconstructed sea surface temperature (ERSST) version 4 (v4). *Journal of Climate*, 29(9), 3119–3142.

Huang, N. E. & Wu, Z. (2008). A review on Hilbert-Huang transform: Method and its applications to geophysical studies. *Reviews of geophysics*, 46(2).

Huang, N. E., Shen, Z., Long, S. R., Wu, M. C., Shih, H. H., Zheng, Q., Yen, N.-C., Tung, C. C. & Liu, H. H. (1998). The empirical mode decomposition and the Hilbert spectrum for nonlinear and non-stationary time series analysis. *Proceedings of the Royal Society of London. Series A: Mathematical, Physical and Engineering Sciences*, 454(1971), 903–995.

Huang, S., Krysanova, V. & Hattermann, F. (2015b). Projections of climate change impacts on floods and droughts in Germany using an ensemble of climate change scenarios. *Regional environmental change*, 15(3), 461–473.

Hulme, M., Barrow, E. M., Arnell, N. W., Harrison, P. A., Johns, T. C. & Downing, T. E. (1999). Relative impacts of human-induced climate change and natural climate variability. *Nature*, 397(6721), 688.

Hulme, M., Doherty, R., Ngara, T., New, M. & Lister, D. (2001). African climate change: 1900-2100. *Climate research*, 17(2), 145–168.

Iizumi, T., Nishimori, M., Dairaku, K., Adachi, S. A. & Yokozawa, M. (2011). Evaluation and intercomparison of downscaled daily precipitation indices over Japan in present-day climate: Strengths and weaknesses of dynamical and bias correction-type statistical downscaling methods. *Journal of Geophysical Research: Atmospheres*, 116(D1).

IPCC. (2001). *Climate Change 2001: The Scientific Basis. Contribution of working group I to the Third Assessment Report of the International Panel on Climate Change e [Houghton, J.T., Y. Ding, D.J. Griggs, M. Noguer, P.J. van der Linden, X. Dai, K. Maskell, and C.A. Johnson (eds.)]*. Cambridge, United Kingdom and New York, NY, USA. 881pp: Cambridge University Press, Cambridge, United Kingdom and New York, NY, USA, 881pp.

IPCC. (2007). *Climate Change 2007: The Physical Science Basis. Contribution of Working Group I to the Fourth Assessment Report of the Intergovernmental Panel on Climate Change [Solomon, S., D. Qin, M. Manning, Z. Chen, M. Marquis, K.B. Averyt, M. Tignor and H.L. Miller (eds.)]*. Cambridge, United Kingdom and New York, NY, USA, 996pp: Cambridge University Press, Cambridge, United Kingdom and New York, NY, USA, 996 pp.

IPCC. (2013a). *Climate Change 2013: The Physical Science Basis. Contribution of Working Group I to the Fifth Assessment Report of the Intergovernmental Panel on Climate Change [Stocker, T.F., D. Qin, G.-K. Plattner, M. Tignor, S.K. Allen, J. Boschung, A. Nauels, Y. Xia, V. Bex and P.M. Midgley (eds.)]*. Cambridge University Press, Cambridge, United Kingdom and New York, NY, USA, 1535 pp.

IPCC. (2013b). Summary for Policymakers. In: Climate Change 2013: The Physical Science Basis. Contribution of Working Group I to the Fifth Assessment Report of the Intergovernmental Panel on Climate Change [Stocker, T.F., D. Qin, G.-K. Plattner, M. Tignor, S.K. Allen, J. Boschung, A. Nauels, Y. Xia, V. Bex and P.M. Midgley (eds.)]. Cambridge, United Kingdom and New York, NY, USA: Cambridge University Press.

IPCC. (2014). *Climate change 2014: Synthesis Report. Contribution of Working Groups I, II and III to the Fifth Assessment Report of the Intergovernmental Panel on Climate Change [Core Writing Team, R.K. Pachauri and L.A. Meyer (eds.)]*. Geneva, Switzerland, 151pp: IPCC.

Jakob Themeßl, M., Gobiet, A. & Leuprecht, A. (2011). Empirical-statistical downscaling and error correction of daily precipitation from regional climate models. *International Journal of Climatology*, 31(10), 1530–1544.

Jiang, P., Yu, Z. & Acharya, K. (2019). Drought in the Western United States: Its Connections with Large-Scale Oceanic Oscillations. *Atmosphere*, 10(2), 82.

Jiménez-Muñoz, J. C., Mattar, C., Barichivich, J., Santamaría-Artigas, A., Takahashi, K., Malhi, Y., Sobrino, J. A. & Van Der Schrier, G. (2016). Record-breaking warming and extreme drought in the Amazon rainforest during the course of El Niño 2015–2016. *Scientific reports*, 6, 33130.

Johnson, N. T., Martinez, C. J., Kiker, G. A. & Leitman, S. (2013). Pacific and Atlantic sea surface temperature influences on streamflow in the Apalachicola–Chattahoochee–Flint river basin. *Journal of hydrology*, 489, 160–179.

Kalnay, E., Kanamitsu, M., Kistler, R., Collins, W., Deaven, D., Gandin, L., Iredell, M., Saha, S., White, G., Woollen, J. et al. (1996). The NCEP/NCAR 40-year reanalysis project. *Bulletin of the American meteorological Society*, 77(3), 437–472.

Kalra, A. & Ahmad, S. (2012). Estimating annual precipitation for the Colorado River Basin using oceanic-atmospheric oscillations. *Water Resources Research*, 48(6).

Karl, T. R. (1986). The sensitivity of the Palmer drought severity index and Palmer's Z-index to their calibration coefficients including potential evapotranspiration. *Journal of Climate and Applied Meteorology*, 25(1), 77–86.

Karlsson, I. B., Sonnenborg, T. O., Refsgaard, J. C., Trolle, D., Børgesen, C. D., Olesen, J. E., Jeppesen, E. & Jensen, K. H. (2016). Combined effects of climate models, hydrological model structures and land use scenarios on hydrological impacts of climate change. *Journal of Hydrology*, 535, 301–317.

Kattelus, M., Salmivaara, A., Mellin, I., Varis, O. & Kummu, M. (2016). An evaluation of the Standardized Precipitation Index for assessing inter-annual rice yield variability in the Ganges–Brahmaputra–Meghna region. *International Journal of Climatology*, 36(5), 2210–2222.

Kay, A. & Davies, H. (2008). Calculating potential evaporation from climate model data: A source of uncertainty for hydrological climate change impacts. *Journal of Hydrology*, 358(3-4), 221–239.

Kay, J., Deser, C., Phillips, A., Mai, A., Hannay, C., Strand, G., Arblaster, J., Bates, S., Danabasoglu, G., Edwards, J. et al. (2015). The Community Earth System Model (CESM) large ensemble project: A community resource for studying climate change in the presence of internal climate variability. *Bulletin of the American Meteorological Society*, 96(8), 1333–1349.

Kelley, C. P., Mohtadi, S., Cane, M. A., Seager, R. & Kushnir, Y. (2015). Climate change in the Fertile Crescent and implications of the recent Syrian drought. *Proceedings of the National Academy of Sciences*, 112(11), 3241–3246.

Kerr, R. A. (2000). A North Atlantic climate pacemaker for the centuries. *Science*, 288(5473), 1984–1985.

Keyantash, J. & Dracup, J. A. (2002). The quantification of drought: an evaluation of drought indices. *Bulletin of the American Meteorological Society*, 83(8), 1167–1180.

Kiem, A. S., Johnson, F., Westra, S., van Dijk, A., Evans, J. P., O'Donnell, A., Rouillard, A., Barr, C., Tyler, J., Thyer, M. et al. (2016). Natural hazards in Australia: droughts. *Climatic Change*, 139(1), 37–54.

Knight, J. R., Allan, R. J., Folland, C. K., Vellinga, M. & Mann, M. E. (2005). A signature of persistent natural thermohaline circulation cycles in observed climate. *Geophysical Research Letters*, 32(20).

Knight, J. R., Folland, C. K. & Scaife, A. A. (2006). Climate impacts of the Atlantic multidecadal oscillation. *Geophysical Research Letters*, 33(17).

Knutson, T. R. & Manabe, S. (1998). Model assessment of decadal variability and trends in the tropical Pacific Ocean. *Journal of Climate*, 11(9), 2273–2296.

Kumar, R., Musuuza, J. L., Loon, A. F. V., Teuling, A. J., Barthel, R., Ten Broek, J., Mai, J., Samaniego, L. & Attinger, S. (2016). Multiscale evaluation of the Standardized Precipitation Index as a groundwater drought indicator. *Hydrology and Earth System Sciences*, 20(3), 1117–1131.

Kundzewicz, Z. & Somlyódy, L. (1997). Climatic change impact on water resources in a systems perspective. *Water Resources Management*, 11(6), 407–435.

Kurtzman, D. & Scanlon, B. R. (2007). El Nino–Southern Oscillation and Pacific Decadal Oscillation impacts on precipitation in the southern and central United States: Evaluation of spatial distribution and predictions. *Water Resources Research*, 43(10).

Kushnir, Y., Seager, R., Ting, M., Naik, N. & Nakamura, J. (2010). Mechanisms of tropical Atlantic SST influence on North American precipitation variability. *Journal of Climate*, 23(21), 5610–5628.

Kwon, M., Kwon, H.-H. & Han, D. (2019). Spatio-temporal drought patterns of multiple drought indices based on precipitation and soil moisture: A case study in South Korea. *International Journal of Climatology*.

Lafon, T., Dadson, S., Buys, G. & Prudhomme, C. (2013). Bias correction of daily precipitation simulated by a regional climate model: a comparison of methods. *International Journal of Climatology*, 33(6), 1367–1381.

Langenbrunner, B. & Neelin, J. D. (2013). Analyzing ENSO teleconnections in CMIP models as a measure of model fidelity in simulating precipitation. *Journal of Climate*, 26(13), 4431–4446.

Leduc, M., Mailhot, A., Frigon, A., Martel, J.-L., Ludwig, R., Brietzke, G. B., Giguére, M., Brissette, F., Turcotte, R., Braun, M. et al. (2019). ClimEx project: a 50-member ensemble of climate change projections at 12-km resolution over Europe and northeastern North America with the Canadian Regional Climate Model (CRCM5). *Journal of Applied Meteorology and Climatology*, (2019).

Lehner, B., Döll, P., Alcamo, J., Henrichs, T. & Kaspar, F. (2006). Estimating the impact of global change on flood and drought risks in Europe: a continental, integrated analysis. *Climatic Change*, 75(3), 273–299.

Lelieveld, J., Proestos, Y., Hadjinicolaou, P., Tanarhte, M., Tyrlis, E. & Zittis, G. (2016). Strongly increasing heat extremes in the Middle East and North Africa (MENA) in the 21st century. *Climatic Change*, 137(1-2), 245–260.

Leng, G., Tang, Q. & Rayburg, S. (2015). Climate change impacts on meteorological, agricultural and hydrological droughts in China. *Global and Planetary Change*, 126, 23–34.

Leng, G., Huang, M., Voisin, N., Zhang, X., Asrar, G. R. & Leung, L. R. (2016). Emergence of new hydrologic regimes of surface water resources in the conterminous United States under future warming. *Environmental Research Letters*, 11(11), 114003.

Lesk, C., Rowhani, P. & Ramankutty, N. (2016). Influence of extreme weather disasters on global crop production. *Nature*, 529(7584), 84.

Li, H., Sheffield, J. & Wood, E. F. (2010). Bias correction of monthly precipitation and temperature fields from Intergovernmental Panel on Climate Change AR4 models using equidistant quantile matching. *Journal of Geophysical Research: Atmospheres*, 115(D10).

Li, S. & Bates, G. T. (2007). Influence of the Atlantic multidecadal oscillation on the winter climate of East China. *Advances in Atmospheric Sciences*, 24(1), 126–135.

Li, T., Angeles, O., Radanielson, A., Marcaida, M. & Manalo, E. (2015). Drought stress impacts of climate change on rainfed rice in South Asia. *Climatic change*, 133(4), 709–720.

Lim, Y.-K., Schubert, S. D., Kovach, R., Molod, A. M. & Pawson, S. (2018). The Roles of Climate Change and Climate Variability in the 2017 Atlantic Hurricane Season. *Scientific reports*, 8(1), 16172.

Lins, H. F. & Cohn, T. A. (2011). Stationarity: wanted dead or alive? 1. *JAWRA Journal of the American Water Resources Association*, 47(3), 475–480.

Linsley, B., Wellington, G., Schrag, D., Ren, L., Salinger, M. & Tudhope, A. (2004). Geochemical evidence from corals for changes in the amplitude and spatial pattern of South Pacific interdecadal climate variability over the last 300 years. *Climate Dynamics*, 22(1), 1–11.

Liu, C., Ikeda, K., Rasmussen, R., Barlage, M., Newman, A. J., Prein, A. F., Chen, F., Chen, L., Clark, M., Dai, A. et al. (2017). Continental-scale convection-permitting modeling of the current and future climate of North America. *Climate Dynamics*, 49(1-2), 71–95.

Liu, W., Huang, B., Thorne, P. W., Banzon, V. F., Zhang, H.-M., Freeman, E., Lawrimore, J., Peterson, T. C., Smith, T. M. & Woodruff, S. D. (2015). Extended reconstructed sea surface temperature version 4 (ERSST. v4): Part II. Parametric and structural uncertainty estimations. *Journal of Climate*, 28(3), 931–951.

Liu, Z. (2012). Dynamics of interdecadal climate variability: A historical perspective. *Journal of Climate*, 25(6), 1963–1995.

Livada, I. & Assimakopoulos, V. (2007). Spatial and temporal analysis of drought in Greece using the Standardized Precipitation Index (SPI). *Theoretical and applied climatology*, 89(3-4), 143–153.

Livezey, R. E. & Chen, W. (1983). Statistical field significance and its determination by Monte Carlo techniques. *Monthly Weather Review*, 111(1), 46–59.

Livneh, B., Rosenberg, E. A., Lin, C., Nijssen, B., Mishra, V., Andreadis, K. M., Maurer, E. P. & Lettenmaier, D. P. (2013). A long-term hydrologically based dataset of land surface fluxes and states for the conterminous United States: Update and extensions. *Journal of Climate*, 26(23), 9384–9392.

Lloyd-Hughes, B. & Saunders, M. A. (2002). A drought climatology for Europe. *International Journal of Climatology: A Journal of the Royal Meteorological Society*, 22(13), 1571–1592.

López-Moreno, J. I. & Vicente-Serrano, S. M. (2008). Positive and negative phases of the wintertime North Atlantic Oscillation and drought occurrence over Europe: a multitemporal-scale approach. *Journal of Climate*, 21(6), 1220–1243.

Lu, R., Dong, B. & Ding, H. (2006). Impact of the Atlantic Multidecadal Oscillation on the Asian summer monsoon. *Geophysical Research Letters*, 33(24).

Mailhot, A. & Duchesne, S. (2009). Design criteria of urban drainage infrastructures under climate change. *Journal of Water Resources Planning and Management*, 136(2), 201–208.

Maleski, J. J. & Martinez, C. J. (2018). Coupled impacts of ENSO AMO and PDO on temperature and precipitation in the Alabama–Coosa–Tallapoosa and Apalachicola–Chattahoochee–Flint river basins. *International Journal of Climatology*, 38, e717–e728.

Mann, M. E. & Gleick, P. H. (2015). Climate change and California drought in the 21st century. *Proceedings of the National Academy of Sciences*, 112(13), 3858–3859.

Mantua, N. J. & Hare, S. R. (2002). The Pacific decadal oscillation. *Journal of oceanography*, 58(1), 35–44.

Mantua, N. J., Hare, S. R., Zhang, Y., Wallace, J. M. & Francis, R. C. (1997). A Pacific interdecadal climate oscillation with impacts on salmon production. *Bulletin of the american Meteorological Society*, 78(6), 1069–1080.

Maraun, D., Wetterhall, F., Ireson, A., Chandler, R., Kendon, E., Widmann, M., Brienen, S., Rust, H., Sauter, T., Themeßl, M. et al. (2010). Precipitation downscaling under climate change: Recent developments to bridge the gap between dynamical models and the end user. *Reviews of Geophysics*, 48(3).

Marcos-Garcia, P., Lopez-Nicolas, A. & Pulido-Velazquez, M. (2017). Combined use of relative drought indices to analyze climate change impact on meteorological and hydrological droughts in a Mediterranean basin. *Journal of Hydrology*, 554, 292–305.

Marengo, J. A., Tomasella, J., Alves, L. M., Soares, W. R. & Rodriguez, D. A. (2011). The drought of 2010 in the context of historical droughts in the Amazon region. *Geophysical Research Letters*, 38(12).

Marengo, J. A. & Espinoza, J. (2016). Extreme seasonal droughts and floods in Amazonia: causes, trends and impacts. *International Journal of Climatology*, 36(3), 1033–1050.

Martel, J.-L., Mailhot, A., Brissette, F. & Caya, D. (2018). Role of Natural Climate Variability in the Detection of Anthropogenic Climate Change Signal for Mean and Extreme Precipitation at Local and Regional Scales. *Journal of Climate*, 31(11), 4241–4263.

Martel, J.-L., Mailhot, A. & Brissette, F. (2020). Global and Regional Projected Changes in 100-Year Sub-Daily, Daily and Multi-Day Precipitation Extremes Estimated from Three Large Ensembles of Climate Simulation. *Journal of Climate*.

Masud, M., Khaliq, N., Wheater, H. & Zilefac, E. (2015). Probabilistic Assessment of Meteorological Drought Risk over the Canadian Prairie Provinces Based on the NARCCAP multi-RCM Ensemble. *AGU Fall Meeting Abstracts*.

Masud, M., Khaliq, M. & Wheater, H. (2017). Future changes to drought characteristics over the Canadian Prairie Provinces based on NARCCAP multi-RCM ensemble. *Climate dynamics*, 48(7-8), 2685–2705.

Matthews, R., Kropff, M., Horie, T. & Bachelet, D. (1997). Simulating the impact of climate change on rice production in Asia and evaluating options for adaptation. *Agricultural systems*, 54(3), 399–425.

Mauger, G., Casola, J., Morgan, H., Strauch, R., Jones, B., Curry, B., Busch Isaksen, T., Whitely Binder, L., Krosby, M. & Snover, A. (2005). State of knowledge: Climate change in Puget Sound.

Maurer, E. P. (2007). Uncertainty in hydrologic impacts of climate change in the Sierra Nevada, California, under two emissions scenarios. *Climatic Change*, 82(3-4), 309–325.

Maurer, E. P., Wood, A., Adam, J., Lettenmaier, D. P. & Nijssen, B. (2002). A long-term hydrologically based dataset of land surface fluxes and states for the conterminous United States. *Journal of climate*, 15(22), 3237–3251.

Mazrooei, A. & Sankarasubramanian, A. (2019). Improving monthly streamflow forecasts through assimilation of observed streamflow for rainfall-dominated basins across the CONUS. *Journal of Hydrology*, 575, 704–715.

McCabe, G. J. & Dettinger, M. D. (1999). Decadal variations in the strength of ENSO teleconnections with precipitation in the western United States. *International Journal of Climatology: a Journal of the Royal Meteorological Society*, 19(13), 1399–1410.

McCabe, G. J., Palecki, M. A. & Betancourt, J. L. (2004). Pacific and Atlantic Ocean influences on multidecadal drought frequency in the United States. *Proceedings of the National Academy of Sciences*, 101(12), 4136–4141.

McCarthy, J. J., Canziani, O. F., Leary, N. A., Dokken, D. J. & White, K. S. (2001). *Climate change 2001: impacts, adaptation, and vulnerability: contribution of Working Group II to the third assessment report of the Intergovernmental Panel on Climate Change*. Cambridge University Press.

McDonald, C. (2016). The Insurance Impact of the Fort McMurray Wildfires. *Risk Management*.

McKee, T. B. (1995). Drought monitoring with multiple time scales. *Proceedings of 9th Conference on Applied Climatology, Boston, 1995*.

McKee, T. B., Doesken, N. J., Kleist, J. et al. (1993). The relationship of drought frequency and duration to time scales. *Proceedings of the 8th Conference on Applied Climatology*, 17(22), 179–183.

Mearns, L. O., Arritt, R., Biner, S., Bukovsky, M. S., McGinnis, S., Sain, S., Caya, D., Correia Jr, J., Flory, D., Gutowski, W. et al. (2012). The North American regional climate change assessment program: overview of phase I results. *Bulletin of the American Meteorological Society*, 93(9), 1337–1362.

Mearns, L., Bogardi, I., Giorgi, F., Matyasovszky, I. & Palecki, M. (1999). Comparison of climate change scenarios generated from regional climate model experiments and statistical downscaling. *Journal of Geophysical Research: Atmospheres*, 104(D6), 6603–6621.

Medellín-Azuara, J., MacEwan, D., Howitt, R. E., Sumner, D. A., Lund, J. R., Scheer, J., Gailey, R., Hart, Q., Alexander, N. D., Arnold, B. et al. (2016). Economic analysis of the 2016 California drought on agriculture. *Center for Watershed Sciences. Davis, CA: UC Davis*.

Meehl, G. A., Covey, C., Delworth, T., Latif, M., McAvaney, B., Mitchell, J. F., Stouffer, R. J. & Taylor, K. E. (2007). The WCRP CMIP3 multimodel dataset: A new era in climate change research. *Bulletin of the American Meteorological Society*, 88(9), 1383–1394.

Meehl, G. A., Hu, A., Santer, B. D. & Xie, S.-P. (2016). Contribution of the Interdecadal Pacific Oscillation to twentieth-century global surface temperature trends. *Nature Climate Change*, 6(11), 1005.

Mehrotra, R., Sharma, A., Bari, M., Tuteja, N. & Amirthanathan, G. (2014). An assessment of CMIP5 multi-model decadal hindcasts over Australia from a hydrological viewpoint. *Journal of hydrology*, 519, 2932–2951.

Messié, M. & Chavez, F. (2011). Global modes of sea surface temperature variability in relation to regional climate indices. *Journal of Climate*, 24(16), 4314–4331.

Minobe, S. (1997). A 50–70 year climatic oscillation over the North Pacific and North America. *Geophysical Research Letters*, 24(6), 683–686.

Minville, M., Brissette, F. & Leconte, R. (2008). Uncertainty of the impact of climate change on the hydrology of a nordic watershed. *Journal of hydrology*, 358(1-2), 70–83.

Mishra, A. K. & Singh, V. P. (2010). A review of drought concepts. *Journal of hydrology*, 391(1-2), 202–216.

Miskus, D. (2017). US Drought Monitor, January 3, 2017.

Mo, K. C. (2008). Model-based drought indices over the United States. *Journal of Hydrometeorology*, 9(6), 1212–1230.

US Drought Monitor (2017). US drought monitor map archive.

Mpelasoka, F. S. & Chiew, F. H. (2009). Influence of rainfall scenario construction methods on runoff projections. *Journal of Hydrometeorology*, 10(5), 1168–1183.

Mukherjee, S., Mishra, A. & Trenberth, K. E. (2018). Climate change and drought: a perspective on drought indices. *Current Climate Change Reports*, 4, 145–163.

Nalbantis, I. (2008). Evaluation of a hydrological drought index. *European Water*, 23(24), 67–77.

Nalbantis, I. & Tsakiris, G. (2009). Assessment of hydrological drought revisited. *Water Resources Management*, 23(5), 881–897.

NCAR. (2019). "The Climate Data Guide: Overview: Climate Indices.". Consulted at https://climatedataguide.ucar.edu/climate-data/overview-climate-indices.

NCDC. (2013). DROUGHT: Monitoring Economic, Environmental, and Social Impacts. Accessed 2013.

NDMC. (2020). Types of Drought. Consulted at https://drought.unl.edu/Education/DroughtIn-depth/TypesofDrought.aspx.

Newman, M., Compo, G. P. & Alexander, M. A. (2003). ENSO-forced variability of the Pacific decadal oscillation. *Journal of Climate*, 16(23), 3853–3857.

Newman, M., Alexander, M. A., Ault, T. R., Cobb, K. M., Deser, C., Di Lorenzo, E., Mantua, N. J., Miller, A. J., Minobe, S., Nakamura, H. et al. (2016). The Pacific decadal oscillation, revisited. *Journal of Climate*, 29(12), 4399–4427.

Nicholson, S. E. (2001). Climatic and environmental change in Africa during the last two centuries. *Climate research*, 17(2), 123–144.

Nigam, S., Barlow, M. & Berbery, E. H. (1999). Analysis links Pacific decadal variability to drought and streamflow in United States. *EOS, Transactions American Geophysical Union*, 80(51), 621–625.

NOAA/NCEI. (2013). *State of the climate: drought for annual 2012*.

NOAA/NCEI. (2019). Billion-dollar weather and climate disasters. Consulted at https://www.ncdc.noaa.gov/billions/.

Okumura, Y. M., DiNezio, P. & Deser, C. (2017). Evolving impacts of multiyear La Niña events on atmospheric circulation and US drought. *Geophysical Research Letters*, 44(22).

Olesen, J. E. & Bindi, M. (2002). Consequences of climate change for European agricultural productivity, land use and policy. *European journal of agronomy*, 16(4), 239–262.

Orlowsky, B. & Seneviratne, S. I. (2013). Elusive drought: uncertainty in observed trends and short-andlong-term CMIP5 projections. *Hydrology and Earth System Sciences*, 17(5), 1765–1781.

Osborn, T., Barichivich, J., Harris, I., Van Der Schrier, G. & Jones, P. (2017). Monitoring global drought using the self-calibrating Palmer Drought Severity Index [in" State of the Climate in 2016"]. *Bulletin of the American Meteorological Society*, 98(8), S32–S33.

Otto-Bliesner, B. L., Brady, E. C., Fasullo, J., Jahn, A., Landrum, L., Stevenson, S., Rosenbloom, N., Mai, A. & Strand, G. (2016). Climate variability and change since 850 CE: An ensemble approach with the Community Earth System Model. *Bulletin of the American Meteorological Society*, 97(5), 735–754.

Oudin, L., Hervieu, F., Michel, C., Perrin, C., Andréassian, V., Anctil, F. & Loumagne, C. (2005). Which potential evapotranspiration input for a lumped rainfall–runoff model?: Part 2—Towards a simple and efficient potential evapotranspiration model for rainfall–runoff modelling. *Journal of hydrology*, 303(1-4), 290–306.

Pai, D., Sridhar, L., Guhathakurta, P. & Hatwar, H. (2011). District-wide drought climatology of the southwest monsoon season over India based on standardized precipitation index (SPI). *Natural hazards*, 59(3), 1797–1813.

Palmer, W. C. (1965). Meteorological drought, Research paper no. 45. *US Weather Bureau, Washington, DC*, 58.

Penalba, O. C. & Rivera, J. A. (2016). Regional aspects of future precipitation and meteorological drought characteristics over Southern South America projected by a CMIP5 multi-model ensemble. *International Journal of Climatology*, 36(2), 974–986.

Perrin, C., Michel, C. & Andréassian, V. (2003). Improvement of a parsimonious model for streamflow simulation. *Journal of hydrology*, 279(1-4), 275–289.

Piani, C., Haerter, J. & Coppola, E. (2010). Statistical bias correction for daily precipitation in regional climate models over Europe. *Theoretical and Applied Climatology*, 99(1-2), 187–192.

Piao, S., Ciais, P., Huang, Y., Shen, Z., Peng, S., Li, J., Zhou, L., Liu, H., Ma, Y., Ding, Y. et al. (2010). The impacts of climate change on water resources and agriculture in China. *Nature*, 467(7311), 43.

Pierce, D., Barnett, T., Schneider, N., Saravanan, R., Dommenget, D. & Latif, M. (2001). The role of ocean dynamics in producing decadal climate variability in the North Pacific. *Climate Dynamics*, 18(1-2), 51–70.

Potop, V. (2011). Evolution of drought severity and its impact on corn in the Republic of Moldova. *Theoretical and Applied Climatology*, 105(3-4), 469–483.

Preethi, B., Ramya, R., Patwardhan, S., Mujumdar, M. & Kripalani, R. (2019). Variability of Indian summer monsoon droughts in CMIP5 climate models. *Climate Dynamics*, 1–26.

Prudhomme, C., Giuntoli, I., Robinson, E. L., Clark, D. B., Arnell, N. W., Dankers, R., Fekete, B. M., Franssen, W., Gerten, D., Gosling, S. N. et al. (2014). Hydrological droughts in the 21st century, hotspots and uncertainties from a global multimodel ensemble experiment. *Proceedings of the National Academy of Sciences*, 111(9), 3262–3267.

Qian, C. & Zhou, T. (2014). Multidecadal variability of North China aridity and its relationship to PDO during 1900–2010. *Journal of Climate*, 27(3), 1210–1222.

Qian, C., Yu, J.-Y. & Chen, G. (2014). Decadal summer drought frequency in China: the increasing influence of the Atlantic Multi-decadal Oscillation. *Environmental Research Letters*, 9(12), 124004.

Quiring, S. M. & Papakryiakou, T. N. (2003). An evaluation of agricultural drought indices for the Canadian prairies. *Agricultural and forest meteorology*, 118(1-2), 49–62.

Rakhecha, P. & Singh, V. P. (2009). *Applied hydrometeorology*. Springer Science & Business Media.

Randall, D. A., Wood, R. A., Bony, S., Colman, R., Fichefet, T., Fyfe, J., Kattsov, V., Pitman, A., Shukla, J., Srinivasan, J. et al. (2007). Climate models and their evaluation. In *Climate change 2007: The physical science basis. Contribution of Working Group I to the Fourth Assessment Report of the IPCC (FAR)* (pp. 589–662). Cambridge University Press.

Rayner, N., Parker, D. E., Horton, E., Folland, C., Alexander, L., Rowell, D., Kent, E. & Kaplan, A. (2003). Global analyses of sea surface temperature, sea ice, and night marine air temperature since the late nineteenth century. *Journal of Geophysical Research: Atmospheres*, 108(D14).

Riahi, K., Rao, S., Krey, V., Cho, C., Chirkov, V., Fischer, G., Kindermann, G., Nakicenovic, N. & Rafaj, P. (2011). RCP 8.5—A scenario of comparatively high greenhouse gas emissions. *Climatic Change*, 109(1-2), 33.

Robeson, S. M. (2015). Revisiting the recent California drought as an extreme value. *Geophysical Research Letters*, 42(16), 6771–6779.

Rogers, J. C. & Coleman, J. S. (2003). Interactions between the Atlantic Multidecadal Oscillation, El Nino/La Nina, and the PNA in winter Mississippi valley stream flow. *Geophysical Research Letters*, 30(10).

Rojas, J. P. & Sheffield, R. E. (2013). Evaluation of daily reference evapotranspiration methods as compared with the ASCE-EWRI Penman-Monteith equation using limited weather data in Northeast Louisiana. *Journal of Irrigation and Drainage Engineering*, 139(4), 285–292.

Rojas, O. (2018). Agricultural extreme drought assessment at global level using the FAO-Agricultural Stress Index System (ASIS). *Weather and Climate Extremes*, 100184.

Rosenberg, E. A., Keys, P. W., Booth, D. B., Hartley, D., Burkey, J., Steinemann, A. C. & Lettenmaier, D. P. (2010). Precipitation extremes and the impacts of climate change on stormwater infrastructure in Washington State. *Climatic Change*, 102(1-2), 319–349.

Roudier, P., Andersson, J. C., Donnelly, C., Feyen, L., Greuell, W. & Ludwig, F. (2016). Projections of future floods and hydrological droughts in Europe under a+ 2 C global warming. *Climatic Change*, 135(2), 341–355.

Ruiz-Barradas, A., Nigam, S. & Kavvada, A. (2013). The Atlantic Multidecadal Oscillation in twentieth century climate simulations: uneven progress from CMIP3 to CMIP5. *Climate dynamics*, 41(11-12), 3301–3315.

Rupp, D. E., Li, S., Mote, P. W., Massey, N., Sparrow, S. N. & Wallom, D. C. (2017). Influence of the ocean and greenhouse gases on severe drought likelihood in the central United States in 2012. *Journal of Climate*, 30(5), 1789–1806.

Räisänen, J. (2001). CO2 Induced Climate Change in CMIP2 Experiments: Quantification of Agreement and Role of Internal Variability. *Journal of Climate*, 14(9), 2088-2104.

Salvi, K., Kannan, S. & Ghosh, S. (2011). Statistical downscaling and bias-correction for projections of Indian rainfall and temperature in climate change studies. *4th International Conference on Environmental and Computer Science*, pp. 16–18.

Santos, J. F., Pulido-Calvo, I. & Portela, M. M. (2010). Spatial and temporal variability of droughts in Portugal. *Water Resources Research*, 46(3).

Schlesinger, M. E. & Ramankutty, N. (1994). An oscillation in the global climate system of period 65–70 years. *Nature*, 367(6465), 723.

Schmidli, J., Frei, C. & Vidale, P. L. (2006). Downscaling from GCM precipitation: a benchmark for dynamical and statistical downscaling methods. *International journal of climatology*, 26(5), 679–689.

Schmidt, N., Lipp, E., Rose, J. & Luther, M. (2001). ENSO influences on seasonal rainfall and river discharge in Florida. *Journal of Climate*, 14(4), 615–628.

Schneider, U., Becker, A., Finger, P., Meyer-Christoffer, A. & Ziese, M. (2018). GPCC Full Data Monthly Product Version 2018 at 0.5°: Monthly land-surface precipitation from rain-gauges built on GTS-based and historical data. *Global Precipitation Climatology Centre*.

Seager, R. & Ting, M. (2017). Decadal drought variability over North America: Mechanisms and predictability. *Current Climate Change Reports*, 3(2), 141–149.

Seager, R. & Vecchi, G. A. (2010). Greenhouse warming and the 21st century hydroclimate of southwestern North America. *Proceedings of the National Academy of Sciences*, 107(50), 21277–21282.

Seiller, G. & Anctil, F. (2014). Climate change impacts on the hydrologic regime of a Canadian river: comparing uncertainties arising from climate natural variability and lumped hydrological model structures. *Hydrology and Earth System Sciences*, 18(6), 2033–2047.

Seneviratne, S. I., Nicholls, N., Easterling, D., Goodess, C. M., Kanae, S., Kossin, J., Luo, Y., Marengo, J., McInnes, K., Rahimi, M. et al. (2012). *Managing the Risks of Extreme Events and Disasters to Advance Climate Change Adaptation: Changes in Climate Extremes and their Impacts on the Natural Physical Environment*.

Shabbar, A. & Skinner, W. (2004). Summer Drought Patterns in Canada and the Relationship toGlobal Sea Surface Temperatures. *Journal of Climate*, 17(14), 2866–2880.

Sharma, T. & Panu, U. (2015). Predicting return periods of hydrological droughts using the Pearson 3 distribution: a case from rivers in the Canadian prairies. *Hydrological Sciences Journal*, 60(10), 1783–1796.

Sheffield, J. & Wood, E. F. (2008). Projected changes in drought occurrence under future global warming from multi-model, multi-scenario, IPCC AR4 simulations. *Climate dynamics*, 31(1), 79–105.

Sheffield, J., Goteti, G., Wen, F. & Wood, E. F. (2004). A simulated soil moisture based drought analysis for the United States. *Journal of Geophysical Research: Atmospheres*, 109(D24).

Sheffield, J., Wood, E. F. & Roderick, M. L. (2012). Little change in global drought over the past 60 years. *Nature*, 491(7424), 435.

Siegel, S. (1956). Nonparametric statistics for the behavioral sciences.

Sigdel, M. & Ikeda, M. (2010). Spatial and temporal analysis of drought in Nepal using standardized precipitation index and its relationship with climate indices. *Journal of Hydrology and Meteorology*, 7(1), 59–74.

Sigmond, M. & Fyfe, J. C. (2016). Tropical Pacific impacts on cooling North American winters. *Nature Climate Change*, 6(10), 970.

Spinoni, J., Barbosa, P., De Jager, A., McCormick, N., Naumann, G., Vogt, J. V., Magni, D., Masante, D. & Mazzeschi, M. (2019). A new global database of meteorological drought events from 1951 to 2016. *Journal of Hydrology: Regional Studies*, 22, 100593.

Steinman, B. A., Mann, M. E. & Miller, S. K. (2015). Atlantic and Pacific multidecadal oscillations and Northern Hemisphere temperatures. *Science*, 347(6225), 988–991.

Stevens, K. (2008). *Statistical associations between large scale climate oscillations and mesoscale surface meteorological variability in the Apalachicola-Chattahoochee-Flint River basin*. (Ph.D. thesis, Florida State University).

Stevens, K. A. & Ruscher, P. H. (2014). Large scale climate oscillations and mesoscale surface meteorological variability in the Apalachicola-Chattahoochee-Flint River Basin. *Journal of hydrology*, 517, 700–714.

Stewart, I. T., Cayan, D. R. & Dettinger, M. D. (2005). Changes toward earlier streamflow timing across western North America. *Journal of climate*, 18(8), 1136–1155.

Stricevic, R., Djurovic, N. & Djurovic, Z. (2011). Drought classification in Northern Serbia based on SPI and statistical pattern recognition. *Meteorological applications*, 18(1), 60–69.

Sushama, L., Khaliq, N. & Laprise, R. (2010). Dry spell characteristics over Canada in a changing climate as simulated by the Canadian RCM. *Global and Planetary Change*, 74(1), 1–14.

Sutton, R. T. & Hodson, D. L. (2005). Atlantic Ocean forcing of North American and European summer climate. *science*, 309(5731), 115–118.

Svoboda, M., Hayes, M. & Wood, D. (2012). Standardized precipitation index user guide. *World Meteorological Organization Geneva, Switzerland*.

Svoboda, M., LeComte, D., Hayes, M., Heim, R., Gleason, K., Angel, J., Rippey, B., Tinker, R., Palecki, M., Stooksbury, D. et al. (2002). The drought monitor. *Bulletin of the American Meteorological Society*, 83(8), 1181–1190.

Svoboda, M., Fuchs, B. et al. (2016). Handbook of drought indicators and indices.

Swann, A. L., Fung, I. Y., Levis, S., Bonan, G. B. & Doney, S. C. (2010). Changes in Arctic vegetation amplify high-latitude warming through the greenhouse effect. *Proceedings of the National Academy of Sciences*, 107(4), 1295–1300.

Tam, B. Y., Szeto, K., Bonsal, B., Flato, G., Cannon, A. J. & Rong, R. (2018). CMIP5 drought projections in Canada based on the Standardized Precipitation Evapotranspiration Index. *Canadian Water Resources Journal/Revue canadienne des ressources hydriques*, 44(1), 90–107.

Taylor, K. E., Stouffer, R. J. & Meehl, G. A. (2012). An overview of CMIP5 and the experiment design. *Bulletin of the American Meteorological Society*, 93(4), 485–498.

Teuling, A. J. (2018). A hot future for European droughts. *Nature Climate Change*, 8(5), 364–365.

Teutschbein, C. & Seibert, J. (2012). Bias correction of regional climate model simulations for hydrological climate-change impact studies: Review and evaluation of different methods. *Journal of Hydrology*, 456, 12–29.

Ting, M., Kushnir, Y., Seager, R. & Li, C. (2009). Forced and internal twentieth-century SST trends in the North Atlantic. *Journal of Climate*, 22(6), 1469–1481.

Tingley, M. P. & Huybers, P. (2013). Recent temperature extremes at high northern latitudes unprecedented in the past 600 years. *Nature*, 496(7444), 201.

Tootle, G. A. & Piechota, T. C. (2006). Relationships between Pacific and Atlantic ocean sea surface temperatures and US streamflow variability. *Water Resources Research*, 42(7).

Torrence, C. & Compo, G. P. (1998). A practical guide to wavelet analysis. *Bulletin of the American Meteorological society*, 79(1), 61–78.

Touma, D., Ashfaq, M., Nayak, M. A., Kao, S.-C. & Diffenbaugh, N. S. (2015). A multi-model and multi-index evaluation of drought characteristics in the 21st century. *Journal of Hydrology*, 526, 196–207.

Trenberth, K., Overpeck, J. & Solomon, S. (2004). Exploring drought and its implications for the future. *Eos, Transactions American Geophysical Union*, 85(3), 27–27.

Trenberth, K. E. (1997). The definition of el nino. *Bulletin of the American Meteorological Society*, 78(12), 2771–2778.

Trenberth, K. E. (1999). Conceptual framework for changes of extremes of the hydrological cycle with climate change. In *Weather and Climate Extremes* (pp. 327–339). Springer.

Trenberth, K. E. & Guillemot, C. J. (1996). Physical processes involved in the 1988 drought and 1993 floods in North America. *Journal of Climate*, 9(6), 1288–1298.

Trenberth, K. E. & Shea, D. J. (2006). Atlantic hurricanes and natural variability in 2005. *Geophysical Research Letters*, 33(12).

Trenberth, K. E. & Stepaniak, D. P. (2001). Indices of el niño evolution. *Journal of climate*, 14(8), 1697–1701.

Trenberth, K. E., Dai, A., Van Der Schrier, G., Jones, P. D., Barichivich, J., Briffa, K. R. & Sheffield, J. (2014). Global warming and changes in drought. *Nature Climate Change*, 4(1), 17.

Trigo, R. M., Osborn, T. J. & Corte-Real, J. M. (2002). The North Atlantic Oscillation influence on Europe: climate impacts and associated physical mechanisms. *Climate research*, 20(1), 9–17.

Troin, M., Arsenault, R. & Brissette, F. (2015). Performance and uncertainty evaluation of snow models on snowmelt flow simulations over a Nordic catchment (Mistassibi, Canada). *Hydrology*, 2(4), 289–317.

Troin, M., Arsenault, R., Martel, J.-L. & Brissette, F. (2018). Uncertainty of hydrological model components in climate change studies over two Nordic Quebec catchments. *Journal of Hydrometeorology*, 19(1), 27–46.

Valdés-Pineda, R., Cañón, J. & Valdés, J. B. (2018). Multi-decadal 40-to 60-year cycles of precipitation variability in Chile (South America) and their relationship to the AMO and PDO signals. *Journal of Hydrology*, 556, 1153–1170.

Valéry, A., Andréassian, V. & Perrin, C. (2014). 'As simple as possible but not simpler': What is useful in a temperature-based snow-accounting routine? Part 2–Sensitivity analysis of the Cemaneige snow accounting routine on 380 catchments. *Journal of Hydrology*, 517, 1176–1187.

Van Lanen, H. A. (2006). Drought propagation through the hydrological cycle. *IAHS publication*, 308, 122.

van Oldenborgh, G. J., Doblas-Reyes, F. J., Wouters, B. & Hazeleger, W. (2012). Decadal prediction skill in a multi-model ensemble. *Climate dynamics*, 38(7-8), 1263–1280.

van Roosmalen, L., Sonnenborg, T. O., Jensen, K. H. & Christensen, J. H. (2011). Comparison of hydrological simulations of climate change using perturbation of observations and distribution-based scaling. *Vadose Zone Journal*, 10(1), 136–150.

Velázquez, J. A., Troin, M., Caya, D. & Brissette, F. (2015). Evaluating the time-invariance hypothesis of climate model bias correction: Implications for hydrological impact studies. *Journal of Hydrometeorology*, 16(5), 2013–2026.

Vicente-Serrano, S. M. & López-Moreno, J. I. (2005). Hydrological response to different time scales of climatological drought: an evaluation of the Standardized Precipitation Index in a mountainous Mediterranean basin.

Vicente-Serrano, S. M., Beguería, S. & López-Moreno, J. I. (2010). A multiscalar drought index sensitive to global warming: the standardized precipitation evapotranspiration index. *Journal of climate*, 23(7), 1696–1718.

Vicente-Serrano, S. M., López-Moreno, J. I., Beguería, S., Lorenzo-Lacruz, J., Azorin-Molina, C. & Morán-Tejeda, E. (2011). Accurate computation of a streamflow drought index. *Journal of Hydrologic Engineering*, 17(2), 318–332.

Vimont, D. J. (2005). The contribution of the interannual ENSO cycle to the spatial pattern of decadal ENSO-like variability. *Journal of Climate*, 18(12), 2080–2092.

von Salzen, K., Scinocca, J. F., McFarlane, N. A., Li, J., Cole, J. N., Plummer, D., Verseghy, D., Reader, M. C., Ma, X., Lazare, M. et al. (2013). The Canadian fourth generation atmospheric global climate model (CanAM4). Part I: representation of physical processes. *Atmosphere-Ocean*, 51(1), 104–125.

von Trentini, F., Schmid, J., Wood, R., Willkofer, F., Leduc, M., Frigon, A. & Ludwig, R. (2018). Natural variability in RCMs: single model 50-member-ensemble (ClimEx) results to better understand variability in multi-model ensembles of CORDEX. *EGU General Assembly Conference Abstracts*, 20, 5244.

Wanders, N. & Wada, Y. (2015). Human and climate impacts on the 21st century hydrological drought. *Journal of Hydrology*, 526, 208–220.

Wanders, N., Wada, Y. & Van Lanen, H. (2015). Global hydrological droughts in the 21st century under a changing hydrological regime. *Earth System Dynamics*, 6(1), 1–15.

Wang, C. & Dong, S. (2010). Is the basin-wide warming in the North Atlantic Ocean related to atmospheric carbon dioxide and global warming? *Geophysical Research Letters*, 37(8).

Wang, H., Fu, R., Kumar, A. & Li, W. (2010). Variability and Predictability of Southeastern United States Summer Precipitation. *J. Hydroclim*, 11, 1007–1018.

Wang, H., Schubert, S. D., Koster, R. D. & Chang, Y. (2019a). Attribution of the 2017 Northern High Plains Drought. *Bulletin of the American Meteorological Society*, 100(1), S25–S29.

Wang, J., Yang, B., Ljungqvist, F. C. & Zhao, Y. (2013). The relationship between the Atlantic Multidecadal Oscillation and temperature variability in China during the last millennium. *Journal of Quaternary Science*, 28(7), 653–658.

Wang, L., Yu, H., Yang, M., Yang, R., Gao, R. & Wang, Y. (2019b). A drought index: The standardized precipitation evapotranspiration runoff index. *Journal of Hydrology*, 571, 651–668.

Wang, S., Yuan, X. & Li, Y. (2017). Does a strong El Niño imply a higher predictability of extreme drought? *Scientific reports*, 7, 40741.

Wang, W., Ertsen, M. W., Svoboda, M. D. & Hafeez, M. (2016). Propagation of drought: from meteorological drought to agricultural and hydrological drought. *Advances in Meteorology*, 2016.

Wayne, C. P. (1965). Meteorological drought. *US Weather Bureau research paper*, (45).

Weare, B. C. (1979). A statistical study of the relationships between ocean surface temperatures and the Indian monsoon. *Journal of the Atmospheric Sciences*, 36(12), 2279–2291.

Weare, B. C. & Nasstrom, J. S. (1982). Examples of extended empirical orthogonal function analyses. *Monthly Weather Review*, 110(6), 481–485.

Wells, N., Goddard, S. & Hayes, M. J. (2004). A self-calibrating Palmer drought severity index. *Journal of Climate*, 17(12), 2335–2351.

Wilby, R. L. & Harris, I. (2006). A framework for assessing uncertainties in climate change impacts: Low-flow scenarios for the River Thames, UK. *Water Resources Research*, 42(2).

Wilby, R. L. & Wigley, T. (1997). Downscaling general circulation model output: a review of methods and limitations. *Progress in physical geography*, 21(4), 530–548.

Wilhelmi, O. V. & Morss, R. E. (2013). Integrated analysis of societal vulnerability in an extreme precipitation event: a Fort Collins case study. *Environmental science & policy*, 26, 49–62.

Wilhite, D. (2006). Drought monitoring and early warning: Concepts, progress and future challenges. *World Meteorological Organization, Geneva, Switzerland. WMO*, (1006).

Wilhite, D. A. & Glantz, M. H. (1985). Understanding: the drought phenomenon: the role of definitions. *Water international*, 10(3), 111–120.

Wu, M.-c. (2013). A brief introduction to Standardized Precipitation Index (SPI). Consulted at https://www.hko.gov.hk/education/edu01met/wxphe/ele_spi_e.htm.

Wu, Z. & Huang, N. E. (2009). Ensemble empirical mode decomposition: a noise-assisted data analysis method. *Advances in adaptive data analysis*, 1(01), 1–41.

Wuebbles, D., Fahey, D. & Hibbard, K. (2016). The Climate Science Special Report (CSSR) of the Fourth National Climate Assessment (NCA4). *AGU Fall Meeting Abstracts*.

Xia, J., Yan, Z. & Wu, P. (2013). Multidecadal variability in local growing season during 1901–2009. *Climate dynamics*, 41(2), 295–305.

Xu, C.-Y. & Singh, V. (2002). Cross comparison of empirical equations for calculating potential evapotranspiration with data from Switzerland. *Water Resources Management*, 16(3), 197–219.

Yang, Q., Ma, Z., Fan, X., Yang, Z.-L., Xu, Z. & Wu, P. (2017). Decadal modulation of precipitation patterns over eastern China by sea surface temperature anomalies. *Journal of Climate*, 30(17), 7017–7033.

Yang, W., Andréasson, J., Phil Graham, L., Olsson, J., Rosberg, J. & Wetterhall, F. (2010). Distribution-based scaling to improve usability of regional climate model projections for hydrological climate change impacts studies. *Hydrology Research*, 41(3-4), 211–229.

Ye, B., Yang, D. & Kane, D. L. (2003). Changes in Lena River streamflow hydrology: Human impacts versus natural variations. *Water resources research*, 39(7).

Youderian, B. D. (2009). *Influence of the Atlantic Multidecadal and the Pacific Decadal Oscillations on Hemispheric Air Temperature and Cloud Cover*. (Ph.D. thesis, The Ohio State University).

Yu, B., Shabbar, A. & Zwiers, F. (2007). The enhanced PNA-like climate response to Pacific interannual and decadal variability. *Journal of Climate*, 20(21), 5285–5300.

Yu, C., Huang, X., Chen, H., Huang, G., Ni, S., Wright, J. S., Hall, J., Ciais, P., Zhang, J., Xiao, Y. et al. (2018). Assessing the impacts of extreme agricultural droughts in China under climate and socioeconomic changes. *Earth's Future*, 6(5), 689–703.

Zarch, M. A. A., Sivakumar, B. & Sharma, A. (2015). Droughts in a warming climate: A global assessment of Standardized precipitation index (SPI) and Reconnaissance drought index (RDI). *Journal of Hydrology*, 526, 183–195.

Zelenhasić, E. & Salvai, A. (1987). A method of streamflow drought analysis. *Water resources research*, 23(1), 156–168.

Zhang, L. & Singh, V. (2006). Bivariate flood frequency analysis using the copula method. *Journal of hydrologic engineering*, 11(2), 150–164.

Zhang, Q., Li, J., Singh, V. P. & Bai, Y. (2012). SPI-based evaluation of drought events in Xinjiang, China. *Natural Hazards*, 64(1), 481–492.

Zhang, R., Delworth, T. L. & Held, I. M. (2007). Can the Atlantic Ocean drive the observed multidecadal variability in Northern Hemisphere mean temperature? *Geophysical Research Letters*, 34(2).

Zhang, Y. (1996). *An observational study of atmosphere-ocean interactions in the northern oceans on interannual and interdecadal time-scale*. (Ph.D. thesis).

Zhang, Y., Wallace, J. M. & Battisti, D. S. (1997). ENSO-like interdecadal variability: 1900–93. *Journal of climate*, 10(5), 1004–1020.

Zhao, P., Lü, H., Yang, H., Wang, W. & Fu, G. (2019). Impacts of climate change on hydrological droughts at basin scale: A case study of the Weihe River Basin, China. *Quaternary international*, 513, 37–46.

Zhao, T. & Dai, A. (2017). Uncertainties in historical changes and future projections of drought. Part II: model-simulated historical and future drought changes. *Climatic Change*, 144(3), 535–548.